Star Formation and Dynamics in the Galactic Centre

Michela Mapelli and Alessia Gualandris

Abstract The centre of our Galaxy is one of the most studied and yet enigmatic places in the Universe. At a distance of about 8 kpc from our Sun, the Galactic centre (GC) is the ideal environment to study the extreme processes that take place in the vicinity of a supermassive black hole (SMBH). Despite the hostile environment, several tens of early-type stars populate the central parsec of our Galaxy. A fraction of them lie in a thin ring with mild eccentricity and inner radius ~ 0.04 pc, while the S-stars, i.e. the ~ 30 stars closest to the SMBH ($\lesssim 0.04$ pc), have randomly oriented and highly eccentric orbits. The formation of such early-type stars has been a puzzle for a long time: molecular clouds should be tidally disrupted by the SMBH before they can fragment into stars. We review the main scenarios proposed to explain the formation and the dynamical evolution of the early-type stars in the GC. In particular, we discuss the most popular *in situ* scenarios (accretion disc fragmentation and molecular cloud disruption) and *migration* scenarios (star cluster inspiral and Hills mechanism). We focus on the most pressing challenges that must be faced to shed light on the process of star formation in the vicinity of a SMBH.

1 Introduction: the Galactic centre as a laboratory for both dynamics and star formation under extreme conditions

The Galactic centre (GC) is a unique laboratory to study physical processes in the vicinity of a supermassive black hole (SMBH). In fact, the GC hosts the only concentration of mass ($\approx 4 \times 10^6 \mathrm{M}_\odot$) that can be identified with a SMBH beyond rea-

Michela Mapelli
INAF, Osservatorio Astronomico di Padova, Vicolo dell'Osservatorio 5, I–35122, Padova, Italy
e-mail: michela.mapelli@oapd.inaf.it

Alessia Gualandris
Department of Physics, University of Surrey, Guildford GU2 7XH, United Kingdom e-mail: a.gualandris@surrey.ac.uk

sonable doubt (Schödel et al. 2002; Ghez et al. 2003). Furthermore, its distance from our Sun (≈ 8 kpc) is several orders of magnitude smaller than the distance from the other SMBH candidates. Despite the hostile environment due to the presence of a SMBH, the GC is an overwhelmingly crowded environment: the observations have revealed the presence of molecular, atomic and ionized gas, of a cusp of late-type stars, and of $\sim 100-200$ early-type stars. About 20-50 % of the early-type stars lie in a relatively thin ring (with inner radius ~ 0.04 pc) and follow a top-heavy mass function (MF, e.g. Paumard et al. 2006; Bartko et al. 2009; Lu et al. 2013; Yelda et al. 2014). The ~ 30 stars closest ($\lesssim 0.04\,\mathrm{pc} \sim 1$ arcsec) to SgrA* (i.e. the radio source that is associated with the central SMBH) are B stars, with an age < 100 Myr. These, named the S-stars, have very eccentric and randomly oriented orbits. The presence of the early-type stars in the central parsec is particularly puzzling, because the gravitational shear exerted by the SMBH disrupts molecular clouds before they can fragment into stars.

Because of its unique characteristics, the GC has been the subject of a plethora of studies and of a few dedicated reviews (e.g. Morris & Serabyn 1996; Genzel, Eisenhauer & Gillessen 2010) over the last ~ 20 years. Our review does not pretend to be either more complete or detailed than previous ones. Rather, it looks at the GC from a slightly different perspective: it focuses on the *young stars* that populate the GC, and on the *theoretical scenarios* that have been proposed to explain *their formation and their dynamical evolution*.

The review is structured as follows. In Sect. 2, we briefly summarize the state-of-the-art knowledge about the GC from an observational point of view, focusing on those aspects that are more relevant for the formation of the early-type stars. In Sect. 3, we discuss the main scenarios that have been proposed for the formation of the early-type stars (including disc fragmentation, molecular cloud disruption, inspiral of a star cluster and tidal break-up of binaries). Sect. 4 is devoted to the dynamical evolution of the early-type stars, considering both different relaxation mechanisms and secular processes. Finally, Sect. 5 deals with the main theoretical scenarios which have been proposed to explain the nature of one of the most peculiar objects that have been observed in the GC: the dusty object G2.

2 A crowded environment

In this Section, we briefly review the most updated observations of the main components of the GC: the SMBH (2.1), the young and old stars (2.2), the gas component (2.3) and the recently discovered, very puzzling G2 cloud (2.4). We also discuss the possibility that the GC hosts one or more intermediate-mass black holes (IMBHs), i.e. black holes with mass in the $10^2 - 10^5\,\mathrm{M}_\odot$ range (2.5).

In the next Sections (3–5), we will focus on the theoretical interpretation of such observations, and in particular on the processes that drive the formation and evolution of stars in the GC.

2.1 The supermassive black hole

The very first hints for the presence of a SMBH candidate in the centre of the Milky Way (MW) came from the detection of a very compact radio source (Balick & Brown 1974) in the innermost parsec.

The first attempts to estimate the mass enclosed in the central parsec are radial velocity measurements of ionized gas located in the structure which is known as minispiral (Lacy et al. 1980). On the other hand, the radial velocity of ionized gas may be affected by a plethora of processes besides gravity. Thus, the first strong claim for a dark mass in the centre of the MW came from radial velocity measurements of stars, obtained by means of near-infrared (NIR) spectra of the stellar population in the central parsecs (e.g. McGinn et al. 1989; Sellgren et al. 1990; Haller et al. 1996). These early measurements indicated the presence of $\sim 3\times10^6\,\mathrm{M}_\odot$ confined in ~ 0.1 pc, corresponding to a minimum density of $\sim 3\times10^9\,\mathrm{M}_\odot\,\mathrm{pc}^{-3}$. Such density is still consistent with a cluster of compact stellar remnants (e.g. Maoz 1998). The first measurements of stellar proper motions with diffraction-limited NIR observations (Genzel et al. 1997; Eckart et al. 1997; Ghez et al. 1998) strengthened the constraints significantly, indicating a $2.6\pm0.6\times10^6\,\mathrm{M}_\odot$ dark mass confined within ~ 0.01 pc, corresponding to a minimum density $\sim 10^{12}\,\mathrm{M}_\odot\,\mathrm{pc}^{-3}$. This density excludes the star cluster of compact remnants (Genzel et al. 1997) and leaves only two possible candidates: either a SMBH or a fermion ball (e.g. Tsiklauri & Viollier 1998). Tracing the orbit of the so called S2 (or S0-2) star (with an orbital period $T_{\rm orb}=15.9$ yr) led to the measurement of $3.7\pm1.5\times10^6\,\mathrm{M}_\odot$ (Schödel et al. 2002) and $4.0\pm0.6\times10^6\,\mathrm{M}_\odot$ (Ghez et al. 2003, see also Ghez et al. 2005 and Ghez et al. 2008) in the inner 0.0006 pc. Finally, the most recent estimate of the S2 orbit leads to $m_{\rm BH}=4.30\pm0.20_{\rm stat}\pm0.30_{\rm sys}\times10^6\,\mathrm{M}_\odot$ (where $m_{\rm BH}$ is the mass of the SMBH, Gillessen et al. 2009b). This value comes from a joint fit of New Technology Telescope (NTT), Very Large Telescope (VLT) and Keck astrometric data ranging from 1992 to 2003 (see Table 1 of Gillessen et al. 2009b). The largest source of uncertainty in this measurement is our distance from the GC ($=8.28\pm0.15_{\rm stat}+0.29_{\rm sys}$ km, Gillessen et al. 2009a; Gillessen et al. 2009b; see also Morris & Ghez 2012).

One of the open questions about the SMBH is its possible past activity. The strongest hint for a past activity is represented by fluorescent X-ray line emission (e.g. Sunyaev et al. 1993), especially the 6.4 keV Fe Kα line. This line is emitted by various molecular clouds in the GC (e.g. Ponti et al. 2010). The lines emitted from different clouds might be triggered by different sources (e.g. different X-ray binaries), but this possibility is not supported by observations of currently active X-ray sources. Thus, if the fluorescent X-ray line emission comes from a single source, such source must have been powerful enough: it might be the 'echo' of an energetic flaring event of Sgr A* that occurred several hundreds years ago, such as the tidal disruption of a star or of a smaller body (e.g. Koyama et al. 1996; Yu et al. 2011; see Morris & Ghez 2012 for a recent review on this and related topics).

Recently, Rea et al. (2013) reported the discovery of a young magnetar (SGR J1745$-$2900) at 2.4 ± 0.3 arcsec projected distance from SgrA*. The probability

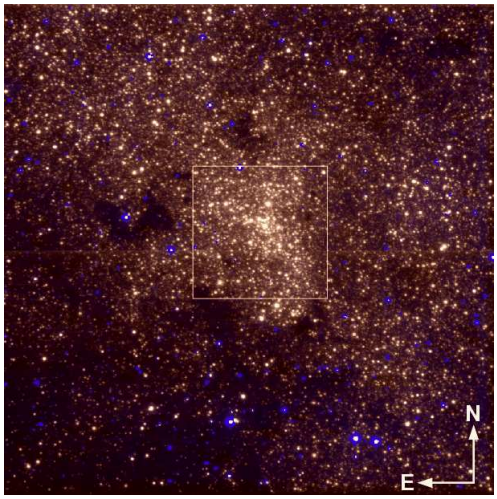

Fig. 1 Colour image composed of ISAAC imaging observations at 2.09 μm and in the J-band. The field-of-view is $150'' \times 150''$. The field of about $40'' \times 40''$ that was observed with adaptive-optics observations is marked by a square. The galactic plane runs approximately southwest-northeast across the image. From Fig. 1 of Schödel et al. (2007).

that the magnetar is a foreground or background object is very low ($\sim 10^{-6}$), while the probability that it is on a bound orbit around the SMBH is non-negligible. If SGR J1745−2900 is on a bound orbit, the fluorescent X-ray line emission in the GC might be easily explained by a past ($\sim$ 100 year ago) giant flare by the magnetar. This scenario is a non-unlikely alternative to a past flare by Sgr A*.

2.2 The stars: old stars, early-type stellar disc(s), and S-stars

2.2.1 The nuclear star cluster

The ensemble of the (both young and old) stars in the central few parsecs is often referred to as the nuclear star cluster (NSC) of the MW. NSCs are located at the photometric and dynamical centre of almost all spiral galaxies (e.g. Côté et al. 2006 and references therein), but the NSC of the MW is the only one where single stars can be resolved and their proper motions measured (Genzel et al. 2003; Schödel et al. 2007; Trippe et al. 2008; Schödel et al. 2009; Schödel et al. 2010). Eckart et al. (1993) and Genzel et al. (1996) derived number density counts from high-resolution NIR speckle imaging observations between 1 and 20 arcsec and found that the stellar density scales as $\rho \propto r^{-2}$ (isothermal profile). Some indication for a cusp (rather than a cored) central density was reported by Eckart et al. (1995) and by Alexander (1999).

Genzel et al. (2003) combined high-resolution stellar number counts from NACO[1] $H-$ and $K-$ band imaging data of the very central region ($0.1 - 10$ arcsec),

[1] The adaptive optics module NAOS and the NIR camera CONICA (abbreviated as NACO) are mounted at the ESO 8 m-class VLT unit telescope 4 on Cerro Paranal, Chile.

with lower resolution number counts from speckle imaging observations at $10 \leq R/\mathrm{arcsec} \leq 100$ (where R is the projected distance from Sgr A*). These data are best-fitted by a broken power-law

$$\rho_* = 1.2 \times 10^6 \mathrm{M}_\odot\,\mathrm{pc}^{-3} \left(\frac{R}{10\ \mathrm{arcsec}}\right)^{-\alpha}, \tag{1}$$

with $\alpha = 2.0 \pm 0.1$ ($\alpha = 1.4 \pm 0.1$) at $R \geq 10$ arcsec ($R < 10$ arcsec).

Schödel et al. (2007) confirm and refine this result, by means of an homogeneous sample of high-resolution data (using the NIR camera and spectrometer ISAAC at the ESO VLT UNIT telescope 4 on Paranal, see Fig. 1). They find a best-fitting power-law

$$\rho_* = 2.8 \pm 1.3 \times 10^6 \mathrm{M}_\odot\,\mathrm{pc}^{-3} \left(\frac{R}{6\ \mathrm{arcsec}}\right)^{-\alpha}, \tag{2}$$

with $\alpha = 1.75$ ($\alpha = 1.2$) at $R \geq 6$ arcsec ($R < 6$ arcsec). Thus, the updated break of the power law is $R_{\mathrm{break}} = 6 \pm 1$ arcsec$= 0.22 \pm 0.04$ pc. This implies that the NSC contains about twice the SMBH mass in < 2 pc (see Fig. 2). The main assumptions that have been done to obtain this result are (i) that the velocity dispersion is constant outside 0.22 pc; (ii) that the NSC is spherically symmetric, does not rotate and is isotropic; (iii) that the Bahcall & Tremaine (1981) mass estimator can be used in the case of NSC; (iv) that the mass-to-light ratio is 2 $\mathrm{M}_\odot/\mathrm{L}_\odot$ at 2μm (Haller et al. 1996), to estimate the unresolved stellar component.

Schödel et al. (2009) use multi-epoch adaptive-optics assisted NIR observations, obtained with NACO at VLT, to study the proper motions of > 6000 stars in the central parsec of the MW (with uncertainties < 25 km s^{-1}). They find that stellar velocities are purely Keplerian only in the inner $\lesssim 0.3$ pc, while the velocity dispersion is nearly constant at $r > 0.5$ pc (see Fig. 3). Furthermore, Schödel et al. (2009) suggest that the velocity dispersion is isotropic. This result has been recently revised by Chatzopoulos et al. (2014), who claim that there are significant differences between proper motion dispersions along different axes, due to a flattening of the NSC. In addition, the NSC is found to rotate parallel to Galactic rotation (Trippe et al. 2008; Schödel et al. 2009; Chatzopoulos et al. 2014).

The mass of the central SMBH is not sufficient to explain the observed proper motions. In particular, Schödel et al. (2009) model the mass distribution as

$$M(r) = m_{\mathrm{BH}} + 4\pi \int_0^r \mathrm{d}\tilde{r}\,\tilde{r}^2\,\rho(\tilde{r}), \tag{3}$$

where

$$\rho(r) = \rho_0 \left(\frac{r}{5\ \mathrm{pc}}\right)^{-\Gamma} \left(1 + \frac{r}{5\ \mathrm{pc}}\right)^{\Gamma-4} \tag{4}$$

and minimize the χ^2 of the proper-motion measurements with three free parameters: m_{BH}, Γ and $M_*(< 1\ \mathrm{pc})$ (where $M_*(< 1\ \mathrm{pc})$ is the mass of stars inside 1 pc). For $\Gamma \geq 0$ and $3.5 \lesssim m_{\mathrm{BH}}/(10^6\,\mathrm{M}_\odot) \lesssim 4.5$, $M_* > 0.4 \times 10^6\,\mathrm{M}_\odot$ (see Fig. 4). Similar results can be found assuming an anisotropic distribution of the velocity dispersion.

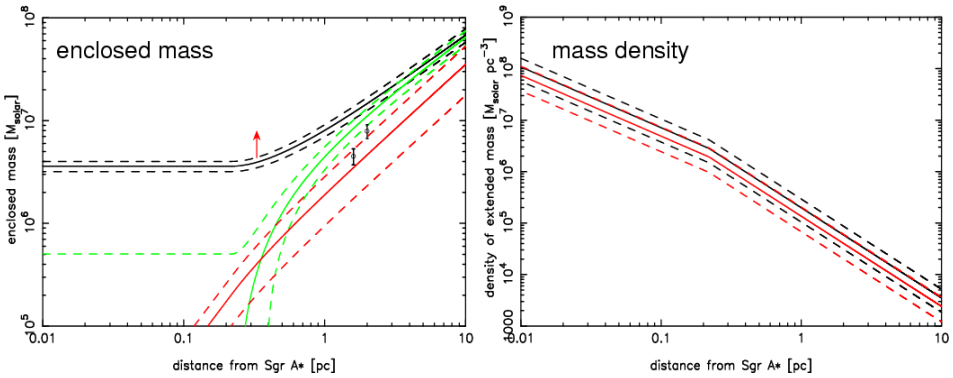

Fig. 2 Left-hand panel: estimate of the enclosed mass versus projected distance (black line), derived with the Bahcall-Tremaine (BT, Bahcall & Tremaine 1981) mass estimator, assuming a broken power-law structure of the stellar cluster and a constant line-of-sight velocity dispersion outside of the break radius (see text for details). The up-pointing red arrow is the enclosed mass estimate based on the bright star IRS 9 (Reid et al. 2007). The circle at 1.6 pc is the mass estimate based on the assumption that the circumnuclear ring (CNR) is a rotating ring with a rotation velocity of 110 km s^{-1} and a radius of 1.6 pc (Christopher et al. 2005). The circle at 2.0 pc is the mass estimate based on the assumption that the CNR is a rotating ring with a rotation velocity of 130 km s^{-1} and a radius of 2.0 pc (Rieke & Rieke 1988; Guesten et al. 1987). Green line: enclosed mass after subtraction of the SMBH mass, derived from the BT mass estimator (black). Red line: estimated mass of the visible stellar cluster. The dashed lines indicate the 1σ uncertainties. Right-hand panel: density of the enclosed mass, after subtraction of the SMBH mass (black). The red line indicates the mass density of the stellar cluster. The dashed lines indicate the 1σ uncertainties. From Fig. 19 of Schödel et al. (2007).

This result strengthens the evidence for a massive NSC. We notice that the best-fitting value for the mass of the SMBH ($m_{\rm BH} = 3.6^{+0.2}_{-0.4} \times 10^6 {\rm M}_\odot$, at 68% confidence level) is smaller than the one derived from the orbits of the S-stars (Gillessen et al. 2009a), although the former is marginally consistent with the latter. Furthermore, even values of $\Gamma < 0$ (i.e. 'centrally evacuated' mass models) are allowed by the fit shown in Fig. 4.

Recently, Chatzopoulos et al. (2014) did a similar analysis using 2500 line-of-sight velocities and 10000 proper motions obtained with VLT instruments, and 200 maser velocities (see Fritz et al. 2014 for a description of the data sample). Using axisymmetric Jeans modeling to fit the proper motion and line-of-sight velocity dispersions, Chatzopoulos et al. (2014) obtain new best estimates for the NSC mass, black hole mass, and distance $M_*(r < 100'') = (9.26 \pm 0.31|_{\rm stat} \pm 0.9|_{\rm syst}) \times 10^6 {\rm M}_\odot$, $m_{\rm BH} = (3.88 \pm 0.14|_{\rm stat} \pm 0.4|_{\rm syst}) \times 10^6 {\rm M}_\odot$, and $R_0 = 8.30 \pm 0.09|_{\rm stat} \pm 0.1|_{\rm syst}$ kpc, respectively.

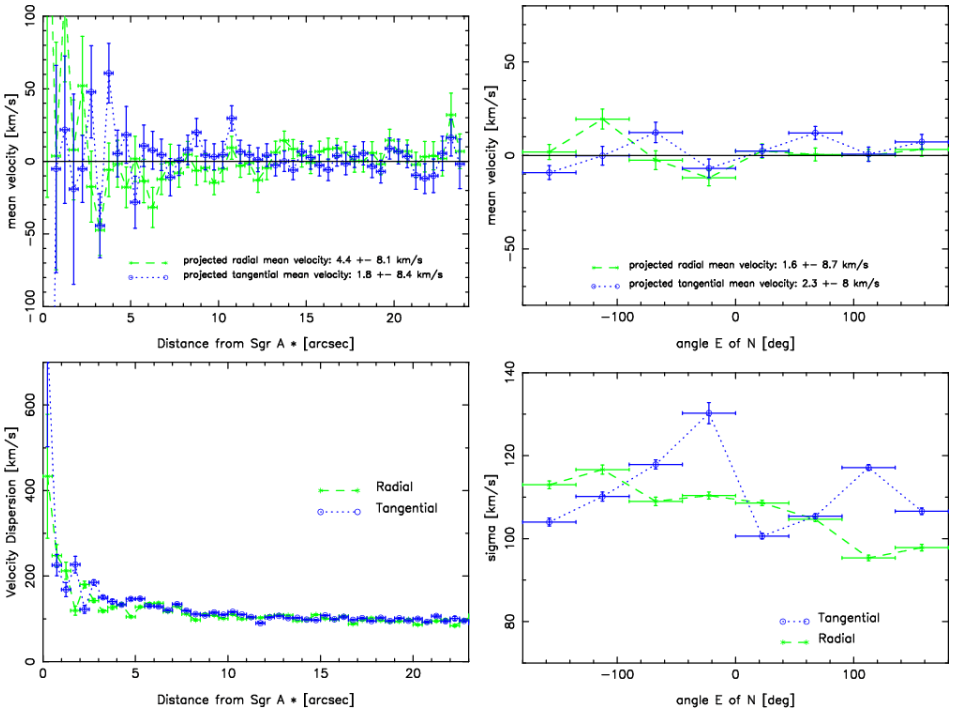

Fig. 3 Top: mean projected radial and tangential velocities versus projected distance from Sgr A* (left) and versus angle east of north (right). Bottom: projected radial (green) and tangential (blue) velocity dispersions in the GC NSC versus projected distance from Sgr A* (left) and versus angle east of north (right). From Fig. 6 of Schödel et al. (2009).

2.2.2 The disc(s) of early-type stars

The presence of young massive stars in the central parsec of the MW has been discussed for a long time (Lacy et al. 1982; Allen 1987; Rieke & Rieke 1989; Allen et al. 1990; see Morris & Serabyn 1996 for a review). So far, more than a hundred young massive stars have been observed in the vicinity of Sgr A* (Krabbe et al. 1991; Morris 1993; Genzel et al. 1994; Blum et al. 1995a; Blum et al. 1995b; Eckart et al. 1995;Krabbe et al. 1995;Libonate et al. 1995; Tamblyn et al. 1996; Genzel et al. 2003; Paumard et al. 2006; Bartko et al. 2009, see Fig. 5). Many of them are O-type and Wolf-Rayet (WR) stars. Radial velocity and spectral type of these stars have been thoroughly investigated thanks to spectroscopy, while proper motions and brightness have been provided by photometry. The most recent spectroscopic data include observations with the integral field spectrograph SINFONI (Bartko et al. 2009 and references therein) at the ESO/VLT, and with the OH-Suppressing Infrared Imaging Spectrograph (OSIRIS) at the Keck II telescope (Do et al. 2013). The most recent photometric data include observations with NACO at the ESO/VLT (Trippe

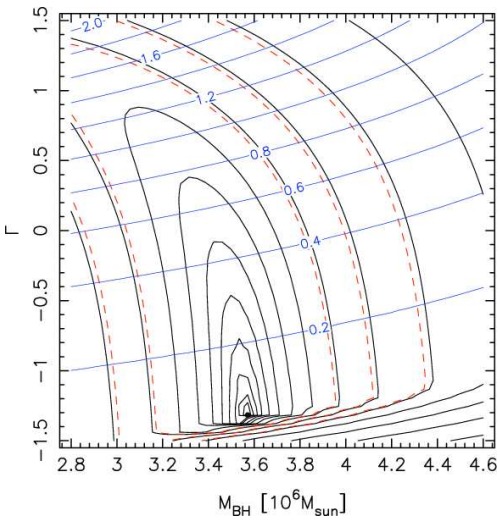

Fig. 4 Results of isotropic modelling of the NSC. The three free parameters ($m_{\rm BH}, M_\star(r<1\,{\rm pc}), \Gamma$) were varied in comparing the fit of the model to the velocity dispersion data. Black thick curves are contours of constant χ^2, separated by a constant factor of 100.3; dashed red curves indicate (68%, 90% and 99%) confidence intervals. Blue thin curves are contours of the best-fit value of $M_\star(r<1\,{\rm pc})$ at each value of ($m_{\rm BH}, \Gamma$); these curves are labelled by $M_\star/10^6\,{\rm M}_\odot$. The overall best-fit model is indicated by the filled circle. From Fig. 14 of Schödel et al. (2009).

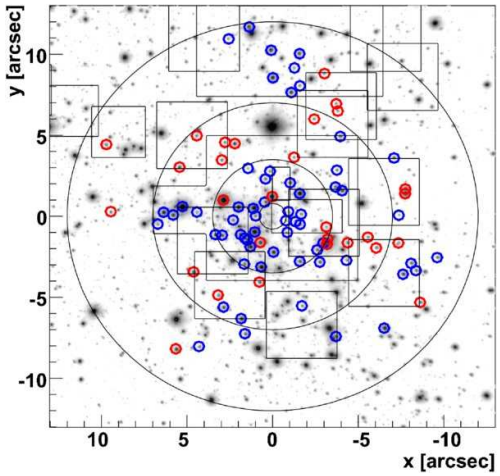

Fig. 5 Sample of 90 WR/O stars ($m_{\rm K}<14$ and $\Delta(v_{\rm z})\leq 100$ km s^{-1}) in the central 0.5 pc of our Galaxy: blue circles indicate CW orbits (61 WR/O stars) and red circles indicate counterclockwise orbits (29 WR/O stars). The black circles show projected distances of 0.”8, 3.”5, 7”, and 12” from Sgr A*. Squares indicate the exposed fields with SINFONI in the 25 mas pixel^{-1} and 100 mas pixel^{-1} scale. The whole inner 0.5 pc region is contained in lower resolution (250 mas pixel^{-1} scale) SINFONI observations (Paumard et al. 2006). From Fig. 1 of Bartko et al. 2009.

et al. 2008; Bartko et al. 2009) and with NIRC2 at the Keck II telescope (Do et al. 2013).

The analysis of orbital angular momentum directions shows that some of the early-type stars lie in a disc (Paumard et al. 2006; Bartko et al. 2009; Lu et al. 2009; Yelda et al. 2012; Do et al. 2013; Lu et al. 2013). This disc is called clockwise (CW) disc, because it shows CW motion when projected on the plane of the sky (Genzel et al. 2003; Paumard et al. 2006). The fraction of early-type stars that actually belong to the CW disc is still debated: the recent study by Yelda et al. (2014) indicates that

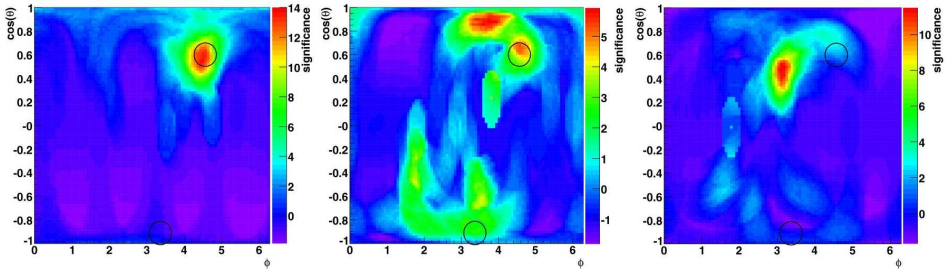

Fig. 6 Cylindrical equal area projections of the distributions of significance in the sky for three radial bins: 32 WR/O stars with projected distances in the bin 0.”8−3.”5 (left-hand panel), 30 WR/O stars in the bin 3.”5 − 7” (central panel), and 28 WR/O stars in the bin 7”−12” (right-hand panel). The position of the CW disc and of the (possible) counterclockwise disc as derived by Paumard et al. (2006) are marked with black circles. In the inner bin there is a maximum excess significance of 13.9 σ at $(\phi, \theta) = (256^\circ, 54^\circ)$, compatible with the CW system of Paumard et al. (2006). The significance map in the middle interval shows two extended excesses, one for CW and one for counterclockwise orbits. The CW excess has a local maximum significance of 5.4 σ at $(\phi, \theta) = (262^\circ, 48^\circ)$, compatible with the orientation of the CW system of Paumard et al. (2006), but a global maximum significance of 5.9 σ at a clearly offset position: $(\phi, \theta) = (215^\circ, 28^\circ)$. The significance map in the outer bin shows a maximum excess significance of 11.5 σ at yet another position $(\phi, \theta) = (179^\circ, 62^\circ)$. The morphology of the excesses in the CW system may indicate a smooth transition of the excess centre with projected radius. From Fig. 11 of Bartko et al. (2009).

only $\sim$ 20 per cent of early-type stars lie in the CW disc, while previous studies (e.g. Do et al. 2013; Lu et al. 2013) suggest a higher fraction ($\sim$ 50 per cent).

Bartko et al. (2009) compute significance maps from the sky maps of the density of reconstructed angular momentum directions of the observed stars ($\rho_{\rm obs}$), by defining the significance for each bin of the sky map as

$$\text{significance} = \frac{\rho_{\rm obs} - \langle \rho_{\rm iso} \rangle}{\rho_{\rm iso,\,rms}}, \tag{5}$$

where $\langle \rho_{\rm iso} \rangle$ and $\rho_{\rm iso,\,rms}$ are the mean density and the root mean square density (of angular momentum directions) for a set of simulated stars following an isotropic distribution, respectively.

From left to right, the three panels of Fig. 6 show the significance maps (derived as described above) for stars with distance 0.”8−3.”5, 3.”5 − 7” and 7”−12” (i.e. 0.032−0.14 pc, 0.14−0.28 pc and 0.28−0.48 pc) from Sgr A*. We recall that a razor-thin disc is expected to define an infinitely small circle in these maps. It is apparent that only the stars in the bin closest to Sgr A* define a unique disc, consistent with the CW disc. In the intermediate bin, various features are present. One of these features is still consistent with the CW disc, while the other features may be interpreted as a second dismembered disc or as outliers of the CW disc. A relevant portion of these ‘outliers’ shows counterclockwise motion, which has been claimed to indicate the presence of a second dissolving disc (Lu et al. 2006, Lu et al. 2009;

Bartko et al. 2009). Finally, the stars in the outer bin mostly belong to a single disc, but offset with respect to the inner bin.

The results shown in Fig. 6 have the following crucial implications.

(i) Only a fraction of the early-type stars in the central parsec are members of the CW disc.
(ii) The probability for an early-type star to be member of the CW disc decreases with increasing distance from the centre.
(iii) The CW disc is likely warped and/or tilted, as the orientation of its normal vector changes by several degrees ($\sim 60^\circ$, Bartko et al. 2009) from its inner to its outer edge.

Recently, Yelda et al. (2014) consider a sample of 116 stars, for which they measure both proper motions and, in a few cases, accelerations. Yelda et al. (2014) compute significance maps from the sky maps of the density of reconstructed angular momentum directions, using a formula very similar to Eq. 5 (Yelda et al. 2014 normalize the significance to the standard deviation rather than to the root mean square density). Similarly to Bartko et al. (2009), they group the stars into three radial bins: 0".8–3".2, 3".2–6".5 and 6".5–13".3 (i.e. 0.032–0.128 pc, 0.128–0.26 pc and 0.26–0.532 pc). Fig. 7 shows the resulting density of normal vectors for the three bins. The main results are:

(i) there are no statistically significant signatures of a counterclockwise disc. It seems that the two discs scenario is definitely dead.
(ii) The existence of a CW disc is confirmed with high significance in the inner bin, but there is no clear evidence that the CW disc extends to the two outermost radial bins. Thus, the outer radius of the CW disc might be as small as ~ 0.13 pc (rather than ~ 0.5 pc, as discussed by Bartko et al. 2009).
(iii) Since the CW disc extends only to ~ 0.13 pc, it is neither significantly warped nor tilted.

The results by Yelda et al. (2014), if confirmed, will significantly change our previous picture of the early-type stars in the GC.

Furthermore, Yelda et al. (2014) measure the orbital eccentricity of stars in their sample (Fig. 8). They confirm that the peak of the eccentricity distribution is at $e \sim 0.2-0.4$ and the distribution of eccentricities is quite broad, as found in previous studies (Bartko et al. 2009; Lu et al. 2009; Yelda et al. 2012; Do et al. 2013; Lu et al. 2013). On the other hand, Yelda et al. (2014) show that the distribution of eccentricities is much narrower if only stars with detected acceleration are considered (Fig. 8). In particular, the resulting average eccentricity is $\langle e \rangle = 0.27 \pm 0.07$ and the high-eccentricity tail disappears.

The most recent estimate of the age of the early-type stars is $t_{\rm age} \approx 2.5-6$ Myr (Lu et al. 2013). This result comes from integral-field spectroscopy (using the OSIRIS spectrometer on Keck II), with a completeness of 50% down to magnitude *K'=15.5* (i.e. stellar mass $\sim 10\,{\rm M}_\odot$), combined with photometry using the NIRC2 instrument on Keck II (Do et al. 2013). The analysis of the data is based on Bayesian inference methods (Lu et al. 2013, see Fig. 9). A previous estimate

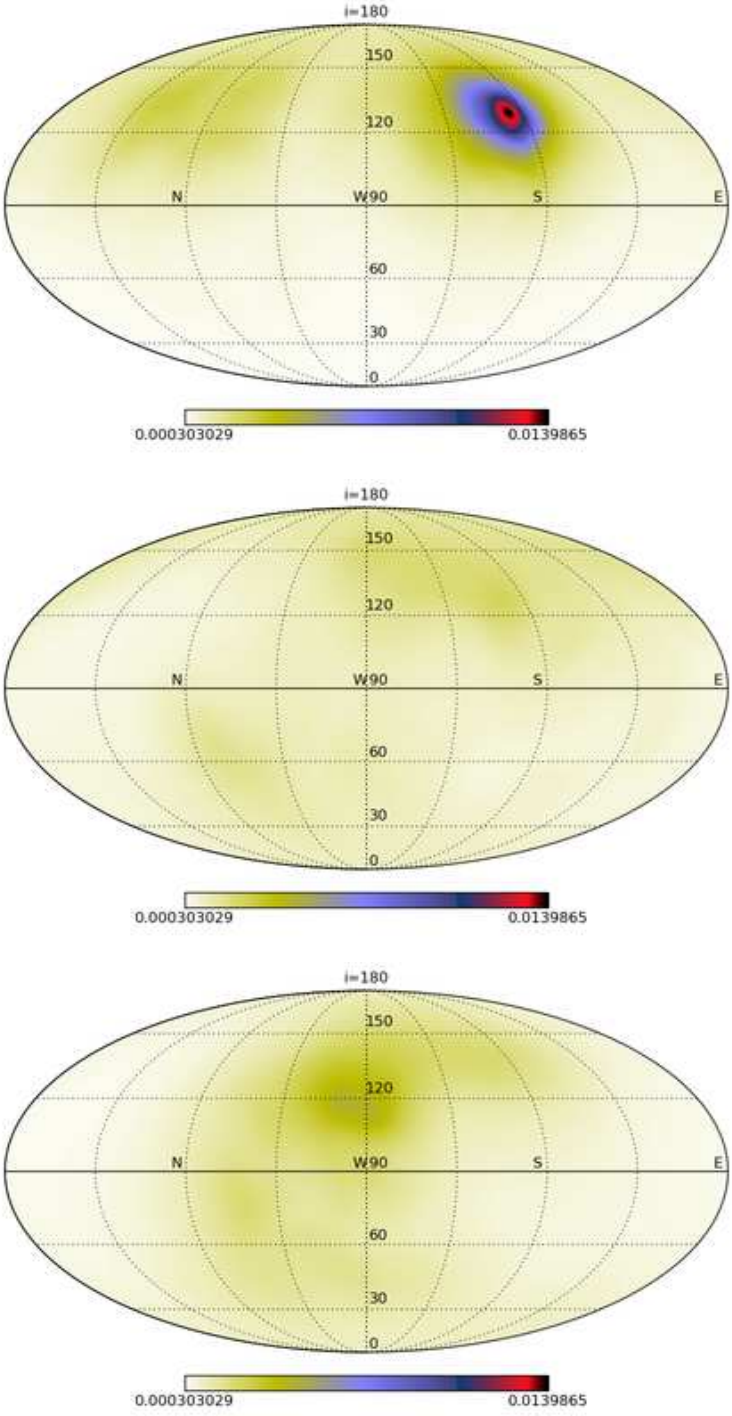

Fig. 7 Density of normal vectors for stars in the three separate radial bins: 0."8-3."2 (*top*), 3."2-6."5 (*middle*), and 6."5-13."3 (*bottom*). The CW disc feature at (i, Ω) = (130°, 96°) is prominent in the inner radial bin and shows a decrease in density with radius. The degenerate orbital solutions associated with the CW disc stars are seen as the slight density enhancement near (i, Ω) $\sim$ (130°, 300°) in the top panel. The middle radial interval shows hints of the CW disc and extended structure around this location. In the outermost radial bin, a density enhancement is seen at (i, Ω) = (117°, 192°). The same scaling is used in each plot to show the relative strength of the features. The horizontal lines represent i and are spaced 30° apart and the longitudinal lines represent Ω and are spaced 45° apart, with the line marked E representing Ω = 0°. Fig. 14 of Yelda et al. (2014).

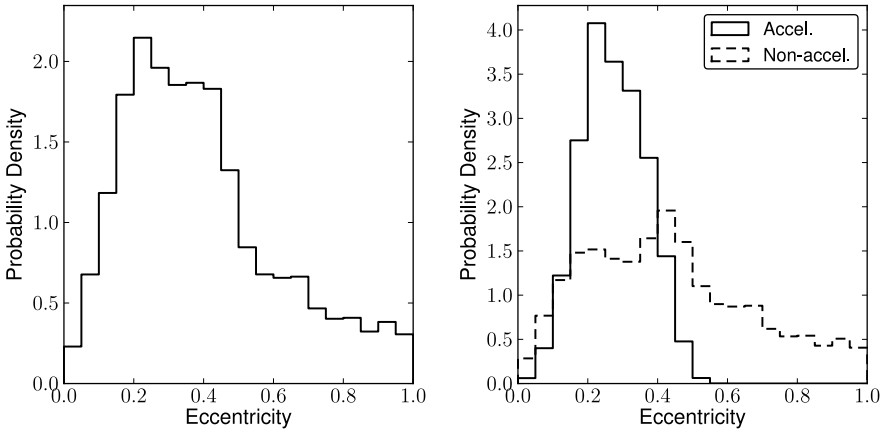

Fig. 8 *Left:* Eccentricity distribution of the CW disc. All orbital solutions falling within 15.2° of the disc are included, thereby weighting the distributions by disc membership probability. *Right:* Eccentricity distributions shown separately for likely disc members with acceleration detections (*solid*) and without (*dashed*). From Fig. 12 of Yelda et al. (2014).

indicated $t_{\rm age} = 6 \pm 2$ Myr (Paumard et al. 2006). Furthermore, Yusef-Zadeh et al. (2013) have found possible indications of gas outflows, suggesting recent star formation (10^{4-5} yr) within 0.6 pc of SgrA*.

The MF of the early-type stars has been claimed to be very top-heavy for a long time. Paumard et al. (2006) suggest an MF similar to $\mathrm{d}N/\mathrm{d}m \sim m^{-\alpha}$, with $\alpha = 0.85$ (we recall that the Salpeter MF has $\alpha = 2.35$, Salpeter 1955) and a total mass $\sim 10^4\,\mathrm{M}_\odot$. The result of Paumard et al. (2006) was obtained from the luminosity function of the most massive WR and O-type stars and suffered from lack of sensitivity for magnitude $K > 13$ (i.e. stellar mass $< 20\,\mathrm{M}_\odot$). Bartko et al. (2010) find an even flatter mass-function, with best-fitting slope $\alpha = 0.45 \pm 0.3$.

Recently, Lu et al. (2013) use the same data and the same Bayesian approach as in Do et al. (2013). They derive a new best-fitting slope $\alpha = 1.7 \pm 0.2$ (see Fig. 9), still flatter than a Salpeter MF, but considerably steeper than previous estimates. Consequently, the total mass of the early-type stars is also revised, suggesting a value in the $1.4 - 3.7 \times 10^4\,\mathrm{M}_\odot$ range (extrapolated down to stars with mass $1\,\mathrm{M}_\odot$).

Finally, by means of stellar evolution models, Löckmann et al. (2010) showed that the total observed luminosity in the central parsec of the NSC is better matched by a continuous star formation over the Galaxy's lifetime, following a Kroupa (2001) MF, than by a long-standing top-heavy MF. This suggests that, if the early-type stars follow a top-heavier MF than the rest of the NSC, the circumstances that led to the formation of the early-type stars must be very peculiar, since these have not affected most of the NSC.

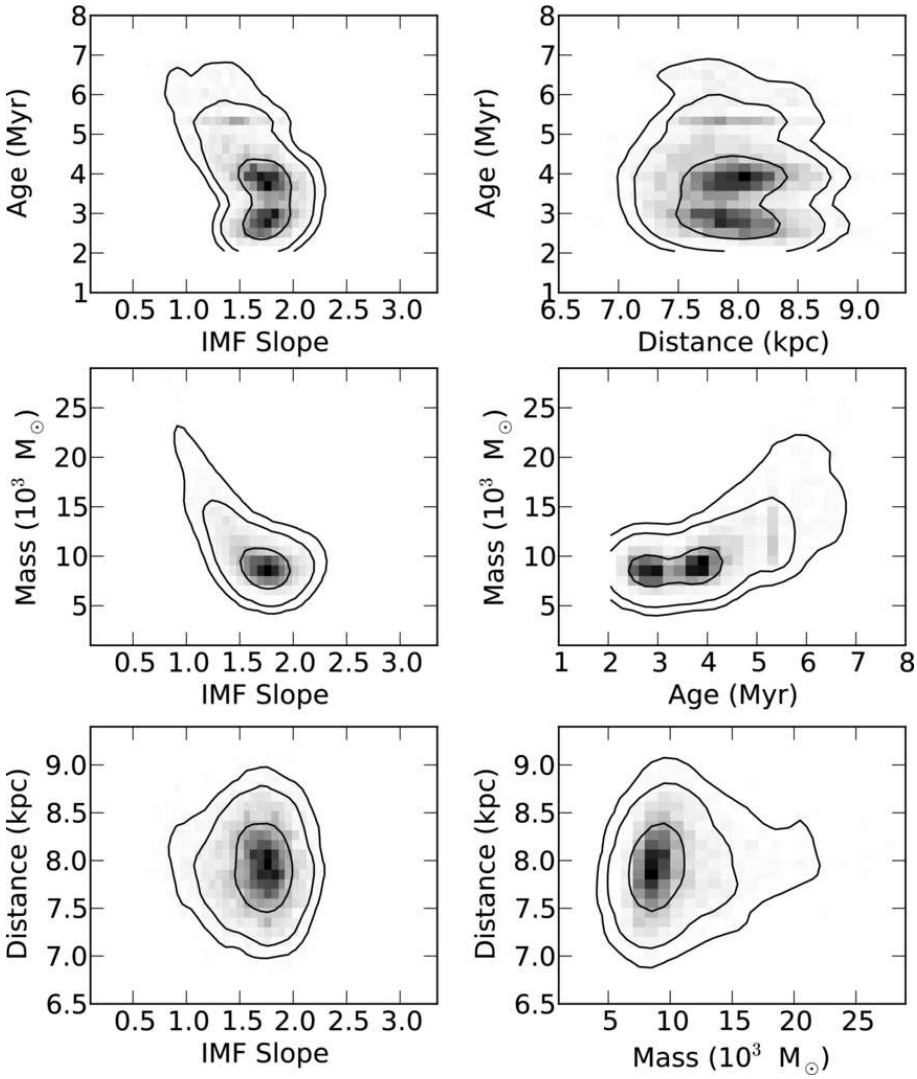

Fig. 9 Two-dimensional posterior probability distribution functions (PDFs) for the observed properties of the early-type stars (from Lu et al. 2013). The over-plotted contours give 68%, 95%, and 99% confidence intervals. Weak correlations exist between age, mass, and initial MF (IMF) slope. The correlation between the total mass and the age or IMF slope is a consequence of the age−IMF slope relationship since, at older ages, the most massive stars have disappeared and the total mass must increase to match the observed numbers of stars brighter than $K_{\rm P} = 15.5$. From Fig. 10 of Lu et al. (2013).

The existence of very young (a few Myr old) stars in the inner parsec has been an enigma for a long time. The observed MF (flatter than the Salpeter MF) and the orbits of these early-type stars (belonging to one or two discs plus a number of

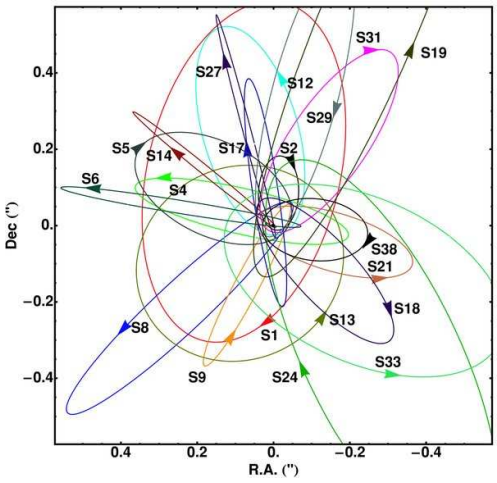

Fig. 10 Stellar orbits of the stars in the central arcsecond for which Gillessen et al. (2009a) determined the orbits. The coordinate system was chosen such that Sgr A* is at rest. From Fig. 16 of Gillessen et al. (2009a).

possible outliers) open several additional questions. The new results by Yelda et al. (2014), which indicate that only 20 per cent of the early-type stars are members of the CW disc (see also Sanchez-Bermudez et al. 2014) and that the CW disc may be much smaller than previously thought, open further issues.

The early-type stars that cannot be considered members of the CW disc, because of the different angular momentum direction (in some cases, they are even counterclockwise), might be either genuine outliers (i.e. stars that were born outside the CW disc) or former members of the CW disc or even members of other (partially dismembered) discs. The existence of other stellar discs (in addition to the CW disc) is still an open question. The mechanisms that can either dismember a disc or perturb the orbits of some of its members are even more debated. In the next sections (Sect. 3 and 4), we will review which theoretical scenarios have been proposed to explain these open questions.

2.2.3 The S-stars

The few stars whose orbits are (totally or partially) inside the innermost arcsecond (~ 0.04 pc) are referred to as the S-star cluster (Schödel et al. 2003; Ghez et al. 2003, Ghez et al. 2005; Eisenhauer et al. 2005; Gillessen et al. 2009a). The orbits of $\sim 25-30$ S-stars are known with accuracy, by means of NIR imaging and spectroscopy. In particular, the motion of the S-stars has been tracked since 1992 at NTT and VLT, and since 1995 at Keck. Most of the S-stars have been classified as B0 – 9 V stars, with ages between 6 and 400 Myr (Eisenhauer et al. 2005). Gillessen et al. (2009a) recently derived the orbital solutions of 28 S-stars: 22 early-type stars and 6 late-type S-stars (S17, S21, S24, S27, S38 and S111). These are the first late-type S-stars with measured orbits. Thus, most of the S-stars (but not all of them) are early-type stars.

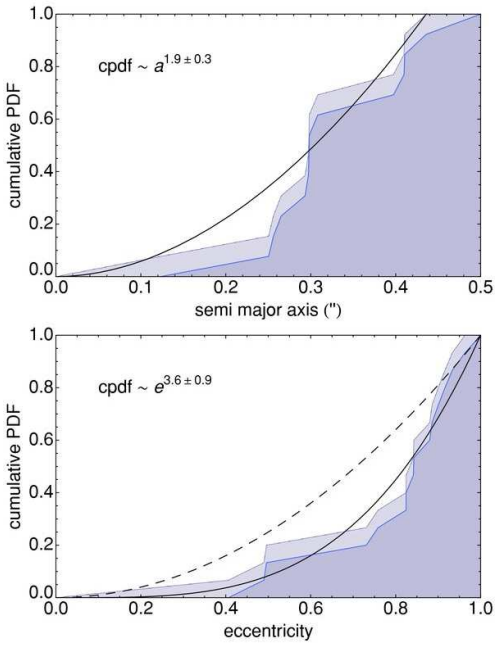

Fig. 11 Top: Cumulative PDF for the semi-major axis of the early-type stars with $a < 0.''5$. The two curves correspond to the two ways to plot a cumulative PDF, with values ranging either from 0 to $(N-1)/N$ or from $1/N$ to 1. Solid line: best fit ($n(a) \sim a^{0.9\pm0.3}$). Bottom: Cumulative PDF for the eccentricities of the early-type stars that are not identified as disc members. As in the top panel, the two curves correspond to the two ways to plot a cumulative PDF. Dashed line: $n(e) \sim e$; Solid line: best fit ($n(e) \sim e^{2.6\pm0.9}$). From Figs. 20 and 21 of Gillessen et al. (2009a).

Six of the 28 S-stars studied by Gillessen et al. (2009a) appear to be members of the CW disc: they have semi-major axis $\approx 1''$, eccentricity $e \approx 0.2-0.4$ and angular distance to the CW disc between 9° and 21°. The orbits of the 22 remaining S-stars do not lie in a disc: they are consistent with a random distribution in space (see Fig. 10).

The distribution of semi-major axes of the 22 'true' S-stars (see Fig. 11) is best-fit (using a log-likelihood fit) by $n(a) \sim a^{0.9\pm0.3}$ (Gillessen et al. 2009a), corresponding to a number density $n(r) \sim r^{-1.1\pm0.3}$, consistent with the mass profile (Genzel et al. 2003; Schödel et al. 2007).

The distribution of eccentricities of the 22 'true' S-stars (see Fig. 11) is best-fit (using a log-likelihood fit) by $n(e) \sim e^{2.6\pm0.9}$ (Gillessen et al. 2009a). This means that the eccentricities of S-stars are much larger than those of the CW disc. The best-fit distribution is somewhat skewed toward larger eccentricity with respect to the thermal distribution ($n(e) \sim e$), typical of two-body relaxed systems.

Among the S-stars, the S2 star is particularly important because so far it has provided the strongest constraints on the SMBH mass (e.g. Ghez et al. 2008; Gillessen et al. 2009a; Gillessen et al. 2009b). S2 has been classified as a B0-2.5 V main sequence star with an estimated zero-age main sequence mass of $19.5\,M_\odot$ (Martins et al. 2008). It is bright ($K \approx 14$) and has a very short orbital period (15.9 years). Astrometric data taken from 1992 to 2003 (see Sect. 2.1) allowed to track one entire orbit. Unfortunately, during pericentre passage (2002) S2 showed a puzzling photometry, which might be due to confusion with a fainter star (see Gillessen et al. 2009a for this issue). For sake of curiosity, S2 is not the shortest-known-period star orbiting

the SMBH: S102 has a period of only 11.5 years (Meyer et al. 2012). Astrometric data (NIRC on Keck) covered one entire orbit of S102. On the other hand, S102 is a factor of 16 fainter than S2.

The S-star cluster is one of the most enigmatic components of the GC: most of the S-stars are early-type stars and cannot have formed *in situ*, with a pericentre so close to the SMBH (this is the so called 'paradox of youth', Ghez et al. 2003). Furthermore, their eccentricities are very high, but these stars are too young to have undergone two-body relaxation. They have different orbital properties with respect to the early-type stars in the CW disc, because of the larger eccentricities and because of the random orientation of their orbital planes. Does this necessarily mean that the S-stars are a different population with respect to the CW disc? If they are a different population, where do they come from? Alternatively, is there any perturbation which can affect the stars in the CW disc and change their orbital properties till they match those of the S-stars? These questions and the main scenarios for the formation of S-stars will be discussed in Sect. 3 and 4.

2.3 The molecular gas and the ionized gas

The GC is a very crowded environment not only from the point of view of the stellar population, but also for the gas. The central ~ 20 parsecs of the MW are rich in molecular, atomic and ionized gas, which form very peculiar structures.

The main reservoirs of ionized gas are Sgr A East and Sgr A West (Novak et al. 2000; Zhao et al. 2009), both observed in radio and both overlapped with Sgr A* (see the schematic illustration in Fig. 12). Sgr A East is a non-thermal elliptical shell source elongated along the Galactic plane with a major axis of length ~ 10 pc (Downes & Martin 1971; Yusef-Zadeh & Morris 1987; Novak et al. 2000). Its centre is displaced by 2.5 pc (in projection) with respect to Sgr A*. Sgr A East is generally thought to be a supernova remnant.

Sgr A West is a spiral-shaped thermal radio source (Ekers et al. 1983; Scoville et al. 2003), which surrounds Sgr A*. For its shape, Sgr A West is often called the 'minispiral'. The three main arms of the minispiral are called the 'Northern Arm' (pointing towards North), the 'Eastern Arm' (pointing towards East) and the 'Western Arc' (pointing towards West). The nature of the minispiral is very debated. According to a popular scenario, the minispiral arms might be streams associated with molecular gas falling in towards the centre (Lo & Claussen 1983; Zhao et al. 2009; Zhao et al. 2010).

A clumpy, inhomogeneous and kinematically disturbed ring of molecular gas, known as the circumnuclear ring (CNR) or the circumnuclear disc (CND), surrounds the minispiral (Fig. 13). The CNR was discovered about 30 years ago (Becklin et al. 1982) via detection of double-lobed emission at 50 and 100 μm, from dust. After the discovery, the CNR has been observed extensively at radio to infrared wavelengths (e.g. Gatley et al. 1986; Serabyn et al. 1986; Guesten et al. 1987; Zylka & Mezger 1988; Depoyy et al. 1989; Sutton et al. 1990; Jackson et al. 1993; Marr et al. 1993;

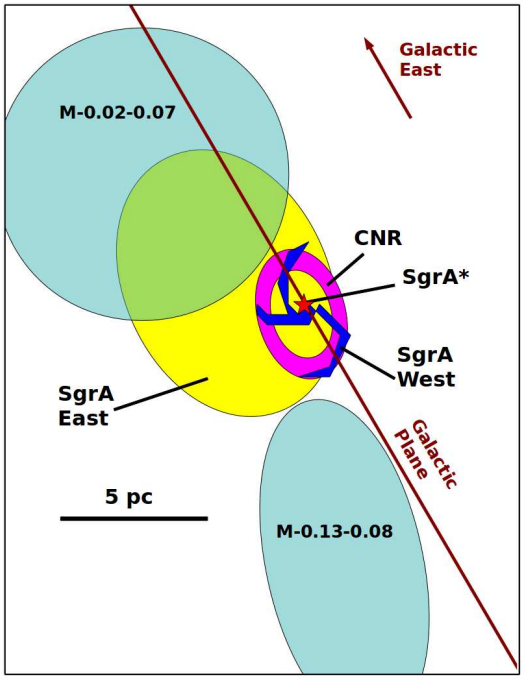

Fig. 12 Schematic diagram showing the sky locations and rough sizes and shapes of GC sources discussed in Sect. 2.3. Red star: Sgr A*; magenta ring: CNR; blue spiral: the minispiral (i.e. Sgr A West); yellow ellipse: Sgr A East; the two turquoise ellipses: the M–0.02–0.07 and the M–0.13–0.08 cloud. A solid red line indicating the orientation of the Galactic plane has been drawn through the position of Sgr A*. The Galactic eastern direction is indicated. One arcminute corresponds to about 2.3 pc at the distance of 8 kpc. This diagram has been inspired by Fig. 1 of Novak et al. (2000).

Telesco et al. 1996; Chan et al. 1997; Coil & Ho 1999; Coil & Ho 2000; Wright et al. 2001; Vollmer & Duschl 2001; Yusef-Zadeh et al. 2004; Christopher et al. 2005; Donovan et al. 2006; Montero-Castaño et al. 2009; Oka et al. 2011; Martín et al. 2012; Mills et al. 2013).

The observations indicate that the CNR is a ring of molecular gas and dust with an inclination of $\sim 50-70^{\circ}$ with respect to the observer. The ring is nearly complete in HCN (Fig. 13), but with a large gap in the north (corresponding to the position of the Northern Arm of the minispiral) and other smaller gaps. The inner radius of the ring is ~ 1.5 pc (de-projected) and it is quite sharp, while the outer radius is less defined: HCN, CO and HCO^+ were observed out to ~ 7 pc, but recent studies (e.g. Wright et al. 2001) suggest an outer edge at $3-4$ pc. The CNR has a thickness of ~ 0.4 pc at the inner edge (Jackson et al. 1993) and expands to ~ 2 pc in the outer parts (Vollmer & Duschl 2001). The total mass of the CNR is highly uncertain. Measurements based on the dust thermal emission indicate a total mass of $\sim 2 \times 10^4$ $M_{\odot}$ (Mezger et al. 1989; Liu et al. 2013, but see Christopher et al. 2005 for a different estimate).

The CNR rotates with a velocity ~ 110 km s^{-1} (Marr et al. 1993; Christopher et al. 2005), but the velocity field shows local perturbations, which may indicate a warp or the presence of different streamers. This is the reason why previous studies proposed that the CNR formed through the collision of two molecular clouds

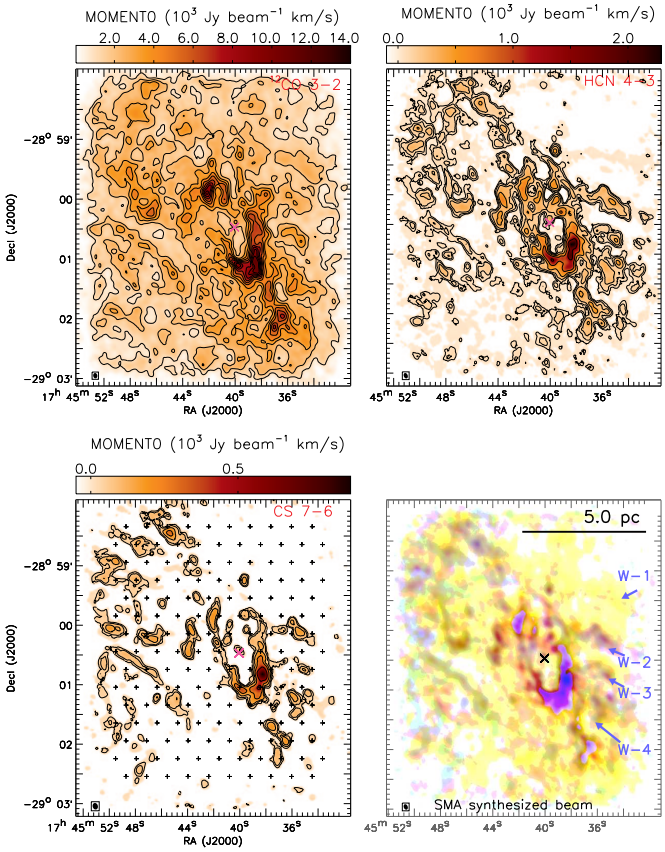

Fig. 13 Velocity integrated (i.e., moment 0) images of the ^{12}CO 3–2, HCN 4–3, and CS 7–6 transitions in the region of the CNR. The synthesized beam of the Submillimeter Array (SMA) observations is shown in the bottom right. The contours of the ^{12}CO 3–2 image start at the value 1000 Jy beam^{-1}km s^{-1}, and are drawn at intervals of 1000 Jy beam^{-1}km s^{-1}. The contours of the HCN 4–3 and CS 7–6 images are 50 Jy beam^{-1}km s^{-1}×[1, 2, 4, 8, 16, 32] and 30 Jy beam^{-1}km s^{-1}×[1, 2, 4, 8, 16], respectively. Integration of the signal over a 20 km s^{-1} velocity range has an rms noise level of 5.8 Jy beam^{-1}km s^{-1} (2.2 K km s^{-1}). The bottom right panel shows an overlay of these lines, in yellow (^{12}CO 3–2), magenta (HCN 4–3) and cyan (CS 7–6) colors. W-1, W-2, W-3 and W-4 in the bottom right panel indicate the four western streamers of the CNR. Crosses in the CS image mark the pointing centers of the SMA mosaic observations. From Fig. 6 of Liu et al. (2012).

(e.g. Guesten et al. 1987) or through the assembly of multiple dynamically different streamers (e.g. Jackson et al. 1993).

Recently, Liu et al. (2012) made wide-field images ($\sim 5''$ resolution) of three high-excitation molecular gas tracers (^{12} CO3–2, HCN 4–3, CS7–6) in the region of the CNR ($\sim 5' \times 5'$ field-of-view), using the Submillimeter Array (SMA). They

also made a 20" resolution CS 1–0 image using the National Radio Astronomy Observatory (NRAO) Green Bank Telescope. The high-excitation lines observed with the SMA trace the dense and warm gas ($> 10^5$ cm^{-3}, > 30 K), while the CS 1–0 traces the less dense and cooler gas ($\sim 5 \times 10^4$ cm^{-3}, < 10 K). Liu et al. (2012) find that several $\sim 5-20$ pc-scale gas streamers either directly connect to the CNR or penetrate inside it (see[2] Fig. 13). Thus, the CNR appears to be the centre of an inflow, quite reminiscent of the molecular gas streaming in the nucleus of NGC 1068 (Müller Sánchez et al. 2009). Liu et al. (2012) speculate that the CNR may be dynamically evolving, continuously fed via gas streamers and in turn feeding gas toward the centre.

The observations also indicate an ongoing interaction between the CNR and the minispiral (Christopher et al. 2005). The strongest interactions likely occur along the Western Arc and the Northern Arm of the minispiral. The ionized gas in the Western Arc is oriented along the CNR and it is immediately interior to the CNR. For this reason, the Western Arc has been proposed to be the inner edge of the CNR, ionized by the central stellar cluster. This idea is confirmed by the velocity field (Christopher et al. 2005). Furthermore, the minispiral Northern Arm may connect with the northeastern extension of the CNR to form a single collimated structure (Christopher et al. 2005).

Christopher et al. (2005) identify 26 resolved molecular gas cores within the CNR. These have a characteristic diameter of ~ 0.25 pc, a typical density of a few $\times 10^7$ cm^{-3} and a typical mass of a few $\times 10^4$ M$_\odot$. The density of the molecular cores is sufficient to prevent tidal disruption at $\sim 1-2$ pc distance from Sgr A*, indicating that the CNR may be a long-lived structure and may be able to form stars. In fact, recent observations with the Green Bank Telescope detect maser lines and both narrow (0.35 km s^{-1}) and broad ($30-50$ km s^{-1}) methanol emission from the CNR (Yusef-Zadeh et al. 2008). This has been interpreted as a signature of massive star formation in its early phases. In the following sections (Sect. 3 and 4), we will see that the CNR may have a crucial role for the formation and for the secular evolution of the young stars in the GC.

Furthermore, several hundreds solar masses of atomic gas (> 300 M$_\odot$) might exist inside the CNR (Jackson et al. 1993; Goicoechea et al. 2013).

Finally, a number of giant molecular clouds are close to the GC (Whiteoak et al. 1974; Guesten & Downes 1980; Dent et al. 1993; Coil & Ho 1999; Coil & Ho 2000; Pierce-Price et al. 2000; Herrnstein & Ho 2002; McGary & Ho 2002; Karlsson et al. 2003; Herrnstein & Ho 2005; Tsuboi et al. 2009; Amo-Baladrón et al. 2011; Tsuboi et al. 2011; Tsuboi & Miyazaki 2012; Ao et al. 2013; Minh et al. 2013). Two molecular clouds (the M–0.02–0.07 and the M–0.13–0.08 cloud, Solomon et al. 1972, Novak et al. 2000) lie within 20 pc of the GC (see Fig. 12). M–0.02–0.07

[2] Liu and collaborators have found that they misplaced CS7–6 as CS^{34}7–6 in their paper (B. Liu private communication). This has been fixed in Fig. 13 with respect to the original figure published on ApJ. See Liu et al. (in preparation) for details.

and M–0.13–0.08 have comparable masses ($\sim 5 \times 10^5 M_\odot$, Lis & Carlstrom 1994), and linear dimensions ($10 - 15$ pc). The centre of M–0.02–0.07 lies ~ 7 pc away from Sgr A* (projected distance). Morphological and kinematic evidence shows that Sgr A East has expanded into M–0.02–0.07, compressing portions of this cloud into a 'curved ridge' (Ho et al. 1985; Genzel et al. 1990; Serabyn et al. 1992, see Fig. 12). The centre of M–0.13–0.08 lies ~ 13 pc away from Sgr A* (projected distance). The cloud is highly elongated. A finger-like structure extends from this cloud toward the Galactic eastern direction, and apparently feeds the CNR (Okumura et al. 1991; Ho et al. 1991).

2.4 The G2 cloud

In the last two years, there has been much excitement about G2: a faint dusty object orbiting the SMBH with a very eccentric orbit (~ 0.98) and an extremely small pericentre (~ 200 AU~ 2000 Schwarzschild radii). The detection of G2 was reported in 2012 (Gillessen et al. 2012), but the first VLT NIR images where G2 can be seen date back to ~ 2003. G2 immediately raised the expectations of the astrophysical community: was this object going to be tidally disrupted by the SMBH? What is its nature?

The observation of a blue-shifted (-3000 km s^{-1}) component in April 2013 indicated that a part of G2 had already passed pericentre (see Fig. 14). The bulk of G2 transited at pericentre in Spring 2014, and was not completely disrupted during its close-up with the SMBH: the object is still point-like (consistent with the point-spread function), even if with a tail of disrupted material. Several authors predicted an enhancement of the X-ray and near-infrared activity of the SMBH in correspondence of G2 pericentre passage, but no significant event has yet been observed (Haggard et al. 2014).

G2 has been observed in L' continuum (3.8 μm, $m_{L'} \sim 14$), in the Br-γ line of hydrogen recombination (Br-γ luminosity $\sim$ a few $\times 10^{30}$ erg s^{-1}, emission measure $\sim 10^{57}$ cm^{-3}), in Paschen-α (1.875 μm) and Helium I (2.058 μm). Its luminosity has remained nearly constant (within a factor of two) since the first observations (Pfuhl et al. 2014; Witzel et al. 2014). The L' continuum emission (corresponding to a luminosity of $\sim 2 \times 10^{33}$ erg s^{-1}, Pfuhl et al. 2014; Witzel et al. 2014) is consistent with the thermal emission of dust at ≈ 560 K (Gillessen et al. 2012; Eckart et al. 2013; Gillessen et al. 2013a; Gillessen et al. 2013b). The combination of line emission and NIR continuum indicates that the cloud is composed mainly of ionized gas ($\sim 10^4$ K) plus some amount of relatively cool dust.

The orbit of G2 was traced back to ~ 2003, thanks to archive VLT data, and showed a three-dimensional velocity increase from 1200 km s^{-1} (in 2004, Gillessen et al. 2012) to 2200 km s^{-1} (in 2013, Gillessen et al. 2013b), consistent with a pure Keplerian motion. The internal velocity dispersion of ≈ 100 km s^{-1} (Gillessen et al. 2013a) is another peculiar feature of the velocity field of G2: this corresponds to the sound speed of gas with temperatures of the order of a few million Kelvin.

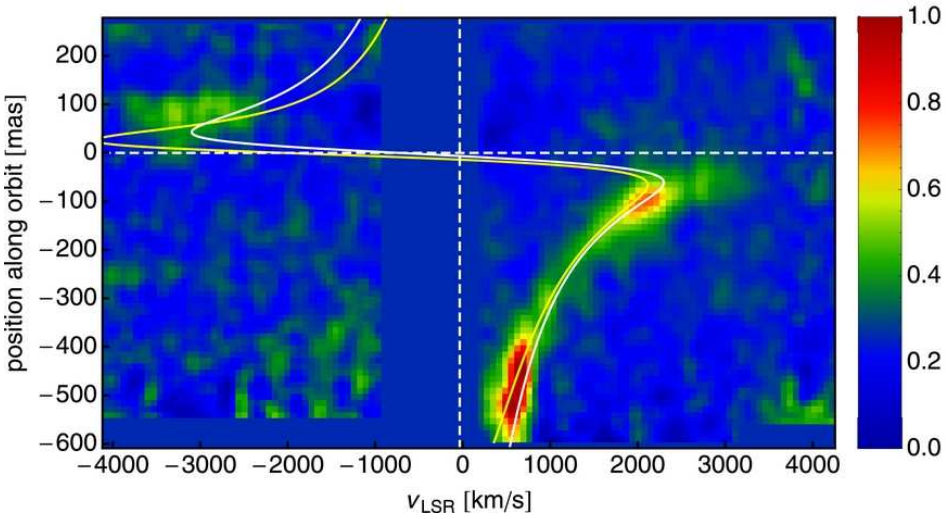

Fig. 14 Position–velocity diagram of G2, extracted from 2013 April SINFONI data set along the orbit projected into the cube. This diagram is a co-add around the lines Br$-\gamma$, Helium I, and Paschen$-\alpha$. The yellow line delineates the $L'-$band based orbit, the white line the Br$-\gamma$ based one. Fig. 2 of Gillessen et al. (2013b).

The best-matching orbital parameters indicate that G2 is almost coplanar with the early-type CW disc (Gillessen et al. 2013b): the orbit of the cloud is $\sim 20^\circ$ tilted with respect to the most recent estimates of the CW disc orientation. Finally, one of the most peculiar features of G2's orbit is its very high eccentricity ($e \sim 0.98$, Phifer et al. 2013; Gillessen et al. 2013a; while the average eccentricity of stellar orbits in the CW disc is ~ 0.3).

Pfuhl et al. (2014) reported the analogy of G2 with another dusty object, the G1 cloud (already observed by Clénet et al. 2004 and Ghez et al. 2005). G1 transited at periapsis in 2001-2002, was observed in Br-γ line and in L' (the same as G2), and has approximately the same dust mass as G2. The eccentricity of G1 is lower (~ 0.86) and the semimajor axis smaller (~ 0.36 arcsec instead of ~ 1.05 arcsec), but its appearance and behaviour are very similar to the ones of G2.

2.5 Does the Galactic Centre host an intermediate-mass black hole?

In this subsection, we discuss the possibility that the GC hosts one or more intermediate-mass black holes (IMBHs, i.e. black holes with mass in the $10^2 - 10^5\,M_\odot$ range). IMBHs have been invoked to explain various phenomena that take place in the GC (such as the ejection of hypervelocity stars).

The presence of an IMBH in the GC might be detected in a number of ways:

1. Reflex motion of the SMBH.
2. A IMBH-SMBH binary might be revealed by emission of gravitational waves (GWs).
3. Stars can remain bound to the IMBH if its Hill sphere is larger than its tidal disruption sphere; this condition is satisfied for SMBH–IMBH separations greater than $\sim 0.05\,\mathrm{mpc}$. The motion of a star bound to the IMBH would be the superposition of a Keplerian ellipse around the SMBH and an additional periodic component due to its motion around the IMBH; the latter would have a velocity amplitude 0.110 times the IMBH orbital velocity and an orbital frequency from several hours to a few years, potentially accessible to astrometric monitoring.
4. In favorable circumstances, a near encounter of the IMBH with a star unbound to it could produce observable changes in the stars orbit over month- or year-long timescales.
5. Interactions with an IMBH may result in ejections of stars to unbound orbits. A star ejected at $\sim 1000\,\mathrm{km\,s^{-1}}$ requires about 100 yr to move beyond 0.1 pc implying a probability $\sim 0.2(N/10^4)$ of observing an escaping star at any given time in the GC region, where N is the number of ejected stars. Interestingly, at least one S-star (S111) in the sample of Gillessen et al. (2009a) appears to be on an unbound trajectory due to its large radial velocity.

In the following two subsections, we focus on points 1. and 2. of the above enumeration.

2.5.1 Constraints on the presence of IMBHs in the GC from radio measurements

At present, the measurements of the proper motion of the radio source associated with SgrA* are the strongest constraints about the presence of IMBHs in the GC (Hansen & Milosavljević 2003; Reid & Brunthaler 2004). In fact, the perturbations induced onto the SMBH by the nearly Keplerian motion of an IMBH orbiting around it are expected to affect the proper motion of SgrA*. In particular, Hansen & Milosavljević (2003) showed that the perturbations induced on the proper motion of SgrA* by an IMBH with mass $10^3 \leq m_{\rm IMBH}/\mathrm{M}_\odot \leq 10^4$, moving in a circular orbit with semi-major axis $10^3 \leq a/\mathrm{AU} \leq 10^4$, can be detected if the proper motion of SgrA* is measured with an accuracy higher than ≈ 0.1 mas. On this basis, measurements of SgrA* proper motion, derived from Very Long Baseline Array (VLBA) data (Reid & Brunthaler 2004), exclude the presence of IMBHs more massive than $\sim 10^4\,\mathrm{M}_\odot$ with $10^3 \leq a/\mathrm{AU} \leq 10^5$.

2.5.2 Gravitational wave signatures of IMBHs in the GC

GWs emitted by an SMBH-IMBH binary in the GC are another possible observational feature of IMBHs. Since the frequency of GWs $f_{\rm GW}$ is twice the or-

bital frequency of a binary, $f_{\rm GW} \sim 10^{-4}{\rm Hz}\left(\frac{m_{\rm BH}}{4.3\times10^3{\rm M}_\odot}\right)^{1/2}\left(\frac{6\times10^{-6}{\rm pc}}{a}\right)^{3/2}$. Thus, an SMBH-IMBH binary enters the frequency range of the future space-borne GW interferometer eLISA (Amaro-Seoane et al. 2013) when $a \lesssim 6\times10^{-6}$pc.

An alternative possible measurement of GWs emitted by an SMBH-IMBH binary might come from pulsar timing, through the so-called pulsar timing array (PTA). GWs are expected to alter the arrival times of pulses from radio pulsars. Thus, observations of a correlated modulation in the time of arrivals of pulses from a network of millisecond pulsars across the sky can be used to observe GWs (Detweiler 1979).

Kocsis et al. (2012) estimate that the maximum distance within which a PTA could measure the GWs of an individual source with a timing precision $\delta t = 10$ ns is

$$D_{\rm source} = 14\,{\rm pc}\left(\frac{m_{\rm IMBH}}{10^3{\rm M}_\odot}\right)\left(\frac{P}{10\,{\rm yr}}\right)^{1/2}\left(\frac{f_{\rm GW}}{10^{-8}{\rm Hz}}\right)^{1/6}\frac{10\,{\rm ns}}{\delta t}, \qquad (6)$$

where P is the orbital period of the IMBH-SMBH binary.

Furthermore, the GW signal from a single source rises above the GW background only when the distance between GW source and PTA is less than

$$D_{\rm bg} = 9\,{\rm pc}\left(\frac{m_{\rm IMBH}}{10^3{\rm M}_\odot}\right)\left(\frac{P}{10\,{\rm yr}}\right)^{1/2}\left(\frac{f_{\rm GW}}{10^{-8}{\rm Hz}}\right)^{11/6}. \qquad (7)$$

Thus, only millisecond pulsars with distance from the GC smaller than both $D_{\rm source}$ and $D_{\rm bg}$ can be used to detect GWs from an hypothetical SMBH-IMBH binary. The GC is expected to host a rich population of pulsars (Pfahl & Loeb 2004), but their detection is challenging because of the high column-density of free electrons toward the GC. Thus, pulsars in the GC can be detected only in relatively high-frequency bands (>10 GHz). This, combined with the very high timing precision required, implies that the aforementioned possible PTA measurement needs (at least) the capabilities of the Square Kilometer Array (SKA, Lazio 2013). Since eLISA is planned for launch in 2034 and SKA is expected to be built in 2018 (phase I) and in the mid 2020s (phase II), the detection of GWs from a possible SMBH-IMBH binary is still quite far-off. As an alternative, GWs from IMBHs in the GC may be detected when they merge with other IMBHs, stellar-mass black holes or neutron stars. Such mergers emit waves in the frequency range that will be observed by forthcoming second-generation ground-based GW detectors (Advanced Ligo, Harry et al. 2010, and Advanced Virgo, Accadia et al. 2012). On the other hand, the probability that such a merger occurs in our GC in the next few years is extremely low (e.g. Mapelli et al. 2010 and references therein).

3 The formation of the early-type stars

A molecular cloud close to the Galactic centre (GC) is tidally disrupted if its number density does not exceed the Roche density

$$n_{\rm RL} \sim 10^7\,{\rm cm}^{-3} \left(\frac{m_{\rm BH}}{3\times10^6\,{\rm M}_\odot}\right) \left(\frac{\rm pc}{r}\right)^3, \quad (8)$$

where $m_{\rm BH}$ is the mass of the SMBH and r the distance of the molecular cloud from the SMBH. Since the density of molecular cloud cores is generally much lower ($\sim 10^{4-6}$ cm^{-3}), molecular clouds are expected to be quickly disrupted when approaching the central SMBH by less than a few parsecs. Thus, the early-type stars inside the central parsec cannot have formed *in situ* from a 'typical' molecular cloud (Phinney 1989; Sanders 1998). And yet, given their young age, they cannot have migrated from larger distances by standard dynamical friction.

Various scenarios have been proposed to solve the 'paradox of youth' and to explain the formation of the early-type stars that orbit within the central parsec. These scenarios can be divided in the following two families: (i) '*in situ*' formation models, which assume local star formation by some non standard process, and the (ii) migration models, which assume formation at larger distances from the SMBH followed by fast migration to their current location.

The inspiral and destruction of a star cluster (Sect. 3.3) belongs to the latter family, together with the tidal breakup of stellar binaries (Sect. 3.4), while the fragmentation of the outer regions of an accretion disc (Sect. 3.1) and the disruption of a molecular cloud (Sect. 3.2) are the most likely '*in situ*' formation pathways.

3.1 Fragmentation of the accretion disc

Keplerian accretion discs around SMBHs may become gravitationally unstable to fragmentation and collapse to form stars (Paczynski 1978; Kolykhalov & Sunyaev 1980; Lin & Pringle 1987; Shlosman & Begelman 1989; Huré 1998; Collin & Huré 1999; Collin & Zahn 1999; Gammie 2001; Goodman 2003; Nayakshin & Cuadra 2005; Thompson et al. 2005; Nayakshin 2006; Nayakshin et al. 2007; Collin & Zahn 2008).

In particular, the Toomre stability parameter for Keplerian rotation (Toomre 1964) is

$$Q = \frac{c_{\rm s}\,\Omega}{\pi G\,\Sigma} = \frac{\Omega^2}{2\,\pi G\,\rho}\,\sqrt{(1+\zeta)}, \quad (9)$$

where $c_{\rm s}$ is the sound speed, Ω is the angular frequency, G is the gravity constant, Σ and ρ are the surface density and the volume density of the disc, respectively. In equation 9, we have taken $\Sigma = 2\,H\,\rho$, where H is the half-disc thickness. The equation of hydrostatic equilibrium writes as $c_{\rm s} = \Omega\,H\,\sqrt{(1+\zeta)}$, where $\zeta \equiv 4\,\pi G\,\rho\,\Omega^{-2}$.

The disc becomes unstable to fragmentation when $Q \leq 1$. This is expected to occur at a radius

$$r_{\rm Q=1} \sim 1.2\,{\rm pc} \left(\frac{m_{\rm BH}}{3\times10^6\,{\rm M}_\odot}\right)^{1/3} \left(\frac{\rho}{2\times10^{-17}\,{\rm g\,cm}^{-3}}\right)^{-1/3}, \quad (10)$$

where we approximated $\Omega^2 = G m_{\rm BH} r^{-3}$ and $\zeta = 0$.

Following Collin & Zahn (1999), the condition necessary for the collapse of a fragment is that the time scale for star formation ($t_{\rm SF}$) and the cooling time ($t_{\rm cool}$) be shorter than the characteristic mass transport time in the disc ($t_{\rm trans}$).

According to Wang & Silk (1994), $t_{\rm SF} = \Omega^{-1} Q/\sqrt{1-Q^2}$. Provided that Q is not too close to 1,

$$t_{\rm SF} \sim \Omega^{-1} = 3 \times 10^{11}\,{\rm s}\,(m_{\rm BH}/3\times10^6\,{\rm M}_\odot)^{-1/2}\,(r/{\rm pc})^{3/2}. \quad (11)$$

For a gravitationally heated disc at nearly solar metallicity,

$$t_{\rm cool} \sim \frac{8\pi\rho H^3}{3\dot{M}} = 8\times10^9\,{\rm s}\left(\frac{\rho}{2\times10^{-17}\,{\rm g\,cm^{-3}}}\right)\left(\frac{H}{0.01\,{\rm pc}}\right)^3\left(\frac{10^{-2}{\rm M}_\odot\,{\rm yr}^{-1}}{\dot{M}}\right) \quad (12)$$

Finally, the mass transport time is

$$t_{\rm trans} \sim \frac{2\pi r^2 \rho H}{\dot{M}} = 6\times10^{13}\,{\rm s}\left(\frac{r}{\rm pc}\right)^2\left(\frac{\rho}{2\times10^{-17}\,{\rm g\,cm^{-3}}}\right)\left(\frac{H}{0.01\,{\rm pc}}\right)\left(\frac{10^{-2}{\rm M}_\odot\,{\rm yr}^{-1}}{\dot{M}}\right). \quad (13)$$

For a wide range of accretion disc parameters, $t_{\rm SF}$ and $t_{\rm cool}$ are shorter than $t_{\rm trans}$. Thus, not only stars are expected to form in the outer parts of accretion discs, but star formation may be sufficiently vigorous to quench accretion and destroy the accretion disc. Thus, recent studies searched for mechanisms that can efficiently transfer angular momentum in the accretion disc, to keep feeding the SMBH. Collin & Zahn (2008) find that gas accretion onto the SMBH is still possible (even if moderate star formation takes place in the accretion disc), provided that supernovae and/or clump collisions enhance the angular momentum transfer.

Nayakshin (2006) find that, if star formation takes place in a marginally stable accretion disc, the protostars heat up and thicken the accretion disc, preventing further fragmentation. This occurs because the accretion luminosity of the protostars exceeds the disc radiative cooling, heating and puffing the disc up. While stellar feedback stops further fragmentation, mass accretion on the already formed protostars continues very efficiently, producing a top-heavy MF. Nayakshin et al. (2007) confirm these findings by means of N-body/smoothed particle hydrodynamics (SPH) simulations of an accretion disc (see Fig. 15). Despite a number of severe approximations (e.g. a constant cooling time, and the usage of sink particles to model star formation without resolving gas fragmentation directly), this is the first self-consistent simulation of an accretion disc showing that (i) the thermal feedback associated with gas accretion on to protostars slows down disc fragmentation, (ii) the initial MF (IMF) of the stars may be considerably top-heavy with respect to Salpeter IMF (Salpeter 1955).

So far, the main issues of the accretion-disc-fragmentation scenario are (i) if the orbits of gas particles in the accretion disc are tidally circularised by viscosity, the orbits of the newly born stars are circular too, and cannot reproduce the observed eccentricity distribution in the GC (Cuadra et al. 2008; on the other hand, this issue

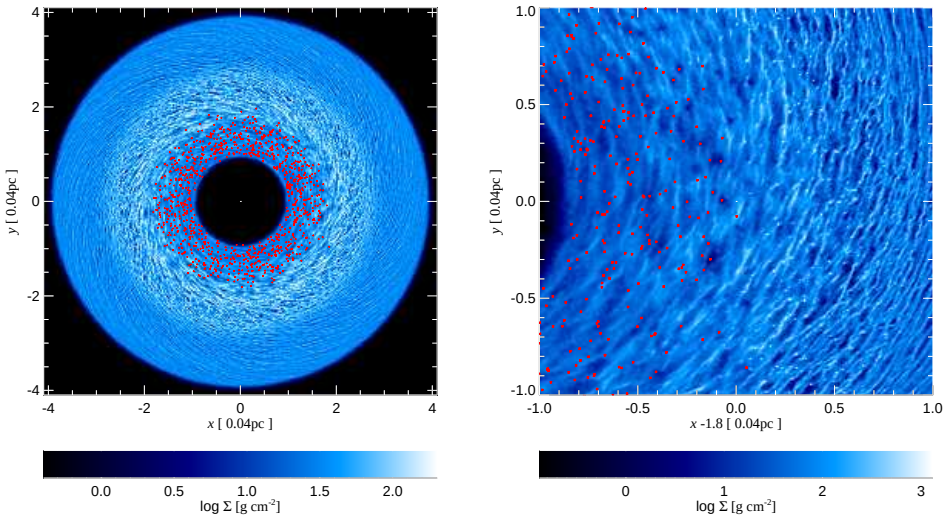

Fig. 15 Snapshot of the disc column density at time $t = 75$ (in N-body units) for run S2 of Nayakshin et al. (2007). In this N-body/SPH simulation, stars form as sink particles from an accretion disc. The left-hand panel shows the full simulation domain, whereas the right-hand one zooms in on a region of the disc centred at $x = 1.8$. Stars with masses greater than $3\,M_\odot$ are plotted as the red asterisks. From Fig. 2 of Nayakshin et al. (2007).

may be overcome by starting with an eccentric accretion disc and by imposing that it forms stars before tidal circularisation, Nayakshin et al. 2007; Alexander et al. 2008); (ii) the newly born stellar disc is expected to be very thin, much thinner (and with smaller individual inclinations) than the observed disc of early-type stars in the GC (e.g. Cuadra et al. 2008); (iii) the MW SMBH is currently quiescent and there is no evidence of an accretion disc: which mechanisms induced the formation of an accretion disc and then destroyed it a few Myrs since the formation of the stellar disc (e.g. Alexander et al. 2012)?

3.2 Molecular cloud disruption

A molecular cloud is disrupted well before reaching the inner parsec. This was the main argument against the *in situ* formation of the early-type stars in the GC. On the other hand, star formation may take place even within a disrupted molecular cloud. The two necessary requirements for a disrupted molecular cloud to form stars in the central parsec of the MW are (i) that the molecular cloud orbit has very low angular momentum; (ii) that the streamers of the disrupted cloud collide with each other and are shocked.

The former requirement is necessary for the streamers to settle on a sufficiently tight orbit (i.e. the initial pericentre of the cloud orbit must be $\lesssim 1$ pc). The latter, i.e. collisions between the filaments, is requested because collisions produce shocks, which induce fast cooling and enhance the gas density by orders of magnitude. In this way, the density of the post-shock streamers can overcome the threshold for tidal disruption (equation 8), and the densest gas clumps collapse into protostars. This is the basic motivation of the pioneering study by Sanders (1998) and of a number of recent papers studying the disruption of a molecular cloud in the surroundings of the GC, by means of *N*-body/SPH simulations (Bonnell & Rice 2008; Mapelli et al. 2008; Hobbs & Nayakshin 2009; Alig et al. 2011; Mapelli et al. 2012; Lucas et al. 2013; Alig et al. 2013).

The aforementioned papers describe simulations of the infall of one or more molecular clouds toward Sgr A*. They consider different cloud masses (ranging from $\sim 10^4$ M$_\odot$ to $\sim 10^6$ M$_\odot$), temperatures[3] (ranging from ~ 10 K to ~ 500 K) and thermodynamics (adiabatic gas, isothermal gas or radiative cooling).

In all the simulations, the cloud is disrupted by the tidal forces of the SMBH and spirals towards it. In less than 10^5 yr, more than one tenth of the gas in the parent cloud ends up in a dense and distorted disc around the SMBH, with a small outer radius (~ 0.5 pc, see e.g. Fig. 16). If the angular momentum of the cloud orbit is low, the resulting gaseous disc is eccentric, consistently with the observations of the stellar orbits in the CW disc. Locally, the surface density of the gaseous disc may overcome the tidal shear from the SMBH and fragmentation may take place.

Among the aforementioned papers, the simulations presented in Mapelli et al. (2012) are the first attempt to trace the fragmentation of the gas disc, without adopting the sink particle technique. The star candidates formed in these simulations are distributed in a thin ring at a distance of $\sim 0.1-0.4$ pc from the SMBH. They have eccentric orbits ($0.2 \leq e \leq 0.4$), with average eccentricity $\langle e \rangle = 0.29 \pm 0.04$ (Fig. 17). Both the semi-major axis and the eccentricity distribution are in agreement with the properties of the observed CW disc (e.g. Fig. 8).

Both Bonnell & Rice (2008) and Mapelli et al. (2012) agree that, if the parent molecular cloud is sufficiently massive (1.3×10^5 M$_\odot$), the total mass of simulated star candidates ($2-5 \times 10^3$ M$_\odot$) is consistent with the estimated mass of the CW disc (e.g. Paumard et al. 2006; Bartko et al. 2009; but see Lu et al. 2013 for a slightly different estimate).

Furthermore, if the minimum temperature (i.e. the temperature floor due to diffuse radiation in the GC) is sufficiently high (T~ 100 K), the MF of stellar candidates is top-heavy (fitted by a single power-law with $\alpha \sim 1.5$ in the case of Mapelli et al. 2012, Fig. 17), in good agreement with the recent measurements by Lu et al. (2013, see Fig. 9). The main reason is that a higher gas temperature corresponds to a higher Jeans mass ($m_{\rm J} \propto T^{3/2}$, Jeans 1919).

All the papers that simulate the infall of a molecular cloud towards the GC (e.g. Mapelli et al. 2008; Bonnell & Rice 2008; Hobbs & Nayakshin 2009; Alig et al.

[3] Many temperature components have been observed in the GC, ranging from ~ 20 K to ~ 200 K, and the temperature distribution is highly non-uniform (e.g. McGary & Ho 2002; Herrnstein & Ho 2002; Herrnstein & Ho 2005; Montero-Castaño et al. 2009; Liu et al. 2013).

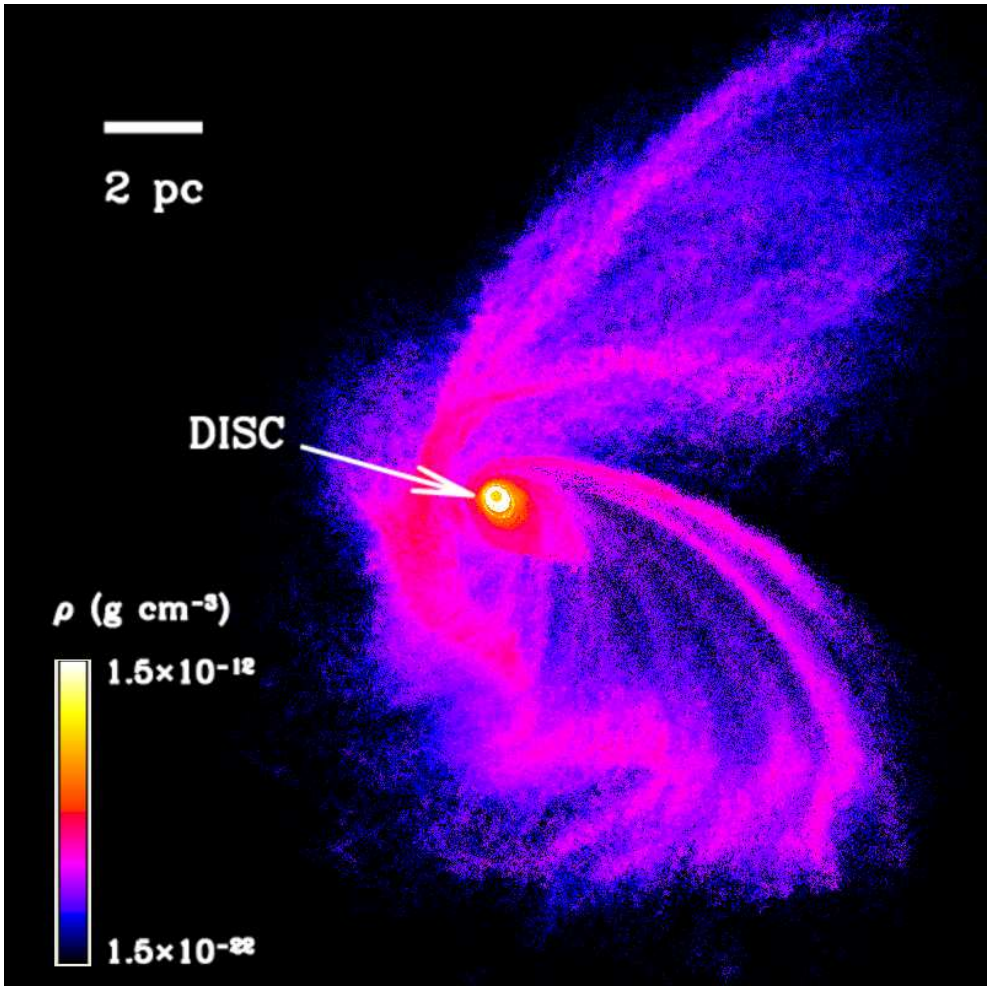

Fig. 16 Density map of the gas in run E of Mapelli et al. (2012) at $t = 4.8 \times 10^5$ yr. Simulation of a $1.3 \times 10^5\,M_\odot$ molecular cloud, disrupted by a $3.5 \times 10^6\,M_\odot$ SMBH. The simulation is projected in the plane where the gaseous disc (at the centre) is seen face-on. The box measures 20 pc per edge. The simulation has been run with the *N*-body/SPH code GASOLINE (Wadsley et al. 2004) and includes radiative cooling (Boley 2009; Boley et al. 2010). The colour-coded map is logarithmic and ranges from 1.5×10^{-22} to 1.5×10^{-12} g cm^{-3}. From Gualandris et al. (2012).

2011) agree on the general picture. However, there are significant differences between these papers, both in the initial conditions and in some of the results.

As to the initial conditions, Mapelli et al. (2008), Bonnell & Rice (2008) and Mapelli et al. (2012) adopt models of gas clouds that are turbulently supported, while Hobbs & Nayakshin (2009) and Alig et al. (2011) consider a simplified model of spherical and homogeneous cloud. The simulations reported in Mapelli et al. (2008) are isothermal, with $T_{MC} = 10$ K (likely too low, if compared to the back-

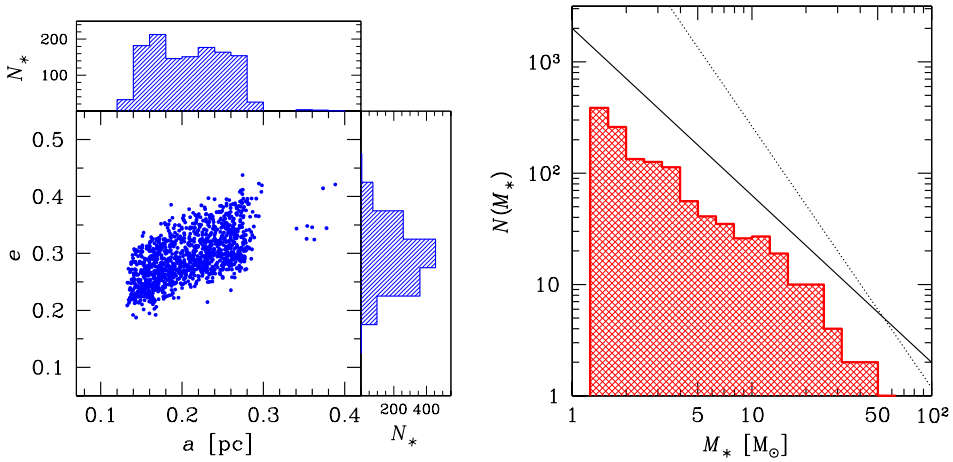

Fig. 17 Left-hand panel: Eccentricity e versus semi-major axis a at $t = 4.8 \times 10^5$ yr in run E of Mapelli et al. (2012) (the same as in Fig. 16). The marginal histograms show the distribution of a (top histogram) and e (right-hand histogram). Right-hand panel: Stellar MF in run E of Mapelli et al. (2012) at $t = 4.8 \times 10^5$ yr (hatched red histogram). $x-$axis: star mass M_*. $y-$axis: number of stars per mass bin $N(M_*)$. Solid (dotted) black thin line: MF $dN/dm \propto m^{-\alpha}$ with $\alpha = 1.5$ ($\alpha = 2.35$). From Mapelli et al. (2012).

ground radiation field in the GC). The simulations in Bonnell & Rice (2008) include an approximate radiative transfer formalism, with compressional heating balanced by cooling rates derived from estimated optical depths. In Hobbs & Nayakshin (2009), the simulations include a very simplified model of cooling, and the initial temperature of the cloud is low ($T_{MC} = 20$ K). In Alig et al. (2011) and Mapelli et al. (2012), the simulations include different thermodynamical treatments for the gas, considering both isothermal and radiative cooling cases. The floor temperature for the simulations with radiative cooling is set to be 50 K in Alig et al. (2011) and 100 K in both Bonnell & Rice (2008) and Mapelli et al. (2012). Alig et al. (2011) stop their simulation before fragmentation takes place in the disc, whereas the other considered papers study the formation of star candidates in the disc. Mapelli et al. (2008), Bonnell & Rice (2008) and Hobbs & Nayakshin (2009) adopt the sink particle technique, to model SF. Only Mapelli et al. (2012) follow the initial fragmentation of the disc. Table 1 is a summary of the differences in the initial conditions of the aforementioned simulations.

The main differences among the results of these papers are about the formation of star candidates, and especially about the MF. The MF in Hobbs & Nayakshin (2009) is quite bottom-heavy, because of the approximations in the cooling recipes and because of the absence of opacity prescriptions.

Bonnell & Rice (2008) adopt a very conservative value of the critical density for converting gaseous particles into sink particles ($= 10^{14}$ $M_\odot$ pc$^{-3} = 1.6 \times 10^{15}$ cm^{-3}, assuming molecular weight $\mu = 2.46$), well above the critical tidal density.

Table 1 Main differences in the initial conditions of simulations of molecular cloud disruption.

Paper	Cloud model	$T_{\rm MC}$ (K)	gas treatment	sink particles
Bonnell & Rice (2008)	turbulently supported	100	radiative cooling	yes
Mapelli et al. (2008)	turbulently supported	10	isothermal	yes
Hobbs & Nayakshin (2009)	homogeneous sphere	20	simplified cooling	yes
Alig et al. (2011)	homogeneous sphere	50	both isothermal and radiative cooling	no
Mapelli et al. (2012)	turbulently supported	100, 500	both isothermal and radiative cooling	no
Lucas et al. (2013)	turbulently supported	100	radiative cooling	yes

Therefore, their MF is consistent with that predicted by the Jeans mass for the local density and temperature of the clouds. Similarly, the MFs derived in Mapelli et al. (2012) are consistent with the predictions from Jeans mass and Toomre instability.

On the other hand, Mapelli et al. (2012) do not observe the formation of the very massive stars ($> 60\,{\rm M}_\odot$) that were found in the massive cloud simulated by Bonnell & Rice (2008). The MF in Mapelli et al. (2012) is consistent with a single power-law with index $\alpha \sim 1.5$, whereas that in Bonnell & Rice (2008) is clearly bimodal, showing two distinct stellar populations (see fig. 4 of Bonnell & Rice 2008). The very massive stars in Bonnell & Rice (2008) are all formed at $r \sim 0.02$ pc, where massive stars have not been observed in the MW (the observed ring of young stars having an inner radius of ~ 0.04 pc). In Mapelli et al. (2012), star candidates do not form at $r < 0.05$ pc, because the shear from the SMBH prevents local collapse. This difference is likely due to the different orbits of the parent clouds, to the different initial densities and to the different recipes for opacity.

Recently, Lucas et al. (2013) showed that the disruption of a single prolate cloud, oriented perpendicular to its orbital plane, produces a spread in angular momenta of gas particles, and leads to the formation of stars with slightly misaligned orbital planes (see Fig. 18). This matches the observations, which indicate that the early-type stars in the CW disc have different orbital inclinations. On the other hand, we will show in Sect. 4 that the misalignment of orbits can be the result of various dynamical processes, taking place after the formation of the first disc.

The main problem with the disruption scenario is the fact that the molecular cloud must have a very low angular momentum. In fact, shock-induced radiative cooling reduces the orbital energy of the cloud rather than its angular momentum. Therefore, the initial mean angular momentum per unit mass of the cloud ($\sim b\,v$, where b is the impact parameter and v the initial velocity of the cloud centre of mass) is nearly preserved during the disruption of the cloud and the settling of the disc. Thus, the radius of the formed gas disc $R_{\rm d}$ will be approximately (Wardle &

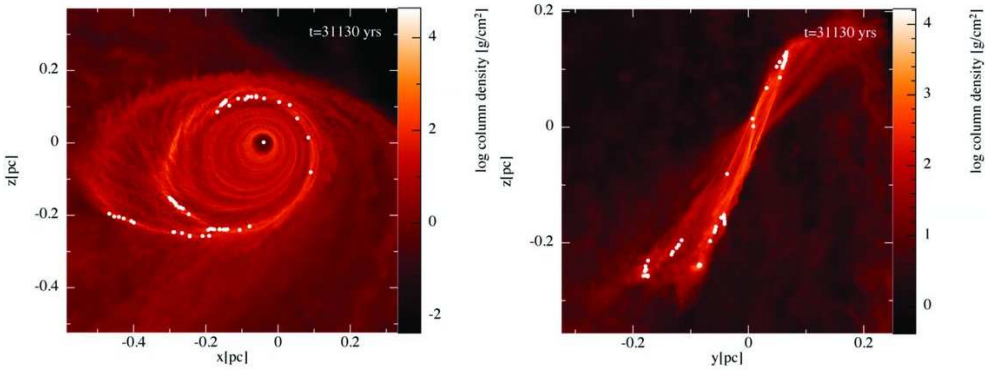

Fig. 18 Column densities for run I10 of Lucas et al. (2013) in the *xz* and *yz* planes at the simulation's end at $t = 3.113 \times 10^4$yr. In this simulation, a prolate molecular cloud, oriented perpendicular to its orbital plane, is disrupted by a SMBH. The white circles mark the position of sink particles. The streamers are oriented 17° out of plane from the disc, resulting in two stellar systems separated by this angle. From Fig. 13 of Lucas et al. (2013).

Yusef-Zadeh 2008):

$$R_{\rm d}\left(\frac{G m_{\rm BH}}{R_{\rm d}}\right)^{1/2} \sim b v. \tag{14}$$

Adopting $m_{\rm BH} = 3.5 \times 10^6\,{\rm M}_\odot$ and $R_{\rm d} \sim 1$ pc, we obtain $b \lesssim 1\,{\rm pc}\,v_{100}^{-1}$ (with $v = v_{100}\,100$ km s^{-1}).

This argument does not hold if a molecular cloud engulfs Sgr A* during its passage through the GC, and it is partially captured by the SMBH (see Fig. 19). The partial capture of a portion of the molecular cloud is enhanced by gravitational focusing. Fluid elements passing on opposite sides of Sgr A* have oppositely directed orbital angular momenta, so that the collision between them leads to a partial cancellation of the specific angular momentum. The efficiency of angular momentum cancellation depends on the density and velocity inhomogeneities in the gas.

An alternative solution to the angular momentum problem is to assume that two molecular clouds collided a few parsecs away from Sgr A*, lost part of their angular momentum during the collision, and fell towards the SMBH with a very small impact parameter. According to this scenario, Hobbs & Nayakshin (2009) simulate the collision between two spherical clouds and the disruption of the collision product by a SMBH. Their *N*-body/SPH simulations reproduce many interesting features of the observed early-type stars in the GC, such as the presence of stars with high orbital inclinations with respect to the main disc (see Fig. 20). Other studies (e.g. Mapelli et al. 2012) simulate clouds with very low initial angular momentum, assuming that this was the result of a previous collision between two different clouds.

Finally, Alig et al. (2013) propose that the young stellar disc is the result of the collision between a molecular cloud and the CNR (see Sect. 2.3 for a description of the observed properties of the CNR). The *N*-body/SPH simulations described in Alig et al. (2013) show that the collision between a molecular cloud and the CNR

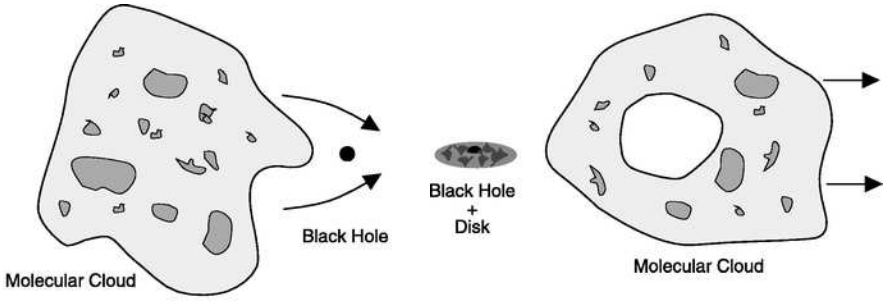

Fig. 19 Schematic diagram of a cloud engulfing Sgr A*, from Fig. 1 of Wardle & Yusef-Zadeh (2008). The left-hand panel indicates the gravitational focusing of incoming molecular cloud material (incident from the left). The right-hand panel shows the carved-out inner region of the cloud that has been captured by Sgr A* and circularised to form a disc. The outer region of the cloud continues its motion in the direction away from Sgr A*.

leads to multiple streams of gas flowing toward the SMBH. This simulation shows that more than a single disc can be formed through this pathway.

3.3 Star cluster disruption

Star formation from standard collapse can proceed outside the central parsec and lead to the formation of young star clusters like the Arches and the Quintuplet, which then inspiral due to dynamical friction and deposit stars while being tidally disrupted (Gerhard, 2001). A dissolving cluster would lead to the formation of a stellar disc similar to the CW disc, possibly accompanied by a number of isolated outliers. It would also preferentially deposit massive stars close to the SMBH, as these would form a compact core and survive tidal effects down to smaller separations than low-mass stars. However, a cluster would need to be very dense and massive to be able to inspiral within the lifetime of its massive stars (Kim & Morris, 2003).

The inspiral would be accelerated by the presence of an IMBH in the centre of the cluster, if this was as massive as 10% of the cluster mass (Kim et al., 2004). Formation of IMBHs has been predicted from a number of N-body simulations. The simulations indicate that a runaway sequence of mergers of massive stars leads to the formation of a very massive object which is assumed to eventually collapse (Portegies Zwart et al., 2004). The evolution of such a very massive star, however, is not well known, and it has been argued that collapse to an IMBH might be prevented by severe mass-loss in the form of stellar winds (Yungelson et al., 2008).

Another potential difficulty of this model is that an inspiralling cluster would deposit stars all along its orbit while being stretched and tidally disrupted. While young stars have been observed outside the central 0.5 pc (Buchholz et al., 2009),

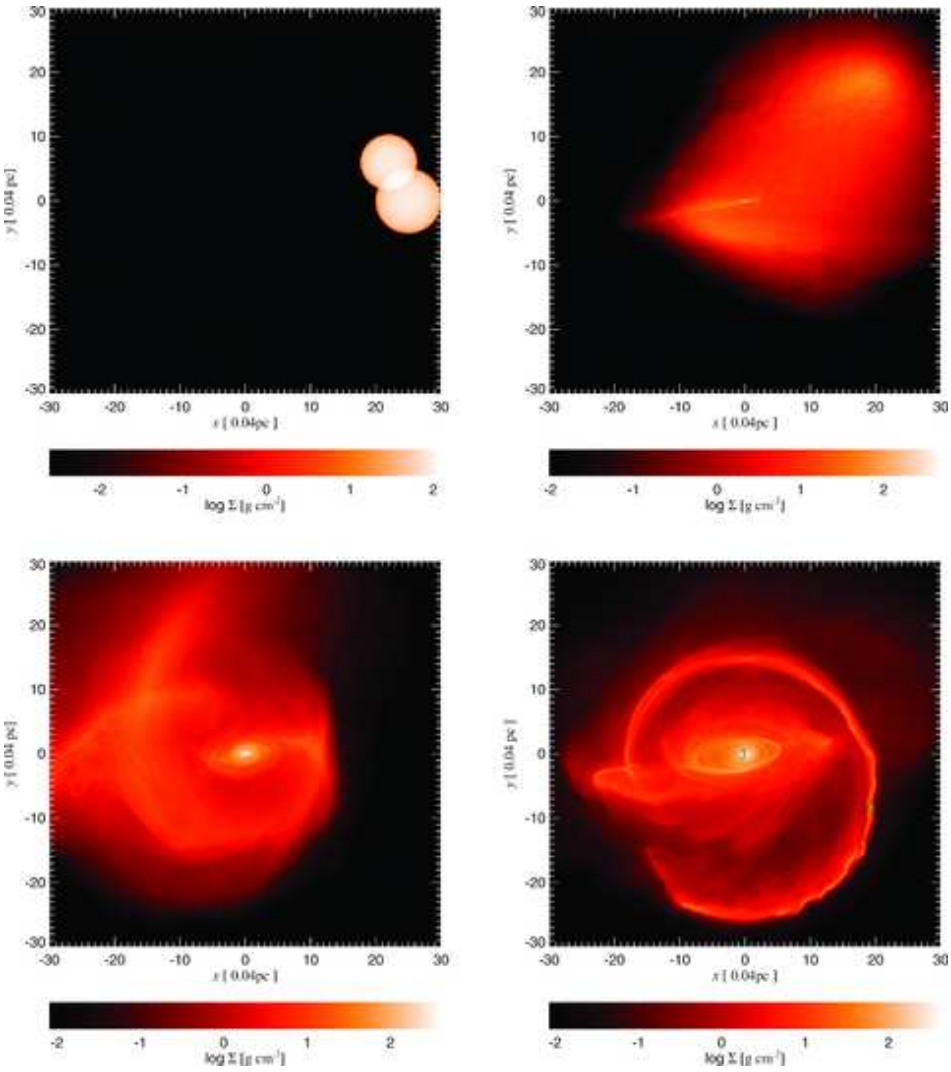

Fig. 20 Gas surface density and star locations (in the bottom right-hand panel) for snapshots from simulation S1 of Hobbs & Nayakshin (2009) taken at times $t = 0, 100, 250$ and 1000 (in N-body units), left to right and top to bottom, respectively. Sgr A* is located at $(0, 0)$, and the line of sight is along the $z-$direction. This simulation follows the collision of two molecular clouds and the infall of the collision product toward the GC. Fig. 1 of Hobbs & Nayakshin (2009).

the required number of young stars is much larger than what currently inferred from observations (Perets & Gualandris, 2010).

Fujii et al. (2008) perform self-consistent simulations of the inspiral of a star cluster in its parent galaxy and find that the inspiral time is somewhat shorter than expected by simple application of Chandraskhar's dynamical friction formula (Chan-

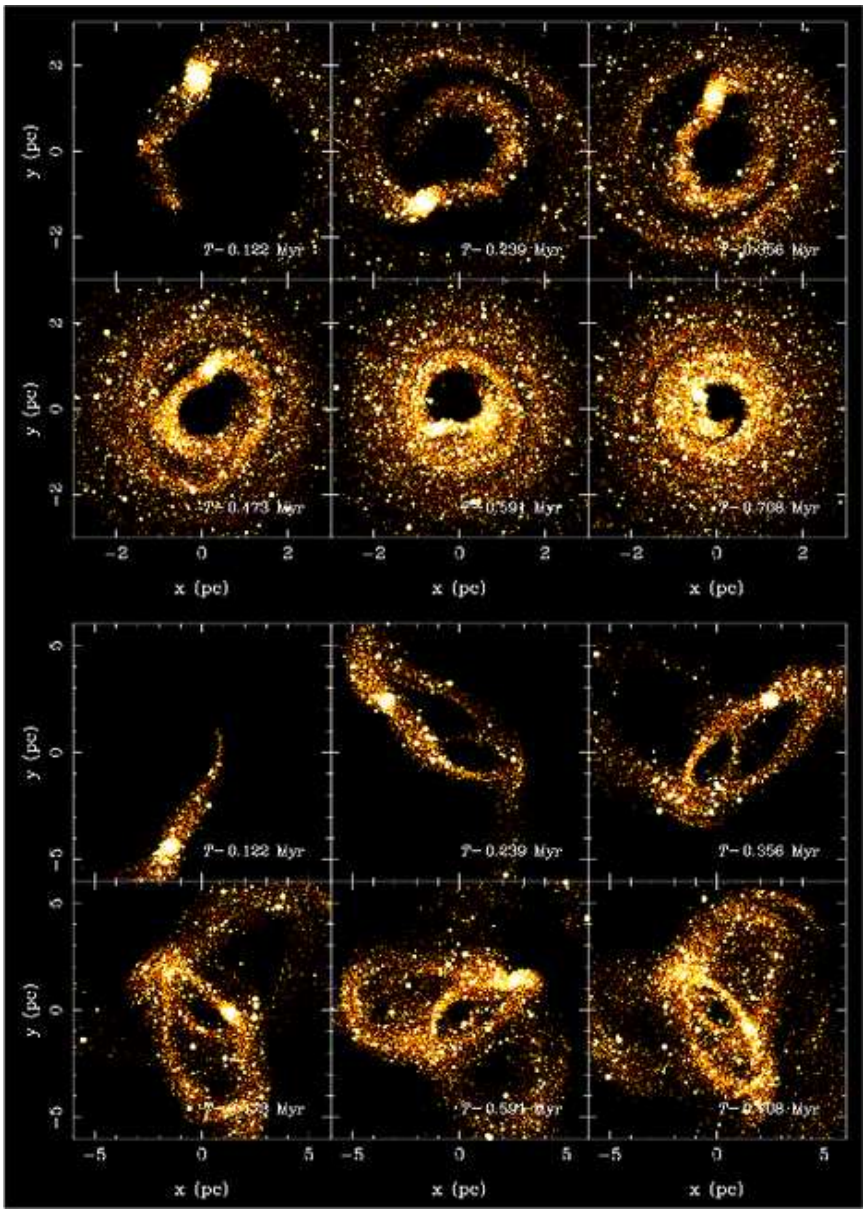

Fig. 21 Snapshots from the simulations of Fujii et al. (2008, Fig.2) of the inspiral of a star cluster in the case of a circular orbit (top panels) and an eccentric orbit (bottom panel).

drasekhar, 1943), especially if the cluster undergoes core collapse. In addition, an eccentric orbit for the star cluster leads to a faster inspiral than a circular orbit, mitigating the requirements on cluster density for survival down to small separations.

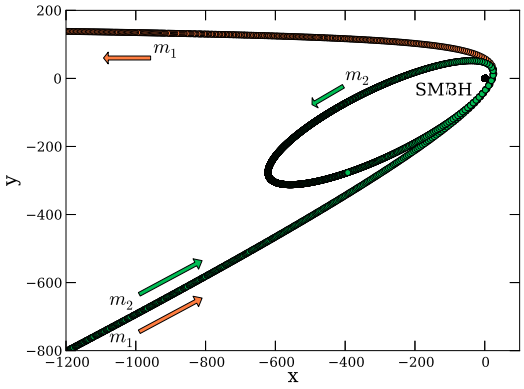

Fig. 22 Example of an encounter between a stellar binary and the SMBH in which the binary is broken apart; one star is ejected while the other is captured by the SMBH into a bound orbit. Distances are expressed in units of the initial binary separation.

Snapshots from simulations of both a circular and an eccentric orbit are shown in Fig. 21. In these simulations, the clusters are positioned at an initial distance of either 2 or 5 parsecs, and no stars are found at distances smaller than 0.5 pc at the end of the integration.

A further speed up of the inspiral is found in simulations in which the star cluster forms an IMBH in its centre in the early stages of evolution (Fujii et al., 2010). In this case, the cluster can deposit massive stars in a disc configuration around the IMBH. Further evolution can quickly randomise the orbital configuration and lead to an isotropic distribution (Merritt et al. 2009, see Sect. 4.5 for details), in agreement with observations of the S-stars. However, for this to happen within the lifetime of the young stars, the cluster needs to be dense and massive and on a very eccentric orbit. While an IMBH of a few thousand solar masses is sufficient for the purpose of randomising the orbits of the bound stars, the simulated cluster in the models of Fujii et al. (2010) forms an IMBH which is more massive than the currently accepted upper limit for a secondary black hole in the GC (Reid & Brunthaler, 2004).

3.4 The binary breakup scenario

Another formation scenario that involves migration from outside the central parsec is the breakup of stellar binaries scattered onto low angular momentum orbits by relaxation processes. A binary scattered to pass very close to the SMBH is likely to undergo an exchange interaction in which one of the stars is ejected to large distances while the other is captured by the SMBH in a wide and eccentric orbit (see Fig. 22).

Theoretically, a binary is expected to be disrupted when it reaches a distance of the order of its tidal radius:

$$r_{\rm t} \simeq \left(\frac{m_{\rm BH}}{M_{\rm b}}\right)^{1/3} a_{\rm b}\,, \tag{15}$$

where $M_{\rm b}$ represents the binary mass and $a_{\rm b}$ its semi-major axis. Simulations show that most binaries approaching the SMBH within the tidal radius are actually disrupted (Hills, 1991, 1992; Bromley et al., 2006). The mean semi-major axis of the captured star is (Hills, 1991)

$$\langle a_{\rm c}\rangle \simeq 0.56\left(\frac{m_{\rm BH}}{M_{\rm b}}\right)^{2/3} a_{\rm b} \simeq 0.56\left(\frac{m_{\rm BH}}{M_{\rm b}}\right)^{1/3} r_{\rm t}\,. \tag{16}$$

This relation shows that harder stellar binaries (i.e. binaries with binding energy larger than average) tend to produce more tightly bound captured stars, and provides a direct mapping between the distribution of semi-major axes of incoming binaries and bound stars. Because the pericentre distance of the captured stars is at the binary tidal radius, the eccentricity is quite high (Hills, 1991; Miller et al., 2005)

$$e \simeq 1 - r_{\rm t}/a_{\rm c} \simeq 1 - 1.78\left(\frac{M_{\rm b}}{m_{\rm BH}}\right)^{1/3} \simeq 0.97 \tag{17}$$

for stellar binaries interacting with the MW SMBH. This is larger than what is derived for any star in the S-cluster and may lead to the conclusion that the binary breakup scenario is inconsistent with the observed properties of the S-stars. Relaxation processes, however, are able to alter the orbital eccentricities of the bound population over the lifetime of the stars, bringing the eccentricity distribution in agreement with the observed one (see section 4.3 for a discussion).

Antonini et al. (2010) study the dynamics of main-sequence binaries on highly elliptical bound orbits with small pericentre distances. They find that bound stars can also be produced when the binary components merge. A coalescence remnant is not able to escape the SMBH gravitational potential if the initial binary is bound to the SMBH unless significant mass loss occurs. The probability for collisions between the components of the binary increases with time, resulting in substantially larger numbers of mergers when allowing for multiple pericentre passages.

Ejection velocities for the unbound star can be large enough to explain the population of hypervelocity stars (HVSs) (Brown et al., 2005) in the halo of the Galaxy. In this model, the HVSs are the former binary companions to the S-stars (Gould & Quillen, 2003).

In addition to an efficient mechanism to thermalise the eccentricities within the lifetime of the stars, in order to be viable the binary breakup model requires a continuous reservoir of binaries at large radii, as well as a mechanism to scatter the binaries onto plunging orbits. Scattering by massive perturbers like star clusters and molecular clouds has been suggested to dominate over two-body relaxation in the central 100 pc of the Galaxy (Perets et al., 2007). Massive perturbers do not significantly contribute to the disruption rate of single stars by the SMBH, but they may

enhance the tidal disruption rate of binaries by a factor $10-1000$, depending on their distribution.

4 Evolution of the early-type stars

The different models described in Sect. 3 for the origin of the young stars predict different distributions for the orbital elements:

- Stars formed from the disruption of a molecular cloud are expected to lie in a disc and have moderate eccentricities ($0.2 \lesssim e \lesssim 0.5$).
- Stars formed from the tidal breakup of stellar binaries are naturally found in an isotropic configuration and with very large eccentricities ($e \gtrsim 0.97$).
- Stars deposited by an inspiralling star cluster with an IMBH in the centre will have distributions of semi-major axes and eccentricities centred on the orbital elements of the IMBH, and will also be orbiting in a plane.

It is interesting to note that none of the suggested models predicts a roughly thermal distribution of eccentricities $N(<e) \sim e^2$, as is observed for the S-stars. The predicted distributions, however, cannot be compared directly with observations, because they evolve during the lifetime of the stars due to relaxation processes and external perturbations. We review these processes in this section.

4.1 Secular processes: precession and Kozai cycles

The motion of a star inside the SMBH sphere of influence can be described as the motion of a test particle in a Keplerian potential (due to the SMBH), perturbed by an external potential. The sources of the external potential may be the spherical cusp of old stars, a stellar disc, a gaseous disc, the circumnuclear ring, a molecular cloud, an IMBH or whatever other perturber is sufficiently massive and sufficiently close to the GC.

Precession is one of the main effects that are induced by the external potential. Precession effects have been invoked to explain the formation of the S-star cluster (e.g. Ivanov et al. 2005; Löckmann et al. 2008; Löckmann et al. 2009) and the broad distribution of angular momentum vectors of the orbits of early-type stars (Šubr et al. 2009; Haas et al. 2011a; Haas et al. 2011b; Mapelli et al. 2013). The strength and the effects of precession depend on the nature of the potential. In particular, the precession induced by a spherically symmetric potential (e.g. the spherical stellar cusp of old stars) is very different from that induced by either an axisymmetric potential (e.g another stellar disc, a gaseous disc/ring) or a single massive object (e.g. an IMBH) orbiting the SMBH. In this section, we briefly describe the precession effects that may affect the early-type stars in the GC, and give an estimate of the corresponding timescales.

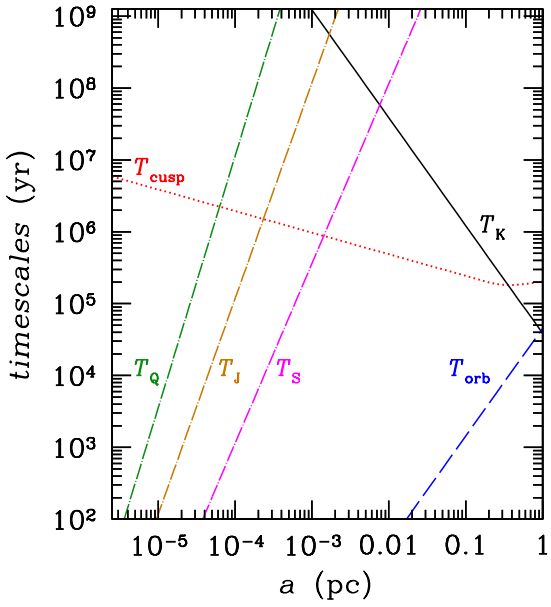

Fig. 23 Comparison of the relevant timescales as a function of the semi-major axis a (see Sect. 4.1 and Sect. 4.2 for details). Solid black line: $T_{\rm K}$ (equation 19, for $m_{\rm BH} = 4.3 \times 10^6\,{\rm M}_\odot$, $M_{\rm DISC} = 10^5\,{\rm M}_\odot$ and $R_{\rm DISC} = 2$ pc); dotted red line: $T_{\rm cusp}$ (equation 18, for $m_{\rm BH} = 4.3 \times 10^6\,{\rm M}_\odot$, $e = 0$ and $M_{\rm cusp}$ derived from equation 2); dashed blue line: $T_{\rm orb}$ (orbital period); dot-dashed green line: $T_{\rm Q}$ (equation 34); dot-dashed ochre line: $T_{\rm J}$ (equation 33); dot-dashed magenta line: $T_{\rm S}$ (equation 28). $T_{\rm S}$, $T_{\rm J}$ and $T_{\rm Q}$ have been derived for $m_{\rm BH} = 4.3 \times 10^6\,{\rm M}_\odot$ and $e = 0$. $\chi = 1$ (i.e. a maximally rotating SMBH) has been assumed for $T_{\rm J}$ and $T_{\rm Q}$.

The orbit of a star in a Keplerian potential dominated by the SMBH mass is an ellipse described by semi-major axis a and eccentricity e. The orientation of the orbital plane in space is defined by two angles: the inclination i with respect to an (arbitrarily chosen) reference plane and the longitude of the ascending node Ω, with respect to the same plane and to an arbitrarily selected direction in this plane, called direction of the γ point. The argument of pericentre (angle ω) describes the orientation of the orbit within its plane. Finally, the true anomaly ψ describes the actual position of the star on the orbit. Precession may affect both Ω and ω or just one of them, depending on the nature of the external potential.

A spherical stellar cusp induces a precession only on the argument of pericentre (ω), because the potential is spherical and all non-spherical effects cancel out. The main effect of this precession is pericentre advance (e.g. Šubr & Haas 2012).

The orbits of disc stars precess on a timescale (Ivanov et al. 2005; Löckmann et al. 2008; Löckmann et al. 2009; Gualandris et al. 2012)

$$T_{\rm cusp} = \frac{m_{\rm BH}}{M_{\rm cusp}}\, T_{\rm orb}\, f(e), \tag{18}$$

where $m_{\rm BH}$ is the mass of the SMBH, $T_{\rm orb}$ is the orbital period of a disc star, $M_{\rm cusp}$ is the mass of the cusp inside the stellar orbit, and $f(e) = \frac{1+\sqrt{1-e^2}}{\sqrt{1-e^2}}$ is a function of the eccentricity e of a disc star. Precession due to a spherical mass distribution, also called *mass precession*, is retrograde, i.e. in the opposite sense to orbital motion. In the limit of $e \to 1$, mass precession becomes unimportant.

In an axisymmetric potential, corresponding to a disc (e.g., a stellar ring or a gas disc or the circumnuclear ring), a star orbiting a SMBH of mass $m_{\rm BH}$ with semi-major axis a, at an inclination i relative to a disc of radius $R_{\rm DISC}$ and mass $M_{\rm DISC}$ precesses on a timescale (Nayakshin 2005; Löckmann et al. 2008; Šubr et al. 2009):

$$T_{\rm K} \equiv \frac{m_{\rm BH}}{M_{\rm DISC}} \frac{R_{\rm DISC}^3}{a^{3/2}\sqrt{G m_{\rm BH}}}. \tag{19}$$

In this case, the equations of motion for mean orbital elements read (Šubr et al. 2009, see also Kozai 1962, Lidov 1962)

$$T_{\rm K}\sqrt{1-e^2}\frac{{\rm d}e}{{\rm d}t} = \frac{15}{8}e(1-e^2)\sin 2\omega \sin^2 i, \tag{20}$$

$$T_{\rm K}\sqrt{1-e^2}\frac{{\rm d}i}{{\rm d}t} = -\frac{15}{8}e^2 \sin 2\omega \sin i \cos i, \tag{21}$$

$$T_{\rm K}\sqrt{1-e^2}\frac{{\rm d}\omega}{{\rm d}t} = \frac{3}{4}\left\{2-2e^2+5\sin^2\omega\left[e^2-\sin^2 i\right]\right\}, \tag{22}$$

$$T_{\rm K}\sqrt{1-e^2}\frac{{\rm d}\Omega}{{\rm d}t} = -\frac{3}{4}\cos i\left[1+4e^2-5e^2\cos^2\omega\right]. \tag{23}$$

In these equations, we chose the plane of the disc that perturbs the stellar orbits as a reference plane. Energy conservation implies that a is approximately constant.

If $i = 0$ (i.e. the star is coplanar with the disc generating the external potential), then only the longitude of the node Ω and the argument of pericentre ω are affected, as all the terms $\propto \sin i$ cancel out. Furthermore, any precession of Ω does not affect the other properties of the orbit, as the plane of the stellar orbit and the plane of the perturbing disc coincide.

If $0 < i < 90^\circ$, then all four quantities (e, i, ω and Ω) are expected to change. Finally, if $i = 90^\circ$, only e and ω are expected to change, as an effect of the perturbation.

It can be shown that the change of both eccentricity and inclination with time is periodic, describing the so called 'Kozai cycles' (Kozai 1962). The change in eccentricity during each 'Kozai cycle' is particularly large if the initial inclination i is high.

If the axisymmetric potential is not the only potential that perturbs the stars, but it combines with a spherical cusp, then things change significantly. The spherical cusp enhances the change in the argument of pericentre. In presence of the spherical cusp, equation 22 can be rewritten as (Ivanov et al. 2005)

$$T_{\rm K}\sqrt{1-e^2}\frac{{\rm d}\omega}{{\rm d}t} = \frac{3}{4}\left\{2-2e^2+5\sin^2\omega\left[e^2-\sin^2 i\right]\right\}(1-\kappa)^{-1}. \tag{24}$$

The term κ is due to the spherical cusp, and can be expressed as (Ivanov et al. 2005)

$$\kappa = \tilde{\kappa}\left(\frac{T_{\rm K}}{T_{\rm orb}}\right)\left(\frac{M_{\rm cusp}(<a)}{m_{\rm BH}}\right), \tag{25}$$

where $\tilde{\kappa}$ is a numeric constant (whose value depends on the shape of the spherical cusp) and $M_{\rm cusp}(<a)$ is the total mass of stars inside a sphere of radius a (i.e. equal to the semi-major axis of the orbit of the considered star).

It can be shown (Ivanov et al. 2005) that if κ is above a certain threshold (i.e. if the spherical cusp is particularly massive with respect to the other involved quantities), then Kozai oscillations are dramatically damped. Thus, the value of the eccentricity remains very close to the initial value.

If $M_{\rm cusp} > 0.1\,M_{\rm DISC}$, the only remaining effect of the gravitational influence of the perturbing disc on the stellar orbits is the precession of the ascending node with frequency (Šubr et al. 2009)

$$\frac{{\rm d}\Omega}{{\rm d}t} = -\frac{3}{4}\cos i \frac{1+\frac{3}{2}e^2}{\sqrt{e^2}}\,T_{\rm K}^{-1}. \tag{26}$$

From equation 26, it is apparent that the precession of the ascending node depends on the semi-major axis of the stellar orbit ($\frac{{\rm d}\Omega}{{\rm d}t} \propto T_{\rm K}^{-1} \propto a^{3/2}$). In particular, stars with larger a will precess faster than stars with smaller a. This is very important for the early-type stars that form the CW disc around Sgr A*, for the following reason. If $i = 0$, this precession has no effect on the inclination of the stellar orbits, as the plane of the perturbing disc and the plane of the star orbit are the same. Instead, if $i > 0$, the orbits of the outer stars will become inclined with respect to the orbits of the inner stars, producing a warp in the stellar disc, and increasing its thickness.

Fig. 23 shows a comparison of the relevant precession timescales in the case of our GC.

4.2 Relativistic effects

According to general relativity, the SMBH itself is a source of precession for the stellar orbits. In the case of a non-rotating black hole, a star orbiting the SMBH experiences an advance of the orbital periapse by an angle

$$\delta\omega_S = \frac{6\pi}{c^2}\frac{Gm_{\rm BH}}{a(1-e^2)}, \tag{27}$$

which depends on the mass of the SMBH and the orbital elements of the star. This apsidal precession (also called geodetic, de Sitter, relativistic or Schwarzschild precession) is an in-plane prograde precession that operates on a time-scale (see Gualandris & Merritt, 2009; Merritt, 2013):

$$\begin{aligned} T_S &= \frac{\pi T_{\rm orb}}{\delta\omega_S} = \frac{T_{\rm orb}\,c^2}{6}\frac{a(1-e^2)}{Gm_{\rm BH}} \\ &= 1.3\times10^3{\rm yr}\left(1-e^2\right)\left(\frac{a}{\rm mpc}\right)^{5/2}\left(\frac{4\times10^6{\rm M}_\odot}{m_{\rm BH}}\right)^{3/2} \end{aligned} \tag{28}$$

In the case of our GC, Schwarzschild precession is large enough to potentially be detectable via ~ 10 years monitoring of identified stars at $\lesssim 10$ mpc separations from the SMBH (Rubilar & Eckart, 2001), see also Fig. 23.

In the case of a rotating black hole, the coupling between the spin of the SMBH and the orbital angular momentum of the stars leads to additional sources of precession, both in-plane and out-of plane. The spin and quadrupole moment contributions to the in-plane precession are, respectively, (Merritt et al., 2010):

$$\delta\omega_J = -\frac{8\pi}{c^3}\chi\left[\frac{Gm_{\rm BH}}{a(1-e^2)}\right]^{3/2}\cos i \tag{29}$$

$$\delta\omega_Q = -\frac{3}{2}\frac{\pi}{c^4}\chi^2\left[\frac{Gm_{\rm BH}}{a(1-e^2)}\right]^2(1-3\cos^2 i) \tag{30}$$

where $\chi = J/(Gm_{\rm BH}^2/c^2)$ is the dimensionless spin parameter of the SMBH. The contributions to the precession of the orbital plane are (Merritt et al., 2010):

$$\delta\Omega_J = \frac{4\pi}{c^3}\chi\left[\frac{Gm_{\rm BH}}{a(1-e^2)}\right]^{3/2} \tag{31}$$

$$\delta\Omega_Q = -\frac{3\pi}{c^4}\chi^2\left[\frac{Gm_{\rm BH}}{a(1-e^2)}\right]^2\cos i. \tag{32}$$

Of these terms, only the quadrupole term is dependent on inclination. The associated timescales are:

$$\begin{aligned} T_J &= \frac{T_{\rm orb}}{4\chi}\left[\frac{c^2 a(1-e^2)}{Gm_{\rm BH}}\right]^{3/2} \\ &= 1.4\times10^5\,{\rm yr}\left(1-e^2\right)^{3/2}\chi^{-1}\left(\frac{a}{\rm mpc}\right)^3\left(\frac{4\times10^6\,{\rm M}_\odot}{m_{\rm BH}}\right)^2 \end{aligned} \tag{33}$$

and

$$\begin{aligned} T_Q &= \frac{T_{\rm orb}}{3\chi^2}\left[\frac{c^2 a(1-e^2)}{Gm_{\rm BH}}\right]^2 \\ &= 1.3\times10^7\,{\rm yr}\left(1-e^2\right)^2\chi^{-2}\left(\frac{a}{\rm mpc}\right)^{7/2}\left(\frac{4\times10^6\,{\rm M}_\odot}{m_{\rm BH}}\right)^{5/2}. \end{aligned} \tag{34}$$

Detection of spin effects in the GC can in principle come from observations of plane precession of stars in the inner mpc. However, gravitational interactions between stars in this region are likely to induce orbital precession of the same approximate amplitude as the precession due to frame dragging, hampering detection. Assuming near-maximal spin for the Milky Way SMBH, detection of frame-dragging precession may be feasible after a few years monitoring with an instrument like GRAVITY (Eisenhauer et al., 2009) for orbits in the radial range $0.2-1$ mpc. At smaller radii

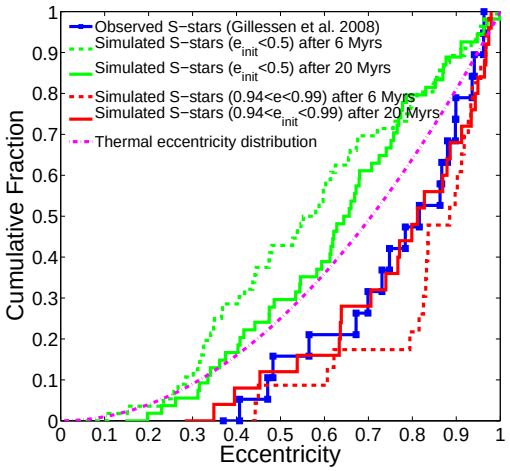

Fig. 24 Cumulative distribution of eccentricities for stars with initially low (green) and high (red) eccentricities, after 6 Myr (dashed) and 20 Myr (solid) of evolution in a relaxed cusp of stars and remnants. The distribution for the S-stars from the sample of Gillessen et al. (2009a) is shown for comparison, as is a line giving the theoretical thermal distribution. The distribution predicted by the binary breakup model is the most consistent with the data. Fig. 2 of Perets et al. (2009).

the number of stars is too small, while at larger radii the star-star and star-remnant perturbations dominate over relativistic effects (Merritt et al., 2010).

4.3 Relaxation processes: two-body relaxation, resonant relaxation

In an isotropic system, the angular momentum of the stars evolves both due to the stochastic two-body relaxation (e.g. Binney &Tremaine, 1987) and to the resonant relaxation (Rauch &Tremaine, 1996). Nonresonant two-body relaxation operates on a timescale (Binney &Tremaine, 1987)

$$T_{\rm NR} = \frac{0.34\,\sigma^3}{G^2\,m\,\rho\,\ln\Lambda} \approx 10^{10}\,{\rm yr}\left(\frac{\sigma}{200\,{\rm km\,s^{-1}}}\right)^3\left(\frac{10^6\,{\rm M_\odot\,pc^{-3}}}{\rho}\right)\left(\frac{\rm M_\odot}{m}\right)\left(\frac{15}{\ln\Lambda}\right) \quad (35)$$

where ρ is the stellar density, σ is the one-dimensional velocity dispersion of the stars, m is the mass of a single star, and $\ln\Lambda$, the Coulomb logarithm, is a numerical factor that corrects for the divergent force in a infinite homogeneous system. Over a time $T_{\rm NR}$, gravitational encounters between stars act to change orbital energies and angular momenta. In particular, angular momentum changes with time in a random walk fashion.

Resonant relaxation occurs when the symmetries of the potential act to constrain the stellar orbits (e.g. closed ellipses in a Kepler potential, or planar rosettes in a spherical one). As long as the symmetry is approximately maintained, gravitational interactions between stars are highly correlated and stars experience coherent

torques. The coherence timescale $T_{\rm coh}$ (the time over which orbits can be considered fixed), is the time associated with the most rapid source of precession of the stellar orbits. Sources of precession (see also section 4.1) are: mass precession, due to the stellar mass distributed around the SMBH, relativistic precession and precession due to resonant relaxation itself. The mass coherence time is always shorter than the self-coherence time, but sufficiently close to the SMBH relativistic precession must dominate.

For a time Δt such that $T_{\rm orb} \ll \Delta t \ll T_{\rm coh}$, the so called *coherent resonant relaxation* is characterised by changes in the angular momentum of a star at a roughly constant rate

$$\frac{dJ}{dt} \sim \sqrt{N}\frac{Gm}{a}, \tag{36}$$

where a is the star's semi-major axis. The angular momentum change is

$$(\Delta J/J_c)_{\rm coh} \sim \sqrt{N}\frac{Gm}{a}\frac{\Delta t}{\sqrt{Gm_{\rm BH}a}}, \tag{37}$$

where $J_c = \sqrt{Gm_{\rm BH}a}$ is the angular momentum of a circular orbit. The coherent resonant relaxation timescale can be defined as the time for which $\Delta J = J_c$

$$\begin{aligned} T_{\rm RR,coh} &= \frac{T_{\rm orb}}{2\pi}\frac{m_{\rm BH}}{m}\frac{1}{\sqrt{N}} \\ &\sim 1.5\times 10^4 {\rm yr}\left(\frac{a}{\rm mpc}\right)^{3/2}\left(\frac{10^6 {\rm M}_\odot}{m_{\rm BH}}\right)^{1/2}\left(\frac{10^{-6}}{m/m_{\rm BH}}\right)\left(\frac{10^3}{N}\right)^{1/2}. \end{aligned} \tag{38}$$

On timescales longer than $T_{\rm coh}$, the field stars precess and the direction of the torque exerted by the N stars changes (while its magnitude remains roughly unchanged). Under the assumption that the direction of the torque is essentially randomised after each $T_{\rm coh}$, the angular momentum of a test star undergoes a random walk, with step size given by the product of the torque and the coherence time. The evolution of the angular momentum in this *incoherent resonant relaxation* regime is qualitatively similar to the evolution under nonresonant two body relaxation, but can be significantly faster. This is due to the fact that the mean free path of the random walk in $\mathbf{J}$ is set by the (large) change accumulated over $T_{\rm coh}$. The incoherent resonant relaxation timescale is then defined by (e.g. Eilon et al., 2009)

$$\Delta J/J_c = (\Delta J/J_c)_{\rm coh}\sqrt{t/T_{\rm coh}} \equiv \sqrt{t/T_{\rm RR}}, \tag{39}$$

$$T_{\rm RR} = \left(\frac{J_c}{\Delta J}\right)^2_{\rm coh} T_{\rm coh}. \tag{40}$$

If the coherence time is determined by mass precession, then

$$T_{\rm RR} \approx \left(\frac{m_{\rm BH}}{m}\right) T_{\rm orb}. \tag{41}$$

If instead relativistic precession dominates,

$$T_{\rm RR} \approx \frac{3}{\pi^2}\frac{r_g}{a}\left(\frac{m_{\rm BH}}{m}\right)^2 \frac{T_{\rm orb}}{N}, \tag{42}$$

where

$$r_g = \frac{G m_{\rm BH}}{c^2} \approx 2\times 10^{-7}\left(\frac{m_{\rm BH}}{4.3\times 10^6 {\rm M}_\odot}\right) {\rm pc} \tag{43}$$

is the gravitational radius of the SMBH.

Merritt (2013) estimates the distance from the SMBH at which incoherent resonant relaxation becomes dominant over nonresonant two body relaxation. In the case of a dynamically relaxed Bahcall-Wolf cusp (Bahcall & Wolf, 1976) this distance is of about 0.06 pc, or $0.025 r_h$, where r_h represents the SMBH's influence radius. In the case of a low-density model for the innermost region of the NSC, resonant relaxation dominates inside ~ 0.18pc $\sim 0.1 r_h$, somewhat further out than in the relaxed model.

Simulations by Perets et al. (2009) show that perturbations from the compact remnants tend to randomise stellar orbits in the GC, partially erasing the dynamical signatures of their origin. The simulations follow the dynamical evolution of a population of stars in the inner ~ 0.3 pc of the Galaxy against a cusp of stars and remnants. The initial conditions are based on the collisionally relaxed cusp of stars and remnants by Hopman & Alexander (2006), and intend to represent products of both the *in situ* formation scenario and the tidal breakup scenario. The former tends to produce stars with low to moderate eccentricities, while the latter leaves stars bound to the SMBH on highly eccentric orbits. The eccentricities of the initially highly eccentric stars evolve, in 20 Myr, to a distribution that is consistent with the observed eccentricity distribution. In contrast, the eccentricities of the initially more circular orbits fail to evolve to the observed values in 20 Myr, arguing against the disc migration scenario. Fig. 24 shows the final cumulative eccentricity distribution of the stars for the two models under consideration and at two different times: 6 Myrs and 20 Myrs. These times are chosen to represent the age of the current CW disc and the canonical S-star lifespan. The binary breakup scenario after 20 Myr of evolution is found to be the preferred model for the origin of the S-stars. In contrast, the disc migration scenarios seem to be excluded (for the given assumptions), since they have major difficulties in explaining the large fraction of eccentric orbits observed for the S-stars in the GC.

Resonant relaxation against the stellar remnants acts to isotropise the inclination distribution of the captured stars for all models, and can not therefore be used to discriminate between them. However, randomisation of the inclinations requires at least 4 Myr when starting from a single plane configuration, and can be used to constrain the lifetime of the S-stars in the *in situ* model.

Monte Carlo simulations by Antonini & Merritt (2013) of the orbital evolution of the S-stars show that the distribution of the semi-major axis a and eccentricity e of the S-stars predicted by the binary disruption model is consistent with the observed orbits even when relativistic effects are considered (see section 4.2 for details). Even though most of the orbits lie initially below the Schwarzschild Barrier (i.e. the locus in the (a, e) plane where resonant relaxation is ineffective at changing

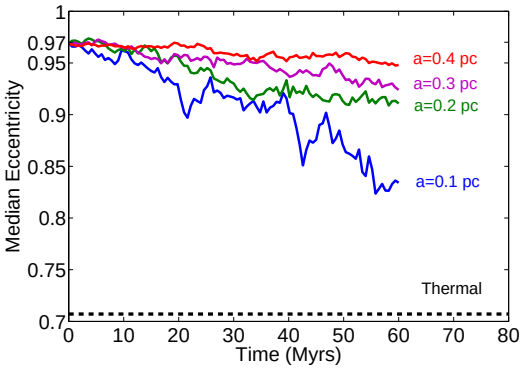

Fig. 25 Evolution of the median eccentricity of a population of B-stars in the central 0.5 pc of the GC, for different initial distances from the SMBH. Relaxation is driven by a cusp of remnants distributed between 0.04 and 0.8 pc. Only stars with initial eccentricity in the range 0.95 – 0.99 are selected to represent captured stars. Fig.2 of Perets & Gualandris (2010).

eccentricities, Merritt et al. 2010), orbits starting sufficiently close to the barrier are sometimes able to penetrate it, diffusing above and reaching a nearly thermal eccentricity distribution. After ~ 20 Myr of evolution the distributions are consistent with the observed ones, if a dynamically relaxed model for the background stellar cusp is assumed. This result is particularly interesting given that relaxed models of the GC are currently disfavored by observations (Buchholz et al., 2009; Do et al., 2009) and by some theoretical arguments (Merritt, 2010; Antonini et al., 2011; Gualandris & Merritt, 2012).

4.4 Impact of relaxation and precession on the early-type stars

Precession of the stellar orbits, due to either stellar perturbations or relativistic effects, has a number of implications for the evolution of the early-type stars in the GC. We here discuss the most relevant to constrain the formation scenarios presented in the previous sections:

Dependence of mean orbital eccentricity on distance. The resonant relaxation timescale increases with distance from the SMBH (e.g. Hopman & Alexander, 2006). Therefore, stars captured/formed further away from the SMBH are expected to have a less relaxed eccentricity distribution than stars closer to the black hole (Perets & Gualandris, 2010). As a result, relaxation processes will give rise, over time, to a correlation between the distance from the SMBH and the orbital eccentricity. Far from the SMBH, where the resonant relaxation timescales are much longer than the typical lifetimes of the B-stars, stars should retain their original eccentricity distribution, i.e., highly eccentric orbits for captured stars after a binary disruption, and likely low eccentricity orbits for stars formed in a stellar disc. Closer to the SMBH, on the other hand, captured stars could have a relaxed (i.e. thermal) eccentricity distribution even after short times. These predictions have been confirmed by the simulations of Perets & Gualandris (2010), who find an increase of the mean eccentricity of the stars with distance from the SMBH (see Fig. 25). Therefore, the

binary capture scenario provides a qualitatively unique signature, in which the typical eccentricity is an increasing function of distance, which can be tested against observations of the B-stars. However, stars with large semi major axes have large orbital periods and it is difficult to determine their dynamical accelerations from astrometric data, from which orbital parameters are derived. Madigan et al. (2014) developed a statistical method which uses only sky positions and proper motions to infer the orbital eccentricities of a stellar population around the SMBH. They confirm the results by Perets & Gualandris (2010) regarding the binary disruption scenario that stellar orbits remain at very high eccentricities outside ~ 0.1 pc. Similarly, stars formed with small eccentricities, as in the case of an in-situ formation from a dissolved disc, maintain small eccentricities at large distances. Applying the statistics to a sample of B-stars at projected radii $\sim 0.004-1$ pc from the SMBH they find that stars with K-band magnitudes $14 \lesssim m_{\rm K} \lesssim 15$ (i.e masses of $15-20\,{\rm M}_\odot$ and ages of $8-13$ Myr) match well to an in-situ formation origin, while those with $m_{\rm K} \geq 15$ (corresponding to masses $\leq 15\,{\rm M}_\odot$ and ages ≥ 13 Myr), if isotropically distributed, form a population that is more eccentric than thermal, suggestive of a binary-disruption origin.

Thickness/warping of the CW disc. As discussed in Sect. 2.2, recent observations (Bartko et al. 2009; Lu et al. 2009; Bartko et al. 2010; Do et al. 2013; Lu et al. 2013; Yelda et al. 2014) show that the opening angle of the CW disc is only $\sim 10^\circ - 14^\circ$, but about half (or even ~ 80 per cent, Yelda et al. 2014) of the early-type stars in the inner $1-10$ arcsec ($0.04-0.4$ pc) do not belong to the CW disc. Furthermore, the probability of early-type stars being members of the CW disc decreases with increasing projected distance from Sgr A* (Bartko et al. 2009; Lu et al. 2009). Finally, the CW disc does not seem a flat structure, but rather a significantly warped ($\sim 64^\circ$, Bartko et al. 2009) and tilted object (but see Yelda et al. 2014 for a different result). Recent studies (e.g. Šubr et al. 2009; Haas et al. 2011a; Haas et al. 2011b; Mapelli et al. 2013) suggest a reasonable interpretation for such observations: the precession exerted by a slightly misaligned gas disc (or ring) enhances the inclinations of the outer stellar orbits with respect to the inner stellar orbits. Thus, while the inner disc remains quite coherent, the outer stellar orbits change angular momentum orientation till they may even lose memory of their initial belonging to the same disc. The result is a tilted/warped disc, which is being dismembered in its outer parts.

The perturbing ring may be the CNR (Šubr et al. 2009; Haas et al. 2011a; Haas et al. 2011b, see[4] Fig. 26) or a transient gas ring that forms from the disruption of a low-angular momentum molecular cloud (Mapelli et al. 2013).

Mapelli et al. (2013) is the first study in which the gas perturber is represented by 'live' SPH particles, rather than by a rigid potential. In particular, Mapelli et al. (2013) simulate the perturbations exerted on a thin stellar disc (with outer radius ~ 0.4 pc) by a molecular cloud that falls towards the GC and is disrupted by the SMBH. The initial conditions for the stellar disc were drawn from the results of

[4] The fiducial run reported in Haas et al. (2011a) includes 200 early-type stars (modelled as N-body particles), a SMBH with mass $m_{\rm BH} = 4 \times 10^6\,{\rm M}_\odot$ (modelled as Keplerian potential), a CNR with mass $0.3\,m_{\rm BH}$ (modelled as a single particle), a stellar cusp with mass $M_{\rm cusp} = 0.03\,m_{\rm BH}$ (modelled as a rigid potential).

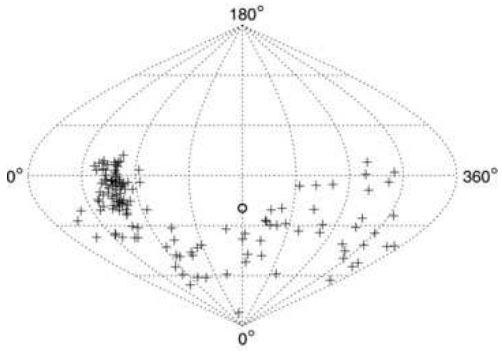

Fig. 26 Angular momenta of individual stars in the young stellar disc after 6 Myr of orbital evolution, integrated through *N*-body simulations (Haas et al. 2011a). The initial state is denoted by an empty circle. The plot is in sinusoidal projection. Latitude on the plots corresponds to i while longitude is related to Ω. Only stars with mass $m > 12\,\mathrm{M}_\odot$ are displayed. From Fig. 2 of Haas et al. (2011a).

previous simulations (Mapelli et al. 2012) of molecular cloud infall and disruption in the SMBH potential. Mapelli et al. (2013) find that most of the gas from the disrupted molecular cloud settles into a dense and irregular disc surrounding the SMBH (see Fig. 27). If the gas disc and the stellar disc are slightly misaligned ($\sim 5-20^\circ$), the precession of the stellar orbits induced by the gas disc significantly increases the inclinations of the stellar orbits (by a factor of $\sim 3-5$ in 1.5 Myr) with respect to the normal vector to the disc. Furthermore, the distribution of orbit inclinations becomes significantly broader (see Fig. 27).

Origin of the S-cluster. Löckmann et al. (2008) propose that the orbits of the S-stars are the result of precession and Kozai resonance due to the interaction between two stellar discs. In this scenario, binary stars in the young stellar disc are first moved to highly eccentric orbits by Kozai resonance with a second stellar disc and then disrupted by the SMBH at pericentre, as in the binary breakup model. The inclusion of a stellar cusp, however, has been shown to damp Kozai oscillations in the disc (Chang 2009; Löckmann et al. 2009, see Fig. 28), which are a key factor in this scenario (see also Gualandris et al., 2012, for a discussion).

Schwarzschild Barrier. Relativistic precession limits the ability of torques from the stellar potential to modify orbital angular momenta via resonant relaxation. This results in a sort of barrier (Merritt et al., 2011) in the (a, e) plane which sets an effectively maximum value of the eccentricity at each value of the semi-major axis (see Fig. 29). The Schwarzschild Barrier inhibits extreme-mass-ratio-inspirals and leads to capture rates that are $\sim 10-100$ times lower than in the non-relativistic case.

Eccentric disc instability. An eccentric stellar disc around the SMBH is expected to exhibit an instability as a result of the eccentricity dependence of the mass precession timescale (Eq. 18). Retrograde precession due to the presence of a stellar cusp induces coherent torques that amplify deviations of individual orbital eccentricities from the average, and thus drives all eccentricities away from their initial value (Madigan et al., 2009), producing a bimodal eccentricity distribution. Gualandris et al. (2012) study the evolution of the ring of stars formed in the GC from fragmentation of the gas disc deposited by an inspiralling molecular cloud. The stars are subject to the potential of the SMBH, a stellar cusp and the parent gas disc. While

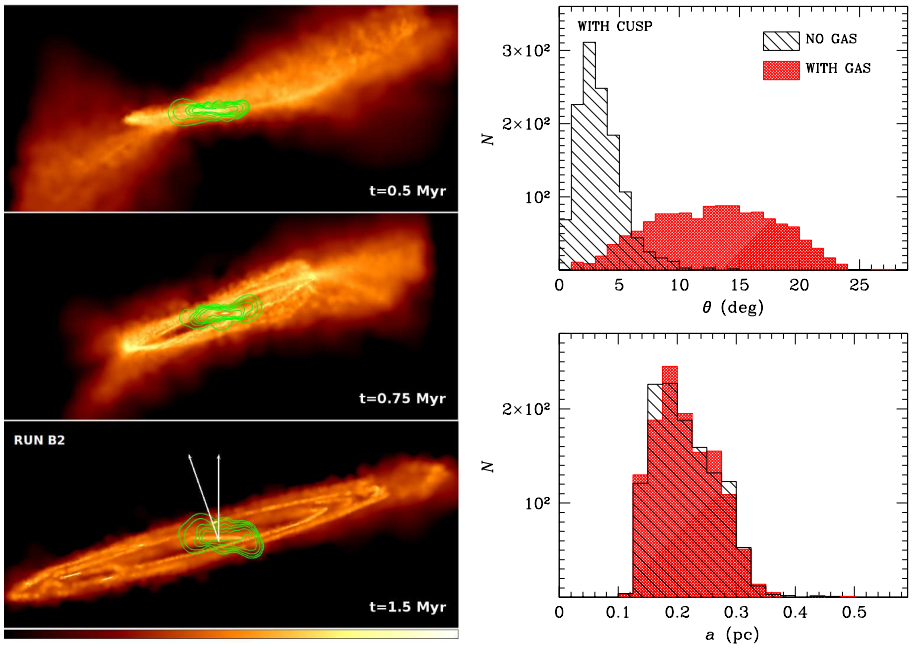

Fig. 27 Left-hand panel: Projected density of gas in run B2 of Mapelli et al. (2013) at $t = 0.5, 0.75$ and 1.5 Myr in the top, central and bottom panel, respectively. In this simulation a pre-existing stellar disc is perturbed by the joint effect of the stellar cusp (modelled as a rigid potential) and of a second molecular cloud (modelled as SPH particles)disrupted by the SMBH. The color map is logarithmic, ranging from 2×10^{-2} to 2×10^{10} $M_\odot$ pc^{-3}. The contours show the projected density of stars in the stellar disc. The box size is 4.0×1.8 pc. The projection was chosen so that the total angular momentum of the stellar disc is aligned to the vertical axis of the plot. The two white arrows in the bottom panel show the direction of the total angular momentum of the stellar disc and the total angular momentum of the outer gas disc. The length of the arrows is arbitrary. Fig. 4 of Mapelli et al. (2013). Right-hand panel: distribution of inclinations (θ) and semi-major axes (a) of the disc stars at $t = 1.5$ Myr in the top and bottom panel, respectively. From the N-body/SPH simulations of Mapelli et al. (2013). Cross-hatched red histogram: simulation including a spherical cusp and a perturbing gas disc (run B2); hatched black histogram: simulation with only a spherical cusp (run A2). From Fig. 9 of Mapelli et al. (2013).

the ring retains the original distribution of semi-major axes, and therefore also the initial inner and outer radius, the distribution of eccentricities evolves in time due to the onset of the eccentric disc instability. Torques exerted by other stars in the ring result in a change in the magnitude of the angular momentum and, as a consequence, in the eccentricity. As stars evolve away from the average eccentricity, a bimodal distribution is established, with a primary peak at $e \sim 0.1$, a secondary peak at $e \sim 0.5$ and a tail that extends to $e \sim 0.7$ (see Fig. 30). This is qualitatively consistent with the distribution found for the CW disc stars (Bartko et al., 2009).

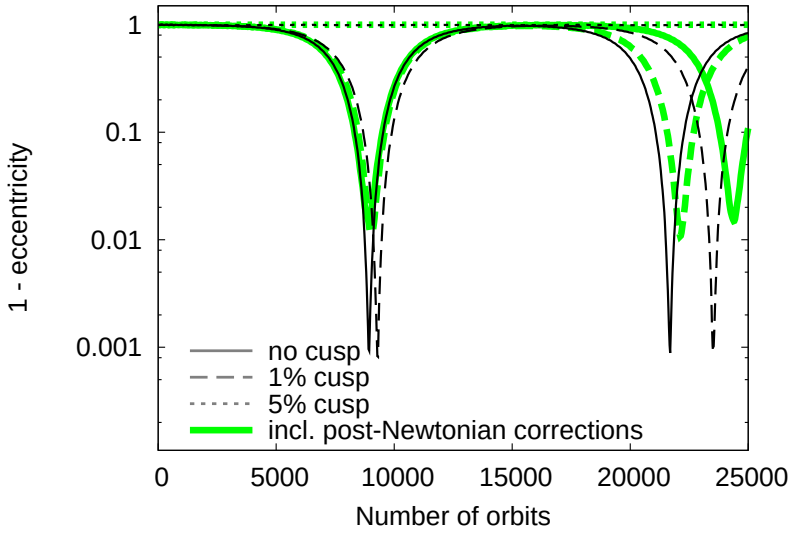

Fig. 28 Eccentricity evolution of a test star undergoing Kozai resonance driven by a fictitious $1.5 \times 10^4\,\mathrm{M}_\odot$ particle representing a disc potential. Both particles have initially circular orbits about the $3.5 \times 10^6\,\mathrm{M}_\odot$ SMBH with semi-major axes of 0.04 and 0.16 pc, respectively. Simulations reported by Löckmann et al. (2009). Solid black line: models without cusp; dashed (dotted) line: models with 1 per cent (5 per cent) of the extended cusp mass observed in the Galactic Centre (modelled as a smooth potential). Each curve is accompanied by a corresponding thick green curve that represents a respective integration including post-Newtonian (PN) terms up to 2.5 PN to account for the effects of general relativity. While relativistic effects damp the Kozai effect at high eccentricities, a stellar cusp with mass of a few per cent of the observed value is sufficient to damp any eccentricity growth (dotted line). Fig. 6 of Löckmann et al. (2009).

4.5 Perturbations from an intermediate-mass black hole

In the cluster inspiral scenario with an IMBH, stars are naturally deposited in a disc structure in the same plane as the IMBH orbit and with orbital elements similar to those of the IMBH itself. The inspiral of the IMBH is expected to slow down or stall completely at a distance $\sim 10(q/10^3)\,\mathrm{mpc}$ from the SMBH, where q is the ratio of IMBH to SMBH masses (Baumgardt et al., 2006; Matsubayashi et al., 2007; Löckmann et al., 2008); this distance is comparable to the sizes of the S-star orbits if $q \approx 10^3$, i.e., if $M_{\mathrm{IMBH}} \sim 10^{3.5}\,\mathrm{M}_\odot$. At this separation, the total binding energy in background stars within the IMBH orbit is comparable to that of the IMBH itself and stars are easily ejected by the slingshot mechanism, thereby causing the frictional force to drop.

The orbit of the IMBH is likely to be quite eccentric at this stage, depending on the initial orbit of the cluster and the detailed history of interactions with the stars (Baumgardt et al., 2006; Matsubayashi et al., 2007). If the eccentricity is not so high ($e \lesssim 0.99$) that energy loss due to emission of GWs results in coalescence

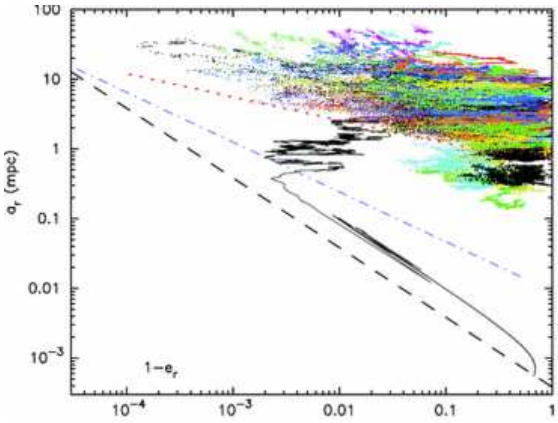

Fig. 29 Trajectories, over a time interval of 2 Myr, of stellar-mass black holes orbiting the SMBH as they undergo gravitational encounters with each other. Dashed line: capture radius around the SMBH; dotted line: the Schwarzschild barrier; dot-dashed line: locus in the $a-e$ plane where angular momentum loss due GW emission dominates over gravitational encounters. From Fig. 5 of Merritt et al. (2011).

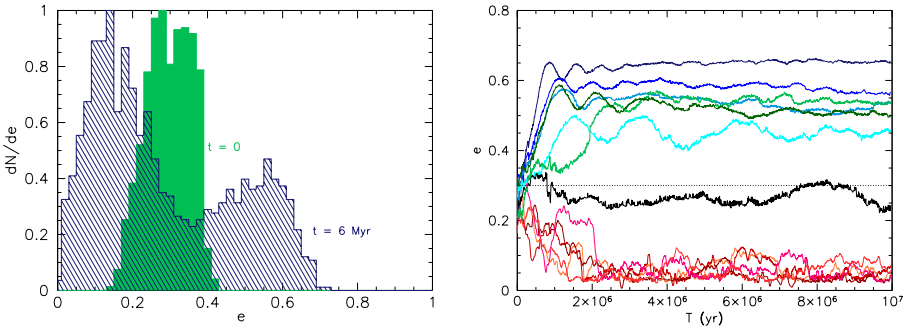

Fig. 30 (Left) Eccentricity distribution of a ring stars at the start of the integration (filled area) and after 6 Myr of evolution (hatched area), subject to the potential of the SMBH, a spherical stellar cusp and the parent gas disc. Adapted from Fig. 5 of Gualandris et al. (2012). (Right) Evidence for the eccentric disc instability (Madigan et al., 2009) in a random subset of stars in the simulation of Gualandris et al. (2012). The time-scale for the process is about 1 Myr. Fig. 6 of Gualandris et al. (2012).

in less than 10^8 years, the semi-major axis of the IMBH orbit remains essentially unchanged for times comparable to the S-stars main-sequence lifetimes. Prolonged gravitational interactions with the IMBH can then scatter the young stars out of the thin disc into which they were originally deposited (Merritt et al., 2009). Fig. 31 shows the result of the simulations of Merritt et al. (2009) following the evolution of a disc of stars around an IMBH with mass ratio of $q = 0.001$. An initially planar configuration for the stars is quickly (~ 1 Myr) turned into an isotropic configuration by perturbations from the IMBH. An eccentricity larger than ~ 0.2 is necessary for stellar inclinations to be excited.

The IMBH also induces evolution in the eccentricities and energies (semi-major axes) of the stars. Eccentricities were found to tend toward a thermal distribution on a timescale of about 0.1 Myr for $q \gtrsim 2.5 \times 10^4$, as illustrated in Fig. 32. The final distribution of stellar semi-major axes depends on the assumed size of the

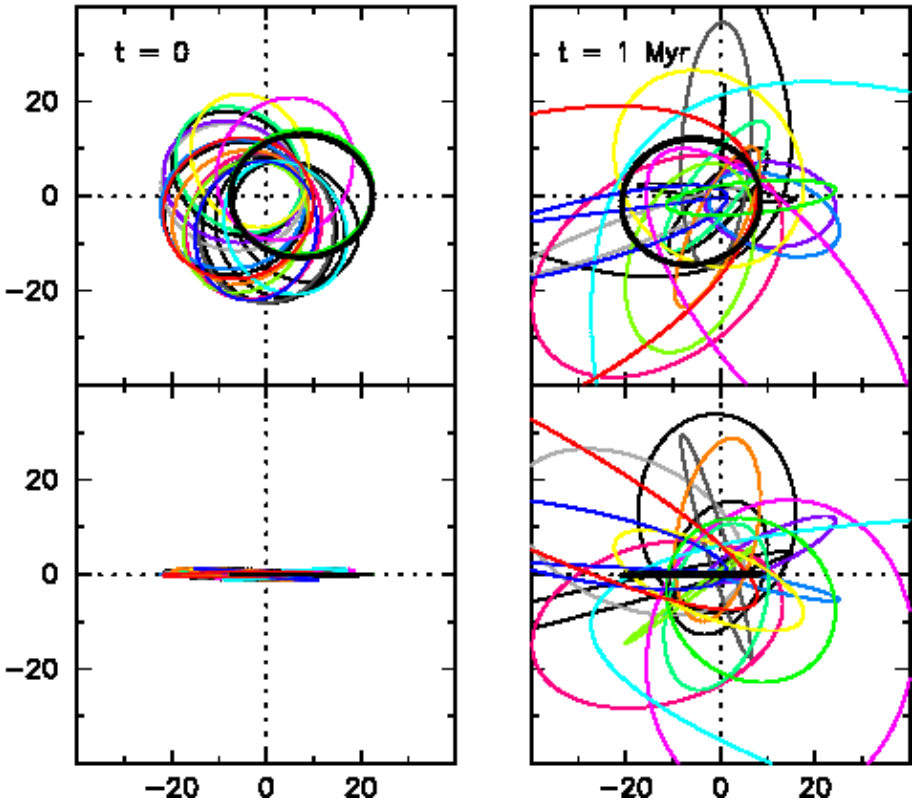

Fig. 31 Initial (left) and final (right, after 1 Myr) orbits of stars in a simulation with IMBH semi-major axis $a = 15\,\mathrm{mpc}$, eccentricity $e = 0.5$, mass ratio $q = 0.001$. Top panels show the view looking perpendicular to the IMBH orbital plane and bottom panels are from a vantage point lying in this plane. The IMBH orbit is the heavy black curve in all panels; the unit of length is milli-parsecs. The initially disc-like, co-rotating distribution of stars is converted, after 1 Myr, into an approximately isotropic distribution of orbits with a range of eccentricities, similar to what is observed for the S-stars. Many of the orbits "flip" in response the perturbation from the IMBH, i.e. their angular momentum vector changes by 180°. Fig. 1 of Merritt et al. (2009).

IMBH orbit, but stars with apastron distances as small as the periastron distance of the IMBH are naturally produced. Therefore, tightly bound orbits like those of the innermost S-stars, e.g., S2, require an IMBH orbit with a periastron distance of about 10 mpc.

If the cluster inspiral scenario with an IMBH is deemed otherwise viable, the results of Merritt et al. (2009) show that the model can also naturally reproduce the random and eccentric character of the stellar orbits, and all in a time that is less than stellar evolutionary timescales – thus providing an essentially complete explanation for the paradox of youth of the S-stars.

In order to avoid making the current epoch special, the IMBH inspiral rate needs to be roughly equal to the inverse of the S-star lifetimes, i.e $\sim 10^7 \mathrm{yr}^{-1}$. Such a rate

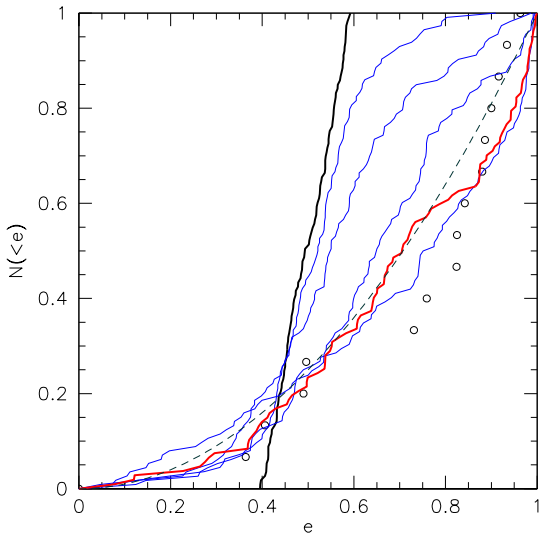

Fig. 32 Evolution of the distribution of stellar orbital eccentricities in a set of simulations with IMBH orbital parameters $q = 5 \times 10^{-4}$, $a = 15\,\mathrm{mpc}$, $e = 0.5$. The initial distribution (thick black line) evolves in time (thin blue lines). After 1 Myr, the distribution (thick red line) is consistent with a thermal distribution (dashed line). Open circles represent the S-stars observed distribution (Gillessen et al., 2009a). Fig. 3 of Merritt et al. (2009).

has been proposed by Portegies Zwart (2006) based on a semi-analytic model of the formation and evolution of star clusters in the galactic bulge.

Gualandris & Merritt (2009) study the short- and long-term effects of an IMBH on the orbits of the S-stars, for different choices of IMBH parameters: mass, semi-major axis, eccentricity, spatial orientation. On long timescales, perturbations from an IMBH can result in : (i) randomization of the inclinations of the stars; (ii) ejection of stars from the region; (iii) scattering of stars onto plunging orbits that result in tidal disruption in the SMBHs tidal field; and (iv) secular effects like Kozai cycles. When considering individual stars, stars with initially large eccentricities are the most susceptible to perturbations.

The result on the distribution of orbital elements for the S-cluster depends on the IMBH parameters. The distribution of S-star semi-major axes and eccentricities are significantly altered from their currently observed form by IMBHs with masses greater than $\sim 1000\,\mathrm{M}_\odot$ if the IMBH–SMBH semi-major axis lies in the range $3 - 10\,\mathrm{mpc}$.

These results can be used to constrain the allowed parameters of an IMBH–SMBH binary at the Galactic centre. The region of parameter space corresponding to masses $\gtrsim 2000\,\mathrm{M}_\odot$ and initial semi-major axes $\sim 2 - 10\,\mathrm{mpc}$ can be excluded. Such region is represented by the shaded box in Fig. 33. All shaded areas in the figure mark regions of parameter space that can be excluded based on theoretical or observational arguments. Interestingly, the IMBH parameters required for an efficient randomization of inclinations (Merritt et al., 2009) in the cluster infall scenario ($M_{\mathrm{IMBH}} \gtrsim 1500\,\mathrm{M}_\odot$ for the simulated range of separations $10 - 50\,\mathrm{mpc}$ - see rectangular box in Fig. 33) are consistent with all the constraints placed so far.

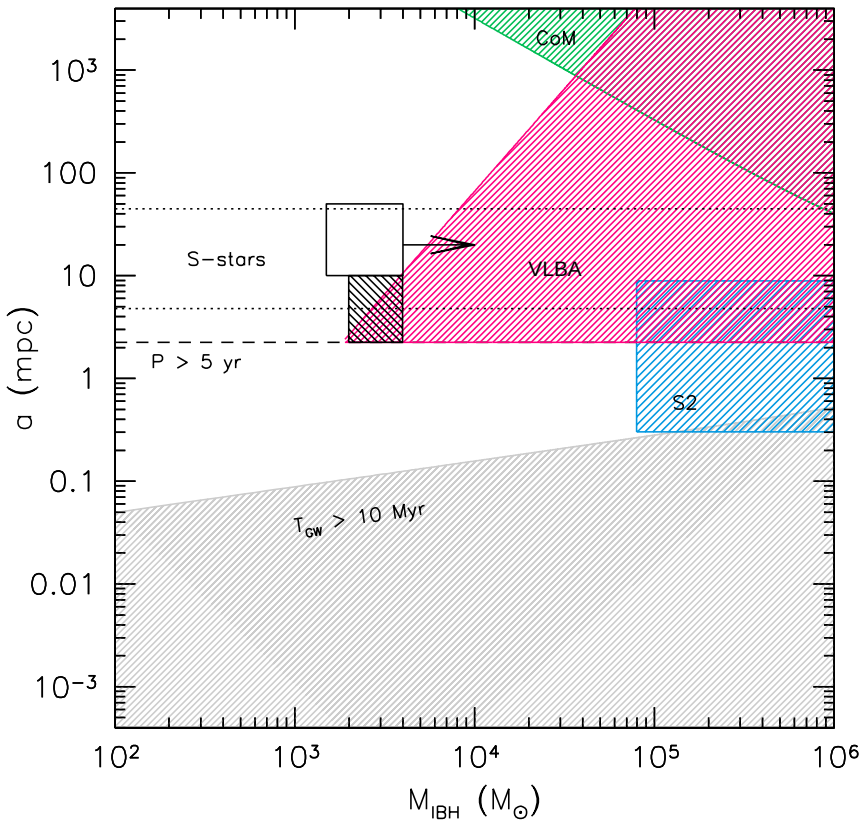

Fig. 33 Constraints on the orbital parameters of a hypothetical IMBH in the Galactic region. The shaded areas represent regions of parameter space that can be excluded based on observational or theoretical arguments. The dotted lines mark the distances at which the S-stars are currently observed. The dashed line represents the five year orbital period corresponding to discoverable systems. The parameters enclosed in the empty rectangular box are required for an efficient randomization of inclinations in the cluster infall scenario (Merritt et al., 2009). The small rectangular region just below the empty box represents the parameter space excluded by Gualandris & Merritt (2009). Adapted from Fig. 13 of Gualandris & Merritt (2009).

Gualandris et al. (2010) study short-term perturbations of an IMBH on star S2, (Schödel et al., 2002; Ghez et al., 2003) whose short orbital period ($P \sim 16$ yr) and large eccentricity ($e \sim 0.88$) (Gillessen et al., 2009a) make it an ideal candidate to detect small deviations from a purely Keplerian orbit. Deviations from a purely Keplerian orbit are expected for star S2 due to relativistic and Newtonian precession (see section 4.1). Their only observable effect is an in-plane advance of the pericentre. None of the other classical elements are affected by precession.

In the absence of spin effects, which would not anyway manifest themselves at the distance of S2 (Merritt et al., 2010), only non spherically symmetric perturbations like those due to an IMBH are able to produce changes in the angular momentum of S2's orbit, leading to changes in eccentricity and the inclination of the orbital plane. Perturbations due to the other S-stars have been shown to be negligible. Combining *N*-body simulations with observational orbital fitting techniques, Gualandris et al. (2010) find that an IMBH more massive than $\sim 1000\,\mathrm{M}_{\odot}$ at a distance of $1-5\,$mpc is potentially discoverable at S2's next pericentre passage in 2018. Evidence for an IMBH would appear as significant deviations from the assumed point mass relativistic potential in S2's orbital fit.

5 Origin and evolution of the G2 cloud

In Sect. 2.4, we discussed the orbital properties of the dusty object G2. Several models were proposed to explain the formation of G2. Despite this, the nature of the G2 cloud remains unclear, because none of the proposed models accounts for all its properties in a satisfactory way. The main open questions are (see Burkert et al. 2012): (i) is G2 only a cloud or is there a compact source hidden inside the gas shell? (ii) where did G2 come from? (iii) why is the orbit so eccentric? (iv) which are the processes that affect G2 close to pericentre? (v) how many clouds like G2 are currently orbiting Sgr A*?

In the following Sections, we review the most popular theoretical scenarios proposed to explain the formation of G2, and we highlight their major drawbacks.

5.1 The pure gas cloud hypothesis

The models proposed to explain the nature of G2 can be grouped in two different families: (i) the 'true' cloud scenarios, and (ii) the 'hidden' central object scenarios. In the present Section we consider the former models, while the latter will be discussed in the next Section. The main difference between the two families of scenarios is that the expected pericentre of the orbit is within (outside) the tidal radius of a gas cloud (star).

According to the cloud scenario, G2 is a cold-ish gas clump, confined by the hot gas surrounding SgrA*. The gas temperature in the inner arcsec is $\sim 10^{7-8}$ K. The cooling timescale of such hot gas is mush longer than the dynamical timescale (Cuadra et al. 2005). Thus, the cloud cannot have formed *in situ* in the central arcsec, but must come from further out.

A possible scenario (e.g. Burkert et al. 2012) is that the cloud originated from the winds of the early-type stars in the CW disc. Winds of a luminous blue variable star can be as slow as $300-500\,\mathrm{km\,s^{-1}}$. When shocked, they are heated to $\sim 10^6$ K and cool quickly to $\sim 10^4$ K (Burkert et al. 2012), leading to the formation of

cold cloudlets embedded in the hot gas (Koo & McKee 1992). The coincidence of the orbital plane of G2 with the orientation of the CW disc encourages the 'shocked wind debris' hypothesis. While 'upstream' winds (i.e. winds emitted in the direction of motion of the parent star) have velocities in excess of $1000\,\mathrm{km\,s^{-1}}$ and are ejected from the GC, 'downstream' winds (i.e. winds emitted against the direction of motion of the parent star) have velocities $< 500\,\mathrm{km\,s^{-1}}$ and may fall toward Sgr A* on a very eccentric orbit.

Alternatively, G2 might have originated from high-velocity stellar winds that collided with each other, losing their initial angular momentum (Cuadra et al. 2006). Furthermore, G2 might have formed as a result of a cooling instability in the accretion flow toward Sgr A* (Gillessen et al. 2013a). In this case, the radial orbit is explained by the fact that the cloud belongs to a gas inflow.

Finally, Guillochon et al. (2014) recently proposed that G2 formed out of the debris stream produced by the removal of mass from the outer envelope of a nearby giant star. Their adaptive mesh hydrodynamical simulations of the returning tidal debris stream show that the stream condenses into clumps that fall periodically onto Sgr A*. G2 might be one of these clumps. Two intriguing results of this model are that (i) the orbits of several observed GC stars are consistent with the debris stream scenario, (ii) there might be several other G2-like clouds in the GC.

The cloud hypothesis (including the aforementioned 'shocked wind debris', 'stellar wind collision', 'cooling instability' and 'debris stream' scenarios) is consistent with existing observations (Gillessen et al. 2013b). The scenarios in which G2 is a collection of smaller droplets might even account for the observed constant luminosity. In fact, G2 is stretched by the SMBH's tidal shear along its orbit, while it is compressed in the transverse direction by the hot gas. This double effect is expected to produce changes in the luminosity. On the other hand, if G2 is composed of many little sub-clumps, the sub-clumps might be less affected by the shear and compression internally. The 'collection of smaller droplets' would allow to explain even another property: the large ($\approx 100\,\mathrm{km\,s^{-1}}$) internal velocity dispersion. In fact, the cold droplets are embedded in diffuse hot gas and might be pressure confined by this hot inter-droplet gas.

The main difficulty of the 'true' cloud models Gillessen et al. (2013b) is their apparent inability to explain the 'compactness' of G2 found in the most recent data: the 'head' of G2 (i.e. the leading bulk of G2 emission) is much more compact than expected (from models and simulations, e.g. Burkert et al. 2012; Schartmann et al. 2012) for a gas cloud starting in pressure equilibrium at the apocentre of the predicted orbit (≈ 0.041 pc, i.e. the inner rim of the ring of early-type stars). Furthermore, the head of G2 survived to the pericentre passage, without undergoing significant disruption.

This issue might be overcome by assuming that the cloud formed closer to the GC (≈ 0.0245 pc, Burkert et al. 2012), or that it is 'magnetically arrested' (Shcherbakov 2014). Alternatively, the cloud might be a spherical shell of gas (Schartmann et al. 2012), or a nova ejecta (Meyer & Meyer-Hofmeister 2012), rather than a compact cloud. Hydrodynamical simulations (see Fig. 34) show that the spherical shell model is in agreement with observations, even if the shell formed at apocentre, in the ring

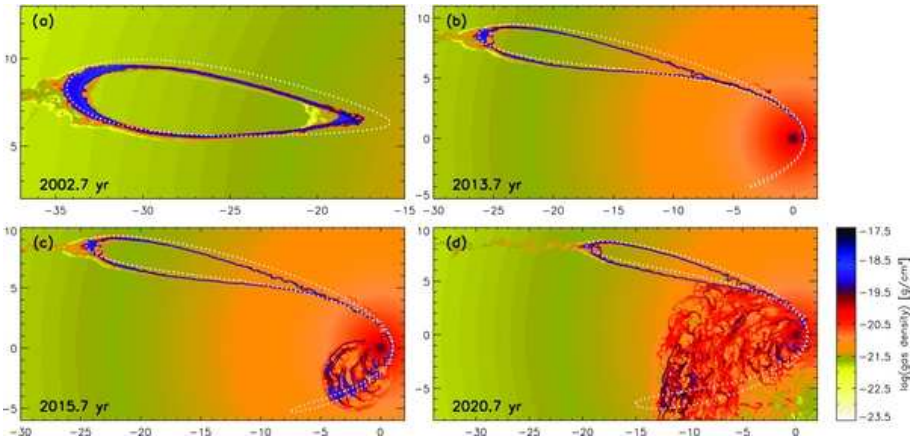

Fig. 34 Density evolution of a spherical shell matching the properties of GC (model SS01 of Schartmann et al. 2012). The simulation was performed with the hydrodynamical code PLUTO (Mignone et al. (2007)). Overlaid as dotted white lines are the positions of test particles initially located at the outer ring boundary. The axis labels are given in mpc. Fig. 5 of Schartmann et al. (2012).

of early-type stars. Finally, it may be that we observe only the 'tip of the iceberg', i.e. that the head of G2 is the very dense top of a much more massive (but less dense) gas inflow.

5.2 The central object scenario

In the central object scenario, G2 is the atmosphere of an unresolved central object that continuously loses gas. Ionizations and recombinations of this gas would be responsible for the observed line emission (Br-γ luminosity $\sim$ a few $\times 10^{30}$ erg s^{-1}, corresponding to an emission measure $\sim 10^{57}$ cm^{-3}). The object might have formed in the disc of early-type stars, and was then scattered into a highly eccentric orbit due to a close encounter with another stellar (or compact) object.

As to the nature of the object, a planetary nebula (Gillessen et al. 2012), a proto-planetary disc around a low-mass star (Murray-Clay & Loeb 2012), a circumstellar gas disc around an old low-mass star, disrupted by a stellar black hole (Miralda-Escudé 2012), the mass-loss envelope of a T Tauri star (Scoville & Burkert 2013, see also Eckart et al. 2013; Ballone et al. 2013; Witzel et al. 2014, and Fig. 35), a merged star (Prodan et al. 2015), and a giant gaseous proto-planet (i.e. a planetary embryo that formed from a gravitational instability in a protoplanetary disc, Mapelli & Ripamonti 2015) have been proposed.

Both the compactness of G2's head and the survival of G2 to pericentre passage can be easily accounted for, in the frame of the compact source scenario, because of the small tidal radius of the central object (≤ 10 AU). In the hypothesis of a T

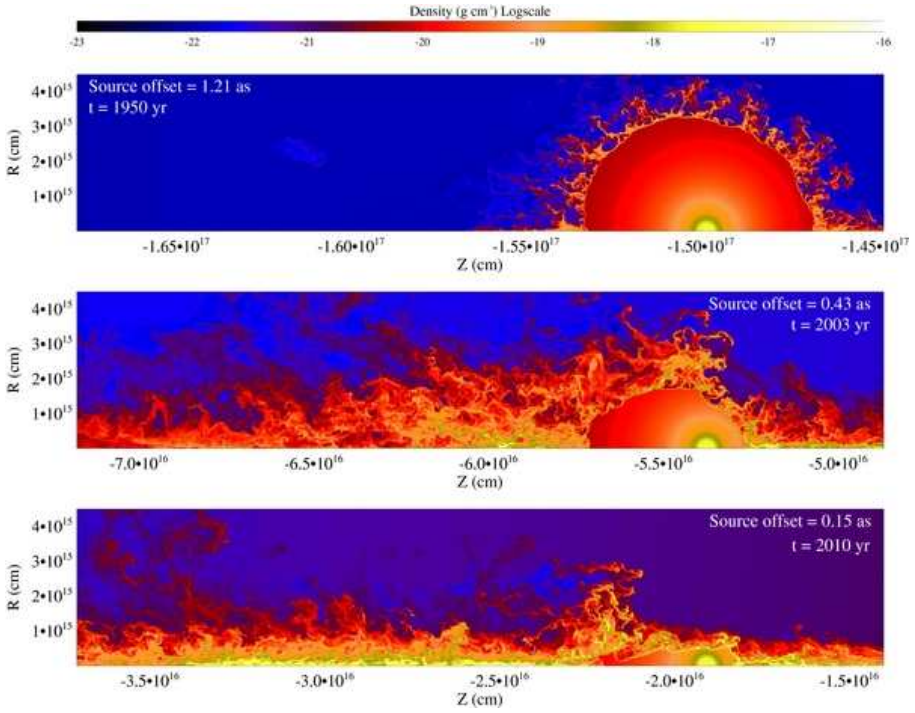

Fig. 35 Density maps of the stellar wind (around a T Tauri star) disrupted by the SMBH, in the fiducial run of Ballone et al. (2013). From top to bottom: source distance of 1".21, 0".43, and 0".15 from Sgr A*. Fig. 2 of Ballone et al. (2013).

Tauri star, the Br-γ emission comes from the inner cold bow shock, where the stellar wind is impacted by the hot gas in proximity of Sgr A* (Scoville & Burkert 2013). In the scenarios of both a giant gaseous protoplanet and a protoplanetary disc, the Br-γ emission arises from photoevaporation due to the ultraviolet background of the nuclear star cluster, and is enhanced by partial tidal stripping (Murray-Clay & Loeb 2012; Mapelli & Ripamonti 2015). Finally, the scenario of a proto-planetary disc (Murray-Clay & Loeb 2012) predicts an increase in the luminosity of the Br$-\gamma$ line by a factor of ≈ 5 at pericentre passage, quite higher than the observed value (which is only a factor of ~ 2, Pfuhl et al. 2014). On the other hand, this mismatch could be due to an overestimate of the recombination rate (see e.g. Mapelli & Ripamonti 2015). As recently highlighted by Witzel et al. 2014, the high L' continuum luminosity (corresponding to $\approx 2 \times 10^{33} \mathrm{erg\,s^{-1}}$) can be easily explained by a dust-enshrouded $1-2$ M$_\odot$ star. If the central source is too weak (e.g. in the case of a protoplanet), the warm dust must be spread over a sufficiently large volume (radius $\gtrsim 5 \times 10^{12}$ cm), to explain the L' continuum luminosity.

In summary, most of the proposed central object scenarios and pure cloud scenarios are still viable to explain the dusty object G2: the nature of this object remains quite elusive.

6 Conclusions: open questions and future work

In this review, we have briefly summarized the most recent observational results about the GC (Sect. 2), and we have discussed the main theoretical scenarios for the formation of the early-type stars (Sect. 3-4) and for the nature of the G2 cloud, Sect. 5) in the GC. In this Section, we would like to summarize the main scenarios for the formation of the early-type stars in the GC and highlight the pros and the cons of each of them.

The main scenarios for the formation of the **CW disc of early-type stars** are the following:

- Fragmentation of the outer parts of a past accretion disc (e.g. Levin & Beloborodov 2003; Nayakshin & Cuadra 2005; Nayakshin 2006; Nayakshin et al. 2007; Collin & Zahn 2008). This scenario appears promising when looking at the relevant timescales, but cannot easily explain (i) the non-zero eccentricity of the stellar orbits, (ii) the observed thickness of the disc, (iii) the absence of any remnant of a past accretion disc. The second issue can be circumvented by invoking some fast mechanism to increase inclinations (e.g. precession exerted by the CNR, Kozai resonance), but the other two issues are more difficult to overcome.
- Disruption of a molecular cloud which results in the formation of a gas disc sufficiently dense to fragment into stars (e.g. Levin & Beloborodov 2003; Bonnell & Rice 2008; Mapelli et al. 2008; Wardle & Yusef-Zadeh 2008; Hobbs & Nayakshin 2009; Alig et al. 2011; Mapelli et al. 2012; Lucas et al. 2013; Alig et al. 2013). Recent simulations show that this scenario can reproduce the observed distribution of eccentricities and semi-major axes of the CW stars, together with the thickness of the disc. A difficulty of this model is that the molecular cloud must have been on a fine-tuned orbit (i.e. with sufficiently low angular momentum, or with nearly zero impact parameter, to engulf Sgr A*). This issue might be overcome by assuming either that a cloud-cloud collision reduced the angular momentum of the cloud or that the disc was formed by gaseous streamers (such as those observed in the region of the CNR) rather than by a coherent molecular cloud.
- Inspiral and disruption of a star cluster (e.g. Gerhard 2001; Kim & Morris 2003). This process appears to be too slow to be consistent with the age of the CW stars and unable to explain the top-heavy MF. The presence of an IMBH at the centre of the cluster mitigates the requirements on the mass and density of the cluster for a fast inspiral but (i) there is so far no observational evidence for an IMBH in the GC, (ii) depending on the mass and eccentricity of the IMBH, interactions may act to randomise the inclinations and thermalise the eccentricities on timescales of 1 Myr or less, producing a system which is consistent with the properties of the S-cluster rather than those of the CW disc.

The main scenarios for the formation of the **early-type stars that do not lie in the CW disc, including the (B-type) S-stars** can be summarized as follows:

- Binary breakup scenario: the SMBH disrupts stellar binaries on eccentric orbits that take them within their tidal radius via the Hill's mechanism and captures one

of the components on an eccentric bound orbit (e.g. Hills, 1991; Miller et al., 2005). The large eccentricities of the stars are thermalised within the B-stars lifetime by resonant relaxation against the background cusp of stars and remnants.

- The inspiral and disruption of a star cluster with an IMBH can explain both the isotropic spatial distribution of the S-stars as well as the roughly thermal eccentricity distribution. However, formation of an IMBH in a cluster has only been predicted from *N*-body simulations. In addition, tidal stripping of stars during the cluster inspiral predicts the deposition of a much larger number of stars outside the S-cluster than are actually observed.

Relaxation processes are necessary ingredients of all above models in that they cause the orbital distributions of the young stars to evolve in time. In particular, resonant relaxation is required for the eccentricity distribution of stars captured from disrupted binaries to be converted into a thermal distribution. In the same model, scattering off massive perturbers is necessary to ensure that a sufficient number of stellar binaries born at large distances are places onto highly eccentric orbits at any time.

Precession in an axisymmetric potential and Kozai-Lidov resonances may explain the formation of the WR/O stars that do not lie in the CW disc (e.g. Löckmann et al. 2008; Löckmann et al. 2009; Šubr et al. 2009; Haas et al. 2011a; Haas et al. 2011b; Mapelli et al. 2013). According to these processes, the early-type stars that do not belong to the CW disc might be the former members of a now dismembered disc and/or the former members of the outer parts of the CW disc. This process can explain the outliers at > 0.04 pc but not the S-stars, unless the perturbing potential in the past was different from the current one (e.g. Chen & Amaro-Seoane 2014 explain the S-stars with Kozai-like resonance, by assuming that the inner edge of the gas disc was $<< 0.04$ pc in the past). Another intriguing idea is that the two-body relaxation time-scale in the inner parts of the disc ($\lesssim 0.05$ pc) might be much shorter than previously thought (Šubr & Haas 2014), leading to a fast relaxation of the innermost stellar orbits.

This short overview of formation scenarios for the young stars shows that there are a number of open questions about the recent star formation history and dynamical evolution of the Galactic Centre. The scenario of molecular-cloud disruption has become increasingly popular to explain the formation of the CW disc, but current simulations are far from realistically tracing the formation of stars in the gaseous disc. The treatment of shocks in the gas is crucial in this context but the SPH codes used so far to simulate the disruption of the molecular cloud are not the most suitable to capture the physics of shocks (e.g. Agertz et al. 2007). Simulations with different techniques (e.g. the adaptive-mesh refinement, AMR, technique) are absolutely needed to confirm these results. Radiative transfer from the newly born stars has never been accounted for (even if this is a likely minor effect with respect to SMBH heating). The explosion of core-collapse supernovae (the stars in the CW disc are $\gtrsim 3$ Myr old) has never been considered: it might have a crucial impact on the evaporation of the gas disc. The adopted cooling functions and recipes for the chemical composition of gas in the GC are critical too (see the discussion about opacity in Mapelli et al. 2012). We also know that the GC hosts strong magnetic

fields: their effects on the formation of the early-type stars have been neglected so far.

Furthermore, we find there has been a gap between *N*-body/SPH codes, used to simulate the evolution of gas, and a dissipationless direct-summation *N*-body codes, used to probe the secular evolution of stars. Only a few studies try to fill this gap (e.g. Mapelli et al., 2013, and references therein). More accurate *N*-body integrators need to be coupled to SPH or AMR codes, in order to have a global picture of the interplay between gas physics and dynamics in the GC. Finally, the formation of the S-stars is far from being understood, as all the proposed mechanisms suffer potential difficulties and/or substantial draw-backs.

From an observational point of view, probably no other region in the sky has been so thoroughly scanned and monitored as the GC, in the last ~ 10 years. ALMA is about to provide an exciting view of molecular gas and ongoing star formation in the GC (Yusef-Zadeh et al., 2013). Forthcoming observations with available facilities (e.g. the 8-m class telescopes VLT and Keck II) will provide more accurate measurements of the orbits of the S-stars, of the mass of the SMBH, of the enclosed mass in the GC and of the main properties of the early-type stars. With an imaging resolution of a few milliarcseconds and an astrometric accuracy of 10μas, the second generation instrument for the VLT Interferometer, GRAVITY, will be able to measure the proper motion of matter (stars or hot spots in the accretion disk) down to the event horizon of the black hole, hereby probing spacetime in its immediate vicinity. Future 30-m class telescopes (the European Extremely Large Telescope, E-ELT, and the Thirty Meter Telescope, TMT) will make a huge difference with respect to the past: a diffraction-limited resolution of ~ 12 mas will be achieved, which will allow for unprecedented astrometric precision (~ 0.1 mas, e.g. Yelda et al. 2013). This will offer a unique laboratory to study the intriguing processes that take place in the neighbourhood of a SMBH. Of particular relevance is the potential detection of relativistic effects, which can be accomplished by a combination of new facilities, longer monitoring of the currently known stars, and the detection of new stars at smaller distances from the SMBH.

Acknowledgements This review is not directly connected with the lectures held by Prof. R. Genzel at the 10$^{\text{th}}$ SIGRAV school on 'Astrophysical black holes'. We would like to thank Prof. R. Genzel, Dr. S. Gillessen, the Organizers of the SIGRAV school and the Editors of this Book for giving us the possibility to write this review. We warmly thank S. Gillessen, H. B. Liu and P. Kroupa for their invaluable comments. MM acknowledges financial support from the Italian Ministry of Education, University and Research (MIUR) through grant FIRB 2012 RBFR12PM1F ('New perspectives on the violent Universe: unveiling the physics of compact objects with joint observations of gravitational waves and electromagnetic radiation'), from INAF through grants PRIN-2011-1 ('Challenging Ultraluminous X-ray sources: chasing their black holes and formation pathways') and PRIN-2014-14 ('Star formation and evolution in galactic nuclei'), and from CONACyT through grant 169554 ('Nearby and distant spheroids: cutting edge theoretical tools for the analysis of stellar populations').

References

Abadi, M.G., Navarro, J.F., Steinmetz, M. 2009, ApJL, 691, L63
Accadia, T., et al. 2012, Virgo Document VIR-0128A-12, https://tds.ego-gw.it/ql/?c=8940
Agertz, O., et al. 2007, MNRAS, 380, 963
Alexander, T. 1999, ApJ, 527, 835
Alexander, R. D., Armitage, P. J., Cuadra, J., Begelman, M. C. 2008, ApJ, 674, 927
Alexander, R. D., Smedley, S. L., Nayakshin, S., King, A. R. 2012, MNRAS, 419, 1970
Alig, C., Burkert, A., Johansson, P. H., Schartmann, M. 2011, MNRAS, 412, 469
Alig, C., Schartmann, M., Burkert, A., Dolag, K. 2013, ApJ, 771, 119
Allen, D. A. 1987, AIP Conference Proceedings, 155, 1
Allen, D. A., Hyland, A. R., Hillier, D. J. 1990, MNRAS, 244, 706
Amaro-Seoane P., et al. 2013, GW Notes, 6, 4
Amo-Baladrón, M. A., Martín-Pintado, J., Martín, S. 2011, A&A, 526, 54
Antonini, F., Faber, J., Gualandris, A., Merritt, D. 2010, ApJ, 713, 90
Antonini, F., Capuzzo-Dolcetta, R., Mastrobuono-Battisti, A., Merritt, D. 2011, ApJ, 750, 111
Antonini, F., Merritt, D. 2013, ApJ, 763, L10
Ao, Y., Henkel, C., Menten, K. M., Requena-Torres, M. A., Stanke, T., Mauersberger, R., Aalto, S., Mühle, S., Mangum, J. 2013, A&A, 550, 135
Arca Sedda, M., Capuzzo-Dolcetta, R. 2014, ApJ, submitted, arXiv:1307.5717
Bahcall, J. N., Tremaine, S. 1981, ApJ, 244, 805
Bahcall, J. N., Wolf, R.A. 1976, ApJ, 209, 214
Balick, B., Brown, R. L. 1974, Intense sub-arcsecond structure in the galactic center, published in 'H II regions and the galactic centre : proceedings of the Eighth ESLAB Symposium', p. 261
Ballone, A., Schartmann, M., Burkert, A., Gillessen, S., Genzel, R., Fritz, T. K., Eisenhauer, F., Pfuhl, O., Ott, T. 2013, ApJ, 776, 13
Bartko, H., Martins, F., Fritz, T. K., Genzel, R., Levin, Y., Perets, H.B., Paumard, T., Nayakshin, S., Gerhard, O., Alexander, T., et al. 2009, ApJ, 697, 1741
Bartko, H., Martins, F., Trippe, S., Fritz, T. K., Genzel, R., Ott, T., Eisenhauer, F., Gillessen, S., Paumard, T., Alexander, T., et al. 2010, ApJ, 708, 834
Baumgardt, H., Gualandris, A., Portegies Zwart, S. 2006, MNRAS, 372, 174
Becklin, E. E., Gatley, I., Werner, M. W. 1982, ApJ, 258, 135
Binney, J., Tremaine, S. 1987, Galactic Dynamics (Princeton, NJ: Princeton University Press)
Blum, R. D., Sellgren, K., Depoy, D. L. 1995a, ApJ, 440, L17
Blum, R. D., Depoy, D. L., Sellgren, K. 1995b, ApJ, 441, 603
Boley, A. C. 2009, ApJ, 695, L53
Boley, A. C., Hayfield, T., Mayer, L., Durisen, R. H. 2010, Icarus, 207, 509
Bonnell, I. A., Rice, W. K. M. 2008, Science, 321, 1060
Bromley, B. C.,Kenyon, S. J.,Geller, M. J., Barcikowski, E.,Brown, W. R., Kurtz, M. J. 2006, ApJ, 653, 1194

Brown, W.R., Geller, M.J., Kenyon, S.J., Kurtz, M.J. 2005, ApJL, 622, L33
Buchholz, R. M., Schödel, R., Eckart, A. 2009, A&A, 499, 483
Burkert, A., Schartmann, M., Alig, C., Gillessen, S., Genzel, R., Fritz, T. K., Eisenhauer, F. 2012, ApJ, 750, 58
Chan, K.-W., Moseley, S. H., Casey, S., Harrington, J. P., Dwek, E., Loewenstein, R., Városi, F., Glaccum, W. 1997, ApJ, 483, 798
Chandrasekhar, S. 1943, ApJ, 97, 255
Chang, Ph. 2009, MNRAS, 393, 224
Chatzopoulos, S., Fritz, T., Gerhard, O., Gillessen, S., Wegg, C., Genzel, R., Pfuhl, O. 2014, MNRAS, submitted, arXiv:1403.5266
Chen, X., Amaro-Seoane, P. 2014, ApJ, submitted, arXiv:1401.6456
Christopher, M. H., Scoville, N. Z., Stolovy, S. R., Yun, Min S. 2005, ApJ, 622, 346
Clénet, Y., Rouan, D., Gendron, E., Lacombe, F., Lagrange, A.-M., Mouillet, D., Magnard, Y., Rousset, G., Fusco, T., Montri, J., et a. 2004, A&A, 417, L15
Coil, A. L., Ho, P. T. P. 1999, ApJ, 513, 752
Coil, A. L., Ho, P. T. P. 2000, ApJ, 533, 245
Collin, S., Huré, J.-M. 1999, A&A, 341, 385
Collin, S., Zahn, J.-P. 1999, A&A, 344, 433
Collin, S., Zahn, J.-P. 2008, A&A, 477, 419
Côté, P., Piatek, S., Ferrarese, L., Jordán, A., Merritt, D., Peng, E. W., Hasegan, M., Blakeslee, J. P., Mei, S., West, M. J., et al. 2006, ApJS, 165, 57
Cuadra, J., Nayakshin, S., Springel, V., Di Matteo, T. 2005, MNRAS, 360, L55
Cuadra, J., Nayakshin, S., Springel, V., Di Matteo, T. 2006, MNRAS, 366, 358
Cuadra J., Armitage, Ph. J., Alexander, R. D. 2008, MNRAS, 388, L64
Dent, W. R. F., Matthews, H. E., Wade, R., Duncan, W. D. 1993, ApJ, 410, 650
Depoy, D. L., Gatley, I., McLean, I. S. 1989, Proceedings of the 136th Symposium of the International Astronomical Union, held in Los Angeles, U.S.A., July 25-29, 1988. Edited by Mark Morris. International Astronomical Union. Symposium no. 136, Kluwer Academic Publishers, Dordrecht, p.411
Detweiler, S. 1979, ApJ, 234, 1100
Do, T., Ghez, A. M., Morris, M. R., Lu, J. R., Matthews, K., Yelda, S., Larkin, J. 2009, ApJ, 703, 1323
Do, T., Lu, J. R., Ghez, A. M., Morris, M. R., Yelda, S., Martinez, G. D., Wright, S. A., Matthews, K. 2013, ApJ, 764, 154
Donovan, J. L., Herrnstein, R., M., Ho, P. T. P. 2006, ApJ, 647, 1159
Downes, D., Martin, A. H. M. 1971, Nature, 233, 112
Eckart, A., Genzel, R., Hofmann, R., Sams, B. J., Tacconi-Garman, L. E. 1993, ApJ, 407, L77
Eckart, A., Genzel, R., Hofmann, R., Sams, B. J., Tacconi-Garman, L. E. 1995, ApJ, 445, L23
Eckart, A., Genzel, R. 1997, MNRAS, 284, 576
Eckart, A., Muzić, K., Yazici, S., Sabha, N., Shahzamanian, B., Witzel, G., Moser, L., Garcia-Marin, M., Valencia-S., M., Jalali, B., et al. 2013, A&A, 551, 18
Eilon, E., Kupi, G., Alexander, T. 2009, ApJ, 698, 641

Eisenhauer, F., Genzel, R., Alexander, T., Abuter, R., Paumard, T., Ott, T., Gilbert, A., Gillessen, S., Horrobin, M., Trippe, S., et al. 2005, ApJ, 628, 246
Eisenhauer, F. et al. 2009, Science with the VLT in the ELT Era, Astrophysics and Space Science Proceedings. ISBN 978-1-4020-9189-6. Springer Netherlands, 2009, p. 361
Ekers, R. D., van Gorkom, J. H., Schwarz, U. J., Goss, W. M. 1983, A&A, 122, 143
Fritz, T. K., Chatzpoulos, S., Gerhard, O., Gillessen, S., Dodd-Eden, K., Genzel, R., Ott, T., Pfuhl, O., Eisenhauer, F., 2014, submitted
Fujii,M.,Iwasawa,M.,Funato,M.,Makino,J. 2008, ApJ, 686, 1082
Fujii,M.,Iwasawa,M.,Funato,M.,Makino,J. 2009, ApJ, 695, 1421
Fujii,M.,Iwasawa,M.,Funato,M.,Makino,J. 2010, ApJ, 716, L80
Gammie, Ch. F. 2001, ApJ, 553, 174
Gatley, I., Jones, T. J., Hyland, A. R., Wade, R., Geballe, T. R., Krisciunas, K. 1986, MNRAS, 222, 299
Genzel, R., Stacey, G. J., Harris, A. I., Townes, C. H., Geis, N., Graf, U. U., Poglitsch, A., Stutzki, J. 1990, ApJ, 356, 160
Genzel, R., Hollenbach, D., Townes, C. H. 1994, 57, 417
Genzel, R., Thatte, N., Krabbe, A., Kroker, H., Tacconi-Garman, L. E. 1996, ApJ, 472, 153
Genzel, R., Eckart, A., Ott, T., Eisenhauer, F. 1997, MNRAS, 291, 219
Genzel, R., Schödel, R., Ott, T., Eisenhauer, F., Hofmann, R., Lehnert, M., Eckart, A., Alexander, T., Sternberg, A., Lenzen, R., et al. 2003, ApJ, 594, 812
Genzel R., Eisenhauer F., Gillessen S. 2010, Reviews of Modern Physics, 82, 3121
Gerhard, O. 2001, ApJ, 546, L39
Ghez, A. M., Klein, B. L., Morris, M., Becklin, E. E. 1998, ApJ, 509, 678
Ghez, A. M., Duchene, G., Matthews, K., Hornstein, S. D., Tanner, A., Larkin, J., Morris, M., Becklin, E. E., Salim, S., Kremenek, T. et al. 2003, ApJ, 586, L127
Ghez, A. M., Salim, S., Hornstein, S. D., Tanner, A., Lu, J. R., Morris, M., Becklin, E. E., Duchene, G. 2005, ApJ, 620, 744
Ghez, A. M., Hornstein, S. D., Lu, J. R., Bouchez, A., Le Mignant, D., van Dam, M. A., Wizinowich, P., Matthews, K., Morris, M., Becklin, E. E., et al. 2005b, ApJ, 635, 1087
Ghez, A. M., Salim, S., Weinberg, N. N., Lu, J. R., Do, T., Dunn, J. K., Matthews, K., Morris, M. R., Yelda, S., Becklin, E. E., et al. 2008, ApJ, 689, 1044
Gillessen, S., Eisenhauer, F., Trippe, S., Alexander, T., Genzel, R., Martins, F., Ott, T. 2009a, ApJ, 692, 1075
Gillessen, S., Eisenhauer, F., Fritz, T. K., Bartko, H., Dodds-Eden, K., Pfuhl, O., Ott, T., Genzel, R. 2009b, ApJ, 707, L114
Gillessen, S., Genzel, R., Fritz, T. K., Quataert, E., Alig, C., Burkert, A., Cuadra, J., Eisenhauer, F., Pfuhl, O., Dodds-Eden, K., Gammie, C. F., Ott, T. 2012, Nature, 481, 51
Gillessen, S., Genzel, R., Fritz, T. K., Eisenhauer, F., Pfuhl, O., Ott, T., Cuadra, J., Schartmann, M., Burkert, A. 2013a, ApJ, 763, 78
Gillessen, S., Genzel, R., Fritz, T. K., Eisenhauer, F., Pfuhl, O., Ott, T., Schartmann, M., Ballone, A., Burkert, A. 2013b, ApJ, 774, 44

Goicoechea, J. R., et al. 2013, ApJ, 769, L13
Goodman, J. 2003, MNRAS, 339, 937
Gould, A,. Quillen, A. 2003, ApJ, 592, 935
Gualandris, A., Merritt, D. 2009, ApJ, 705, 361
Gualandris, A., Gillessen, S. , Merritt, D. 2010, MNRAS, 409, 1146
Gualandris, A., Mapelli, M., Perets, H.B. 2012, MNRAS, 427, 1793
Gualandris, A., Merritt D. 2012, ApJ, 744, 74
Guesten, R., Downes, D. 1980, A&A, 87, 6
Guesten, R., Genzel, R., Wright, M. C. H., Jaffe, D. T., Stutzki, J., Harris, A. I. 1987, ApJ, 318, 124
Guillochon, J., Loeb, A., MacLeod, M., Ramirez-Ruiz, E. 2014, ApJ, 786, L12
Gvaramadze, V. V., Gualandris, A., Portegies Zwart, S. 2009, MNRAS, 396, 570
Gvaramadze, V.V., Gualandris, A. 2011, MNRAS, 410, 304
Haas, J., Šubr, L., Kroupa, P. 2011a, MNRAS, 412, 1905
Haas, J., Šubr, L., Vokrouhlický, D. 2011b, MNRAS, 416, 1023
Haggard, D., Baganoff, F. K., Rea, N., Coti Zelati, F., Ponti, G., Heinke, C., Campana, S., Israel, G. L., Yusef-Zadeh, F., Roberts, D. 2014, The Astronomer's Telegram, # 6242
Haller, Joseph W., Rieke, M. J., Rieke, G. H., Tamblyn, P., Close, L., Melia, F. 1996, ApJ, 456, 194
Hansen, B. M. S., Milosavljević, M. 2003, ApJ, 593, L77
Harry, G. M. and the LIGO Scientific Collaboration 2010, Classical and Quantum Gravity 27, 084006
Heber, U., Edelmann, H., Napiwotzki, R., Altmann, M., Scholz, R.-D. 2008, A&A, 483, L21
Herrnstein, R. M., Ho, P. T. P. 2002, ApJ, 579, L83
Herrnstein, R. M., Ho, P. T. P. 2005, ApJ, 620, 287
Hills, J.G. 1991, AJ, 102, 704
Hills, J.G. 1992, AJ, 103, 1955
Hills, J.G. 1992, Nature, 331, 687
Ho, P. T. P., Jackson, J. M., Barrett, A. H., Armstrong, J. T. 1985, ApJ, 288, 575
Ho, P. T. P., Ho, L. C., Szczepanski, J. C., Jackson, J. M., Armstrong, J. T. 1991, Nature, 350, 309
Hobbs, A., Nayakshin, S. 2009, MNRAS, 394, 19
Hopman, C., Alexander, T. 2006, ApJ, 645, L133
Huré, J.-M. 1998, A&A, 290, 625
Irrgang, A., Przybilla, N., Heber, U., Nieva, M.F., & Schuh, S. 2010, ApJ, 711, 138
Ivanov, P. B., Polnarev, A. G., Saha, P. 2005, MNRAS, 358, 1361
Jackson, J. M., Geis, N., Genzel, R., Harris, A. I., Madden, S., Poglitsch, A., Stacey, G. J., Townes, C. H. 1993, ApJ, 402, 173
Jeans, J. H.: Problems of cosmogony and stellar dynamics, 1919, Cambridge, University press, LCCN: 20-9684 (PREM), CALL NUMBER: QB981 .J4
Karlsson, R., Sjouwerman, L. O., Sandqvist, Aa., Whiteoak, J. B. 2003, A&A, 403, 1011
Kim, S. S., Morris, M. 2003, ApJ, 597, 312

Kim, S. S., Figer,D.F., Morris, M. 2004, ApJL, 607, L123
Kocsis, B., Ray, A., Portegies Zwart, S. 2012, ApJ, 752, 67
Kolykhalov, P. I., Syunyaev, R. A. 1980, Soviet Astronomy Letters, 6, 357
Koo, B.-C., McKee, C. F. 1992, ApJ, 388, 93
Koyama, K., Maeda, Y., Sonobe, T., Takeshima, T., Tanaka, Y., Yamauchi, S. 1996, PASJ, 48, 249
Kozai, Y. 1962, AJ, 67, 591
Krabbe, A., Genzel, R., Drapatz, S., Rotaciuc, V. 1991, ApJ, 382, L19
Krabbe, A., Genzel, R., Eckart, A., Najarro, F., Lutz, D., Cameron, M., Kroker, H., Tacconi-Garman, L. E., Thatte, N., Weitzel, L., et al. 1995, ApJ, 447, L95
Kroupa, P. 2001, MNRAS, 322, 231
Lacy, J. H., Townes, C. H., Geballe, T. R., Hollenbach, D. J. 1980, ApJ, 241, 132
Lacy, J. H., Townes, C. H., Hollenbach, D. J. 1982, ApJ, 262, 120
Lazio, T. J. W. 2013, Classical and Quantum Gravity, 30, 224011
Levin, Y., Beloborodov, A. M. 2003, ApJ, 590, L33
Libonate, S., Pipher, J. L., Forrest, W. J., Ashby, M. L. N. 1995, ApJ, 439, 202
Lidov, M. L. 1962, Planetary and Space Science, 9, 719
Lin, D. N. C., Pringle, J. E. 1987, MNRAS, 225, 607
Lis, D. C., Carlstrom, J. E. 1994, ApJ, 424, 189
Liu, H. B., Hsieh, P.-Y., Ho, P. T. P., Su, Y.-N., Wright, M., Sun, A.-L., Minh, Y. C. 2012, ApJ, 756, 195
Liu, H. B., Ho, P. T. P., Wright, M. C. H., Su, Y.-N., Hsieh, P.-Y., Sun, A.-L., Kim, S. S., Minh, Y. C. 2013, ApJ, 770, 44
Lo, K. Y., Claussen, M. J. 1983, Nature, 306, 647
Löckmann, U., Baumgardt, H. 2008, MNRAS, 384, 323
Löckmann, U., Baumgardt, H., Kroupa, P. 2008, ApJ, 683, L151
Löckmann, U., Baumgardt, H., Kroupa, P. 2009, MNRAS, 398, 429
Löckmann, U., Baumgardt, H., Kroupa, P. 2010, MNRAS, 402, 519
Lu, J. R., Ghez, A. M., Hornstein, S. D., Morris, M., Matthews, K., Thompson, D. J., Becklin, E. E. 2006, Journal of Physics: Conference Series, Volume 54, Proceedings of ”The Universe Under the Microscope - Astrophysics at High Angular Resolution”, held 21-25 April 2008, in Bad Honnef, Germany. Editors: Rainer Schoedel, Andreas Eckart, Susanne Pfalzner and Eduardo Ros, pp. 279-287
Lu, J. R., Ghez, A. M., Hornstein, S. D., Morris, M. R., Becklin, E. E., Matthews, K. 2009, ApJ, 690, 1463
Lu, Y., Zhang, F., Yu, Q. 2010, ApJ, 709, 1356
Lu, J. R., Do, T., Ghez, A. M., Morris, M. R., Yelda, S., Matthews, K. 2013, ApJ, 764, 155
Lucas, W. E., Bonnell, I. A., Davies, M. B., Rice, W. K. M. 2013, MNRAS, 433, 353
Madigan, A., Levin, Y., Hopman, C. 2009, ApJ, 697, L44
Madigan, A., Pfuhl, O., Levin, Y., Gillessen, S., Genzel, R., Perets, H.B. 2014, ApJ, submitted, arXiv:1305.1625
Maoz, E. 1998, ApJ, 494, L181
Mapelli, M., Hayfield, T., Mayer, L., Wadsley, J. 2008, arXiv0805.0185

Mapelli, M., Huwyler, C., Mayer, L., Jetzer, Ph., Vecchio, A. 2010, ApJ, 719, 987
Mapelli, M., Hayfield, T., Mayer, L., Wadsley, J. 2012, ApJ, 749, 168
Mapelli, M., Gualandris, A., Hayfield, T. 2013, MNRAS, 436, 3809
Mapelli, M., Ripamonti, E. 2015, ApJ, submitted
Marr, J. M., Wright, M. C. H., Backer, D. C. 1993, ApJ, 411, 667
Martín, S., Martín-Pintado, J., Montero-Castaño, M., Ho, P. T. P., Blundell, R. 2012, A&A, 539, 29
Martins, F., Gillessen, S., Eisenhauer, F., Genzel, R., Ott, T., Trippe, S. 2008, ApJ, 672, L119
Matsubayashi, T., Makino, J., Ebisuzaki, T. 2007, ApJ, 656, 897
McGary, R. S., Ho, P. T. P. 2002, ApJ, 577, 757
McGinn, M. T., Sellgren, K., Becklin, E. E., Hall, D. N. B. 1989, ApJ, 338, 824
Merritt, D., Gualandris, A., Mikkola, S. 2009, ApJL, 693, L35
Merritt, D. 2010, ApJ, 718, 739
Merritt, D., Alexander, T., Mikkola, S., Will, C.M. 2010, Phys.Rev.D, 81, 6
Merritt, D., Alexander, T., Mikkola, S., Will, C.M. 2011, Phys.Rev.D, 84, 044024
Merritt, D. 2013, Loss Cone Dynamics, Invited article for the focus issue on "Astrophysical Black Holes" in Classical and Quantum Gravity, guest editors: D. Merritt and L. Rezzolla
Merritt, D. 2013, Dynamics and Evolution of Galactic Nuclei (Princeton: Princeton University Press)
Meyer, L., Ghez, A. M., Schödel, R., Yelda, S., Boehle, A., Lu, J. R., Do, T., Morris, M. R., Becklin, E. E., Matthews, K. 2012, Science, 338, 84
Meyer, F., Meyer-Hofmeister, E. 2012,A&A, 546, L2
Mezger, P. G., Zylka, R., Salter, C. J., Wink, J. E., Chini, R., Kreysa, E., Tuffs, R. 1989, A&A, 209, 337
Mignone, A., Bodo, G., Massaglia, S., Matsakos, T., Tesileanu, O., Zanni, C., Ferrari, A. 2007, ApJS, 170, 228
Miller, M. C., Freitag, M., Hamilton, D. P., Lauburg, V. M. 2005, ApJ, 631, L117
Mills, E. A. C., Güsten, R., Requena-Torres, M. A., Morris, M. R. 2013, ApJ, 779, 47
Minh, Y. C., Liu, H. B., Ho, P. T. P., Hsieh, P.-Y., Su, Y.-N., Kim, S. S., Wright, M. 2013, ApJ, 773, 31
Miralda-Escudé, J. 2012, ApJ, 756, 86
Montero-Castaño, M., Herrnstein, R. M., Ho, P. T. P. 2009, ApJ, 695, 1477
Morris, M. 1993, ApJ, 408, 496
Morris, M. R., Meyer, L., Ghez, A. M. 2012, Research in Astronomy and Astrophysics, 12, 995
Morris, M., Serabyn, E. 1996, Annual Review of Astronomy and Astrophysics, 34, 645
Müller Sánchez, F., Davies, R. I., Genzel, R., Tacconi, L. J., Eisenhauer, F., Hicks, E. K. S., Friedrich, S., Sternberg, A. 2009, ApJ, 691, 749
Murray-Clay, R. A., Loeb, A. 2012, Nature Communications, 3
Nayakshin, S., Cuadra, J. 2005, A&A, 437, 437
Nayakshin, S. 2005, MNRAS, 359, 545

Nayakshin, S. 2006, MNRAS, 372, 143
Nayakshin, S., Cuadra, J., Springel, V. 2007, MNRAS, 379, 21
Novak, G., Dotson, J. L., Dowell, C. D., Hildebrand, R. H., Renbarger, T., Schleuning, D. A. 2000, ApJ, 529, 241
Oka, T., Nagai, M., Kamegai, K., Tanaka, K. 2011, ApJ, 732, 120
Okumura, S. K., Ishiguro, M., Fomalont, E. B., Hasegawa, T., Kasuga, T., Morita, K.-I., Kawabe, R., Kobayashi, H. 1991, ApJ, 378, 127
Paczynski, B. 1978, Acta Astronomica 28, 91
Paumard, T., Genzel, R., Martins, F., Nayakshin, S., Beloborodov, A. M., Levin, Y., Trippe, S., Eisenhauer, F., Ott, T., Gillessen, S., et al. 2006, ApJ, 643, 1011
Perets, H.B., Hopman, C., Alexander, T. 2007, ApJ, 656, 709
Perets, H.B, Gualandris, A., Kupi, G., Merritt, D., Alexander, T. 2009, ApJ, 702, 884
Perets, H.B., Gualandris, A. 2010, ApJ, 719, 220
Pfahl, E., Loeb, A. 2004, ApJ, 615, 253
Pfuhl, O., Gillessen, S., Eisenhauer, F., Genzel, R., Plewa, P. M., Ott, T., Ballone, A., Schartmann, M., Burkert, A., Fritz, T. K. 2014, ApJ, accepted
Phifer, K., Do, T., Meyer, L., Ghez, A. M., Witzel, G., Yelda, S., Boehle, A., Lu, J. R., Morris, M. R., Becklin, E. E., Matthews, K. 2013, ApJ, 773, L13
Phinney, E. S. 1989, In: The Center of the Galaxy: Proceedings of the 136th Symposium of the International Astronomical Union, held in Los Angeles, U.S.A., July 25-29, 1988. Edited by Mark Morris. International Astronomical Union. Symposium no. 136, Kluwer Academic Publishers, Dordrecht, 543
Pierce-Price, D., et al. 2000, ApJ, 545, L121
Piffl, T., Williams, M., Steinmetz, M. 2011, A&A, 535, A70
Ponti, G., Terrier, R., Goldwurm, A., Belanger, G., Trap, G. 2010, ApJ, 714, 732
Prodan, S., Antonini, F., Perets, H. B. 2015, ApJ, accepted, arXiv1405.6029
Przybilla, N., Nieva, M.F., Heber, U., & Butler, K. 2008, ApJL, 684, L103
Portegies Zwart, S., Baumgardt, H., Hut, P., Makino, J., McMillan S. L. W. 2004, Nature 428, 724
Portegies Zwart, S., 2006, ApJ, 641, 319
Rauch, K.P., Tremaine, S. 1996, NewA, 1, 149
Rea, N., Esposito, P., Pons, J. A., Turolla, R., Torres, D. F., Israel, G. L., Possenti, A., Burgay, M., Viganò, D., Papitto, A., et al. 2013, ApJ, 775, L34
Reid, M. J., Brunthaler, A. 2004, ApJ, 616, 872
Reid, M. J., Menten, K. M., Trippe, S., Ott, T., Genzel, R. 2007, ApJ, 659, 378
Rieke, G. H., Rieke, M. J. 1988, ApJ, 330, L33
Rieke, G. H., Rieke, M. J. 1989, ApJ, 344, L
Rubilar,G.F., Eckart,A. 2001, A&A, 374, 95
Salpeter, E. E. 1995, ApJ, 121, 161
Sanchez-Bermudez, J., Schödel, R., Alberdi, A., Muzić, K., Hummel, C. A., Pott, J.-U. 2014, A&A, 567, 16
Sanders, R. H. 1998, MNRAS 294, 35
Schartmann, M., Burkert, A., Alig, C., Gillessen, S., Genzel, R., Eisenhauer, F., Fritz, T. K. 2012, ApJ, 755, 155

Schödel, R., Ott, T., Genzel, R., Hofmann, R., Lehnert, M., Eckart, A., Mouawad, N., Alexander, T., Reid, M. J., Lenzen, R., et al. 2002, Nature, 419, 694
Schödel, R., Ott, T., Genzel, R., Eckart, A., Mouawad, N., Alexander, T. 2003, ApJ, 596, 1015
Schödel, R., Eckart, A., Alexander, T., Merritt, D., Genzel, R., Sternberg, A., Meyer, L., Kul, F., Moultaka, J., Ott, T., Straubmeier, C. 2007, A&A, 469, 125
Schödel, R., Merritt, D., Eckart, A. 2009, A&A, 502, 91
Schödel, R., Najarro, F., Muzic, K., Eckart, A. 2010, A&A, 511, 18
Scoville, N. Z., Stolovy, S. R., Rieke, M., Christopher, M., Yusef-Zadeh, F. 2003, ApJ, 594, 294
Scoville, N., Burkert, A. 2013, ApJ, 768, 108
Sellgren, K., McGinn, M. T., Becklin, E. E., Hall, D. N. 1990, ApJ, 359, 112
Serabyn, E., Guesten, R., Walmsley, J. E., Wink, J. E., Zylka, R. 1986, A&A, 169, 85
Serabyn, E., Lacy, J. H., Achtermann, J. M. 1992, ApJ, 395, 166
Shcherbakov, R. V. 2014, ApJ, 783, 31
Shlosman, I., Begelman, M. C. 1989, ApJ, 341, 685
Solomon, P. M., Scoville, N. Z., Penzias, A. A., Wilson, R. W., Jefferts, K. B. 1972, ApJ, 178, 125
Šubr, L., Schovancová, J., Kroupa, P. 2009, A&A, 496, 695
Šubr, L., Haas, J. 2012, Journal of Physics: Conference Series, 372
Šubr, L., Haas, J. 2014, ApJ, 786, 121
Sunyaev, R. A., Markevitch, M., Pavlinsky, M. 1993, ApJ, 407, 606
Sutton, E. C., Danchi, W. C., Jaminet, P. A., Masson, C. R. 1990, ApJ, 348, 503
Tamblyn, P., Rieke, G. H., Hanson, M. M., Close, L. M., McCarthy, D. W., Jr., Rieke, M. J. 1996, ApJ, 456, 206
Telesco, C. M., Davidson, J. A., Werner, M. W. 1996, ApJ, 456, 541
Thompson, T. A., Quataert, E., Murray, N. 2005, ApJ, 630, 167
Tillich, A., Przybilla, N., Scholz, R.-D., Heber, U. 2009, A&A, 507, L37
Toomre, A. 1964, ApJ, 139, 1217
Trippe, S., Gillessen, S., Gerhard, O. E., Bartko, H., Fritz, T. K., Maness, H. L., Eisenhauer, F., Martins, F., Ott, T., Dodds-Eden, K., Genzel, R. 2008, A&A, 492, 419
Tsiklauri, D., Viollier, R. D. 1998, ApJ, 500, 591
Tsuboi, M., Miyazaki, A., Okumura, S. K. 2009, PASJ, 61, 29
Tsuboi, M.,Tadaki, K.-I., Miyazaki, A., Handa, T. 2011, PASJ, 63, 763
Tsuboi, M., Miyazaki, A. 2012, PASJ, 64, 111
Vollmer, B., Duschl, W. J. 2001, A&A, 367, 72
Wadsley, J. W., Stadel, J., Quinn, T. 2004, New Astronomy, 9, 137
Wang, B., Silk, J. 1994, ApJ, 427, 759
Wardle, M., Yusef-Zadeh, F. 2008, ApJ, 683, L37
Whiteoak, J. B., Rogstad, D. H., Lockhart, I. A. 1974, A&A, 36, 245
Witzel, G., Ghez, A. M., Morris, M. R., Sitarski, B. N., Boehle, A., Naoz, S., Campbell, R., Becklin, E. E., Canalizo, G., Chappell, S., et al. 2014, ApJ, 796, L8

Wright, M. C. H., Coil, A. L., McGary, R. S., Ho, P. T. P., Harris, A. I. 2001, ApJ, 551, 254
Yelda, S., Ghez, A. M., Lu, J. R., Do, T., Meyer, L., Morris, M. R. 2012, Adaptive Optics Systems III. Proceedings of the SPIE, 8447, 7 pp.
Yelda, S., Meyer, L., Ghez, A. M., Do, T. 2013, Proceedings of the Third AO4ELT Conference. Firenze, Italy, May 26-31, 2013, Eds.: Simone Esposito and Luca Fini Online at http://ao4elt3.sciencesconf.org/, id. #83
Yelda, S., Ghez, A. M., Lu, J. R., Do, T., Meyer, L., Morris, M. R., Matthews, K. 2014, ApJ, 783, 131
Yu, Y.-W., Cheng, K. S., Chernyshov, D. O., Dogiel, V. A. 2011, MNRAS, 411, 2002
Yu, Q., & Tremaine, S. 2003, ApJ, 599, 1129
Yungelson, L. et al. 2008, A&A, 477, 223
Yusef-Zadeh, F., Morris, M. 1987, ApJ, 320, 545
Yusef-Zadeh, F., Hewitt, J. W., Cotton, W. 2004, ApJS, 155, 421
Yusef-Zadeh, F., Braatz, J., Wardle, M., Roberts, D. 2008, ApJ, 683, L147
Yusef-Zadeh, F., Royster, M., Wardle, M., Arendt, R., Bushouse, H., Lis, D. C., Pound, M. W., Roberts, D. A., Whitney, B., Wootten, A. 2013, ApJ, 767, L32
Zhao, J.-H., Morris, M. R., Goss, W. M., An, T. 2009, ApJ, 699, 186
Zhao, J.-H., Blundell, R., Moran, J. M., Downes, D., Schuster, K. F., Marrone, D. P. 2010, ApJ, 723, 1097
Zylka, R., Mezger, P. G. 1988, A&A, 190, L25

Index